NASA/CR-1998-207448

THE GLOBAL CORONAL STRUCTURE INVESTIGATION

NASA Grant NAG5-5075

Annual Report

For the Period 1 April 1997 through 31 March 1998

Principal Investigator
Dr. Leon Golub

February 1998

Prepared for:

GSFC/Wallops Flight Facility
Wallops Island, VA 23337

Smithsonian Institution
Astrophysical Observatory
Cambridge, Massachusetts 02138

The Smithsonian Astrophysical Observatory is a member of the Harvard-Smithsonian Center for Astrophysics

The NASA Technical Officer for this grant is Bobby J. Flowers, Code 830.0, GSFC/Wallops Flight Facility, Wallops Island, VA 23337

I. Work Completed During the Past Year:

During the past year we have completed the changeover from the NIXT program to the new TXI sounding rocket program. The NIXT effort, aimed at evaluating the viability of the remaining portions of the NIXT hardware and design, has been finished and the portions of the NIXT which are viable and flightworthy, such as filters, mirror mounting hardware, electronics and telemetry interface systems, are now part of the new rocket payload.

The backup NIXT multilayer-coated x-ray telescope and its mounting hardware have been completely fabricated and are being stored for possible future use in the TXI rocket. The H-alpha camera design is being utilized in the TXI program for real-time pointing verification and control via telemetry. A new H-alpha camera has been built, with a high-resolution RS-170 CCD camera output.

Two papers, summarizing scientific results from the NIXT rocket program, have been written and published this year:

1. "The Solar X-ray Corona," by L. Golub, *Astrophysics and Space Science,* **237**, 33 (1996).

This is an invited contribution to a Festschrift in honor of Sir Robert Wilson, representing an introduction to the physics of the solar corona. A major portion of the discussion is a summary of results from the series of NIXT sounding rocket flights.

A copy of this paper is appended to this report as Appendix 1.

2. "Difficulties in Observing Coronal Structure," Keynote Paper, Proceedings STEPWG1 Workshop on *Measurements and Analyses of the Solar 3D Magnetic Field, Solar Physics*, **174**, 99 (1997).

There has developed in recent years a substantial body of evidence to indicate that the temperature and density structure of the corona are far more complicated than had previously been thought. We review some of the evidence and discuss some specific examples: observations of a limb flare, showing that the cool H-alpha material is *cospatial* with the hot x-ray emitting material; simultaneous NIXT and Yohkoh SXT observations of an active region,

showing that loops seen in one instrument are not seen in the other, and that the effect works in *both* directions.

Comparisons of extrapolated magnetic field measurements to the observed coronal structure, indicating that neither potential nor constant-alpha force-free fits are adequate. We conclude with a description of two new instruments, the TRACE and the TXI, which will help to resolve some of these difficulties.

A copy of this paper is appended to this report as Appendix 2.

3. Both a PIC and a CDR were held at Wallops Island FLight Facility during the past year. The presentation packages for these meetings are appended to this report as Appendices.

II. Future plans: Preparation of the payload for launch continues.

THE SOLAR X-RAY CORONA

L. GOLUB
Smithsonian Astrophysical Observatory
60 Garden St., Cambridge MA.

Abstract. The solar corona, and the coronae of solar-type stars, consist of a low-density magnetized plasma at temperatures exceeding 10^6 K. The primary coronal emission is therefore in the UV and soft x-ray range. The observed close connection between solar magnetic fields and the physical parameters of the corona implies a fundamental role for the magnetic field in coronal structuring and dynamics. Variability of the corona occurs on all temporal and spatial scales – at one extreme, as the result of plasma instabilities, and at the other extreme driven by the global magnetic flux emergence patterns of the solar cycle.

1. Introduction

The corona is a portion of the Sun's outer atmosphere beginning slightly above the visible surface and extending many solar radii out. A precise definition of the term "corona" is to some extent dependent on one's theoretical bias, and one may choose to think in terms of a modified plane-parallel model, or in terms of a composite, multi-component model made up of relatively isolated individual structures.

In either case, the most important physical fact about the corona is that it reaches very high temperatures, more than 10^6 K. Moreover, this temperature increase is found to occur over very short distances, with the rise from $< 10^4$ K to $> 10^6$ K occurring within less than a thousandth of the solar radius. If we pick a temperature well above that of the photosphere, such as 10^5 K, then we may define any portion of the atmosphere above this temperature as *corona*. Because the rise in temperature is so dramatically steep, this choice is adequate for many purposes, since a large change in this cutoff value will correspond to only a very small change in actual physical location.

At visible wavelengths, the corona is extremely faint relative to the disk, having a maximum brightness ratio of $\approx 10^{-6}$, decreasing to $\approx 10^{-9}$ within a single solar diameter away from the visible limb. However, at UV and soft x-ray wavelengths, the situation is reversed. Because of the high temperature of the coronal gas, its primary emission is in the UV and soft x-ray portion of the spectrum. Therefore, an instrument in which the visible light is blocked while the short wavelengths are transmitted permits viewing of the coronal emission on the disk and out to several solar radii above the limb.

Figure 1 shows a superposition of both on-disk and limb observations. It was obtained during a total solar eclipse in 1991, using ground-based data from the CFH-T in Hawaii and x-ray data from the NIXT sounding

Astrophysics and Space Science **237**: 33–48, 1996.

rocket (Golub *et al.* 1990). The ground-based eclipse permitted the white-light photo of the outer corona to be obtained, while the *uneclipsed* sun was viewed at the same time from above White Sands, New Mexico, where the eclipse had not yet started. The combination of the two observations shows that the streamer structures originate at the solar surface, typically in the brighter places called "active regions." This type of comparison brings home clearly the point that the corona is three-dimensional, with its roots at or below the solar photosphere and outer extension far into interplanetary space.

Observations of the high-temperature solar emission were first carried out from sounding rockets (Baum *et al.* 1946) and techniques for high resolution x-ray imaging were developed under NASA's Suborbital program (Vaiana, Krieger & Timothy 1973) during the late 60's and early 70's. The high temperature corona emits predominantly in isolated spectral lines which fall in the XUV and soft x-ray spectral regions, and many of the important lines were observed and identified by Sir Robert and co-workers in the 60's (Wilson 1964; Jones, Freeman & Wilson 1968). These studies and technological development efforts led to the first series of high resolution studies with extended temporal coverage, carried out from *Skylab* (*viz.* Orrall 1981); these will be discussed in the next section. Most recently, the *Yohkoh* satellite has significantly advanced the study of coronal activity and variability, using a combination of soft x-ray and hard x-ray imaging to study coronal activity, and a major new solar observatory – the Solar and Heliospheric Observatory (SoHO) – carries a large complement of instruments which are expected to provide a comprehensive view of the sun from its interior out to the solar wind.

The solar-stellar connection

If our sun, which is a typical middle-aged low-mass star, has a corona and is a source of x-ray emission, then it is reasonable to ask whether other stars also have coronae and emit x-rays. Within the past two decades this question has been answered in the affirmative: not only do other stars emit x-rays, but the sun is rather below average in activity level. Stars of nearly all spectral types are found to emit UV and x-rays and to display tracers of activity which are detectable in ground-based observations.

Ground-based observations may be used to determine the level of activity on stars, using methods which range from detection of chromospheric lines (Wilson 1963) to direct detection of magnetic fields (Robinson, Worden & Harvey 1980). Surveys of all spectral types, but especially of solar-type stars, have been carried out, most notably at Mt. Wilson (Vaughan 1980).

The direct detection of material at transition region and coronal temperatures had to await observations from space: the International Ultraviolet

Fig. 1. Composite photo showing the white-light corona seen from the CFH-T in Hawaii at the 11 July 1991 eclipse and the on-disk x-ray corona observed from the NIXT sounding rocket at the same time.

Explorer (IUE) was launched into a quasi-geosynchronous * orbit on 26 January 1978. The satellite provided ultraviolet spectra of astronomical objects ranging from comets and planets to active galactic nuclei and quasars. For stellar studies, the spectra extended the ground-based observations to more highly ionized species, such as Si IV, C IV and N V, thus permitting the extension of ground-based chromospheric studies into what would appear to

* The satellite circulates over Central and South America in a pattern which allows access by ground stations feeding both Europe and North America.

be temperatures more characteristic of the chromosphere-corona transition region.

Early IUE surveys extended our knowledge of high-temperature atmospheres on solar-type stars, and also showed a cutoff in coronal emission for late-type giants and supergiants (Linsky & Haisch, 1979). Detailed analysis of emission from late-type stars shows that in general they are solar-like in their properties, as was shown by data from both the IUE (Linsky 1980) and the *Einstein* Observatory, launched on 13 November 1978.

The *Einstein* Observatory had higher sensitivity to x-rays than previous experiments and it also had the ability to produce high resolution images, which yields a high signal-to-noise ratio. As it turns out, flare stars and RS CVn stars are only a few orders of magnitude brighter than "normal" stars, so that the increase in sensitivity of the *Einstein* observations was more than enough to allow the less active solar-type stars to be seen. A survey published after the first year of observation (Vaiana *et al.*, 1981), showed an "x-ray H-R diagram" nearly indistinguishable from its optical counterpart.

2. Magnetic Fields and X-ray Emission

In seeking to explain the existence of a corona on the sun, the major questions to be answered concern:

- coronal heating: the high temperature seems to compel the need to invoke some non-thermal, i.e., mechanical, source of energy. What is that source and how does it transfer energy to the coronal plasma?
- coronal structure: in addition to the gross correlation between magnetic fields and coronal heating, there is fine structure in the corona. What determines the scale size of the "loops"?
- stability: the overall appearance of the corona is stable on several days' timescale, but instabilities and rapid energy release occur on timescales of minutes and seconds.
- currents: how is energy stored in the corona and what causes its sudden release?

The key to answering these questions seems to be in the close connection between the presence, at and above the photosphere, of strong magnetic fields and the locations of the brightest, hottest regions in the corona. Magnetic flux is seen to emerge from the solar interior, rising and breaking through the surface in the form of bipolar regions. Here 'bipolar' indicates that the magnetic field is re-entrant to the solar surface – field of one polarity emerges and field of the opposite polarity re-enters, usually at a nearby location. The overall appearance is roughly that of the field from a magnetic dipole lying horizontally just below the surface. Corresponding to this magnetic structure, the hot coronal plasma is seen to form loop-shaped structures which appear to trace the magnetic topology.

The life of such a region is divided into two main stages, the emergence of magnetic flux and then the subsequent diffusion of that flux across the solar surface. The x-ray loop structures are seen to emerge and grow in accordance with the evolution of the magnetic field.

These processes are directly observed in the corona by x-ray imaging techniques, and at the photospheric level by magnetic field maps, or magnetograms, which can measure the field strength* directly. The regions of emerged flux are seen in magnetograms as neighboring patches of opposite polarity fiel. The bottom panel of Fig. 2 shows such a magnetogram.

For large regions containing more than 10^{20} Mx [1 Mx $\equiv$ 1 gauss-cm^2] total flux, the field is seen to emerge, grow in size and then gradually spread out across the solar surface. The calculated timescale for ohmic diffusion of the magnetic field in the photosphere by classical collisional electric resistivity is too slow by many orders of magnitude. It appears necessary to invoke turbulent diffusion, in which the field is moved about by the convective motions at or below the photosphere, in order to account for the rapid spreading of emerged magnetic flux. This process is also, in some theories, closely connected with the heating of the corona, by one of any number of proposed mechanisms whereby the convective motions feed energy into the coronal plasma via the magnetic field (for a recent review, see Narain & Ulmschneider 1990).

Fig. 2 also shows a near-simultaneous coronal x-ray image, taken with the NIXT sounding rocket payload (Golub *et al.* 1990)**. The x-ray image covers temperatures from $1 - 3 \times 10^6$ K, and the hottest, brightest locations coincide with the strongest concentrations of emerged magnetic flux. This can be seen by locating the x-ray bright regions in the top photo and comparing to the black-and-white bipolar magnetic areas in the bottom photo.

Note also that there are extensive regions of weaker magnetic flux in the magnetogram. However, the measured values of magnetic field strength are now known to be deceptively low. The actual photospheric strength of the magnetic field is found to be well over 10^3 G, (Frazier & Stenflo 1972) so that the appearance of weaker average field means that the B is concentrated into small magnetic elements with a low filling factor: the photospheric field is intermittent. In the corona, the field cannot be measured directly, but appears to be space-filling, as expected from the low plasma β. Above the weak-field regions the loop structures are larger and weaker than in active regions; such locations have sometimes been called "quiet corona", but time resolved observations show that it is not at all quiet, as we describe in the next section.

* Either just the line of sight component, or more recently the full vector field.

** The data could not be taken exactly simultaneously because of a total eclipse; note the shadow of the moon entering the x-ray f.o.v. from the west.

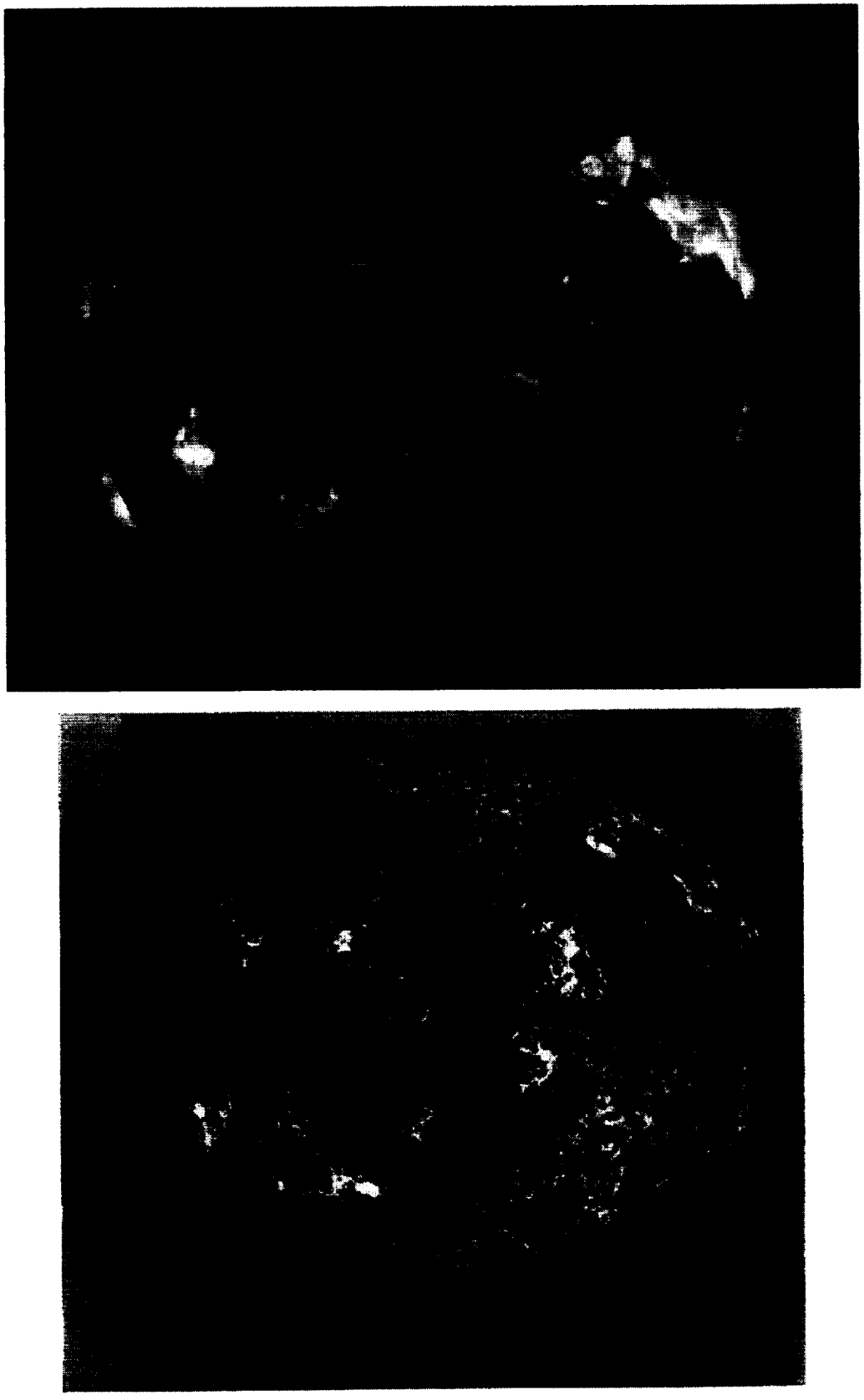

Fig. 2. Near-simultaneous longitudinal magnetic field map (bottom, from NSO/Kitt Peak), and x-ray images of the sun (top, from the NIXT rocket), 11 July 1991.

3. Short-term Variability

X-ray variability.

Prior to *Skylab* it was generally expected that the x-ray corona would show variations on time scales governed by the emergence and diffusion of magnetic flux. Although flares certainly were known, the general view concerning rapid events was that "Coronal events are rare." (Dunn, 1971). This view was completely reversed by the *Skylab* data, leading to the realization that all parts of the corona are varying on nearly every possible timescale (Vaiana & Rosner 1978) and that future instruments should be designed with the capability to obtain both high spatial and temporal resolution coronal imaging (Golub 1991).

An example of the dynamic changes seen in active regions is shown in Fig. 3. The four panels cover about 1-1/2 days and show the changes in the corona induced by the emergence of new magnetic flux near a pre-existing region. The older region is seen to consist of closed (re-entrant) loops and follows the magnetic field in being spread-out and fairly diffuse. To the west (right in this image) a newly emerging region is compact and very bright, with correspondingly strong emerging magnetic field. The dynamic and highly variable x-ray emission in the newly emerging region is evident, as is also the flare-like activity associated with the formation of interconnecting loops between the two regions. The complexity of the coronal structures, i.e. of the magnetized plasma loops, is also quite evident.

Transient loop brightenings.

A study carried out by Sheeley & Golub (1979) using *Skylab* data from the NRL S-082 and AS&E S-054 instruments provided one of the only studies of coronal variability at high spatial and temporal resolution. The study consisted of a set of nested exposures with time resolution down to two minutes at the center of the set, and focussed on two x-ray bright points (XBPs). These are defined as small, short-lived, magnetically bipolar regions of enhanced x-ray emission in the low corona (Golub *et al.* 1974). Active regions (ARs) were also seen in the data, but were excluded from the study because the large number of loops in the ARs made tracking of individual structures difficult.

The XBPs were seen to consist of a small number of loops, the number varying from two to six from one observation to another. Individual loops were seen to brighten and fade rapidly on timescales of about six minutes, which corresponds to the timescale for cooling by radiation and conduction in a plasma with the observed temperature and density. At any given moment, the "bright point" is seen to consist of several "independently-evolving miniature loops". This study concluded that the coronal structures

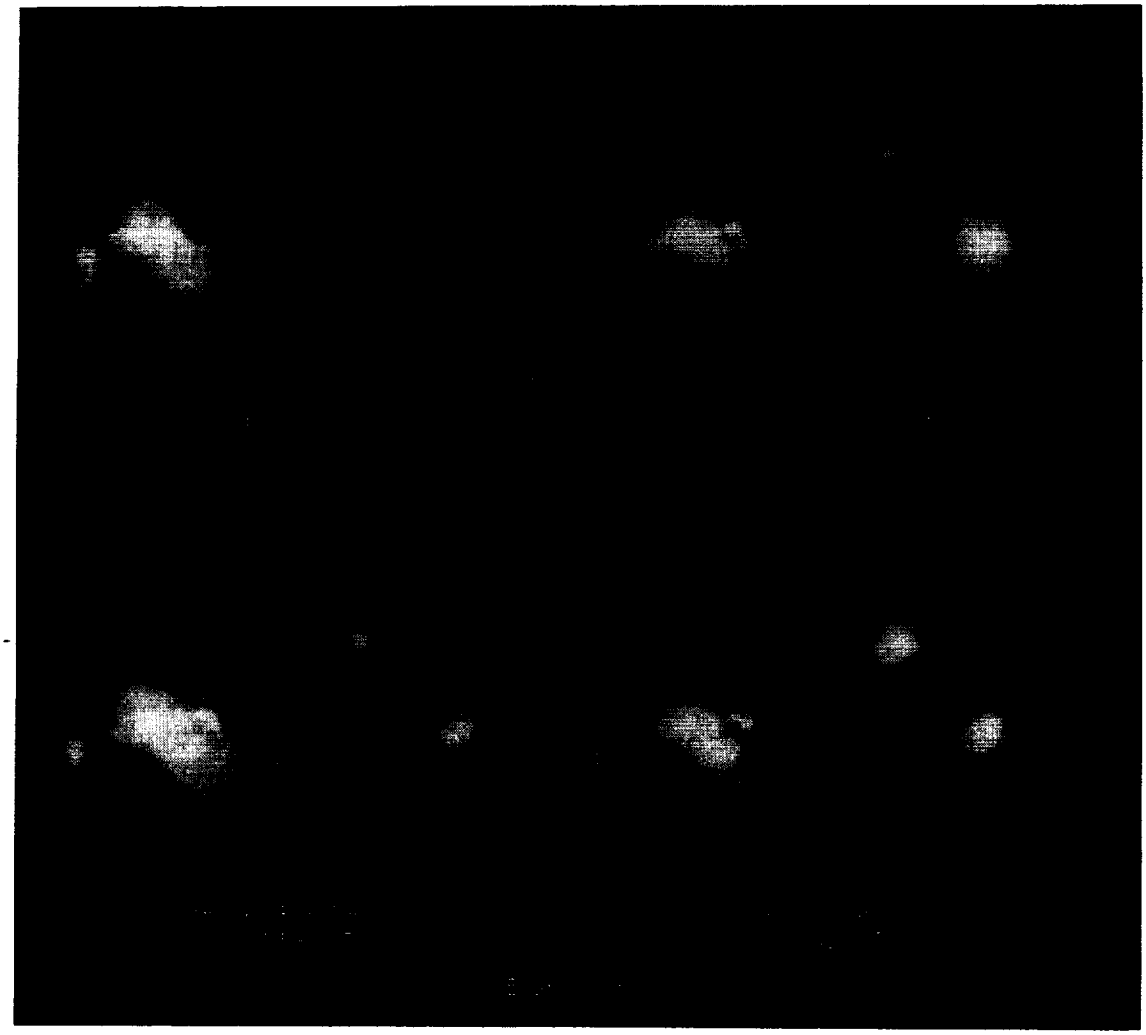

Fig. 3. The rapid reorganization of coronal loop structures in response to newly emerging magnetic flux.

are brightening and fading as fast as they can, and that the observed variability is consistent with an intermittent delta-function energy input, followed by energy redistribution by conduction and radiative losses without significant additional energy input.

The Yohkoh soft x-ray telescope (SXT) has provided the clearest images to date of the extremely dynamic and variable nature of the solar corona. While originally designed primarily as a flare mission, this satellite has proven to be extremely useful for studying the activity of the corona on spatial scales consistent with the resolution (2.5 arcsec pixels) and on temporal scales from seconds to months, and even years.

One of the finest examples of this variability are the so-called "transient brightenings" seen in active regions (Shimizu *et al.* 1992). Some (but not all) active regions are particularly dynamic in showing repeated, small flare-

like brightenings, which are clearly seen to take place in closed magnetic structures, i.e., in "loops". An example of this phenomenon is shown in Fig. 4, from Shimizu *et al.* (1992).

The brightenings have a power-law spectrum of energy, from 10^{29} erg down to the instrumental threshold at $\approx 10^{25}$ erg, with a slope $\alpha = 1.7$. Thus, the larger events blend into the distribution of events which one would normally call "flares", but the slope is not consistent with the suggestion that these brightenings make a significant contribution to the heating of active region coronae (Shimizu 1994).

Flares in x-rays.

Solar flares emit high levels of radiation at nearly all wavelengths, from the radio to x-rays and even gamma rays. Flares and the large-scale magnetic rearrangements in the corona associated with flares, eject relativistic electrons, protons, heavy ions and perhaps neutrinos. They produce microwave radio bursts with timescales of milliseconds and long wavelength radio noise storms lasting days. Coronal soft x-ray emission may increase temporarily by a factor of 1000 in a flare, and enhancements may last several minutes up to tens of hours. At the earth, upper atmospheric disturbances, auroral displays, ground-level particle events and a host of related phenomena are produced.

The definition of a flare is somewhat controvertial. An often-used classification defines a flare as 'a rapid temporary heating of a restricted part of the solar corona and chromosphere.' However, 'rapid' might mean a few seconds or it might mean several hours. 'Restricted' may mean a volume so small that it is below our ability to resolve, or it may mean a volume nearly as large as the sun itself. If we ask, how much heating must occur for an event to be called a flare, the possible answers cover a range of six to nine orders of magnitude.

Of course, some things are considered nearly certain. There is nearly universal agreement that magnetic fields play a crucial role in controlling solar activity in general, and flares in particular. We cannot do justice to the extensive range of ideas in the literature on this subject; for details of present flare theory the reader is referred to Tandberg-Hanssen & Emslie (1988) and to the article by Priest in this volume.

As an indication of the possible upper end of the flare size scale in the solar corona, Fig. 5 shows the coronal brightening associated with a large filament eruption. This event evolves to a size greater than a solar radius in extent, and such events often are responsible for major readjustments of the large-scale coronal structure. The timescale of this event is long, taking nearly an hour to brighten and several hours to fade away. The latter timescale typically does not agree with the somewhat shorter times calculated for radiative and conductive cooling, so that continued energy input

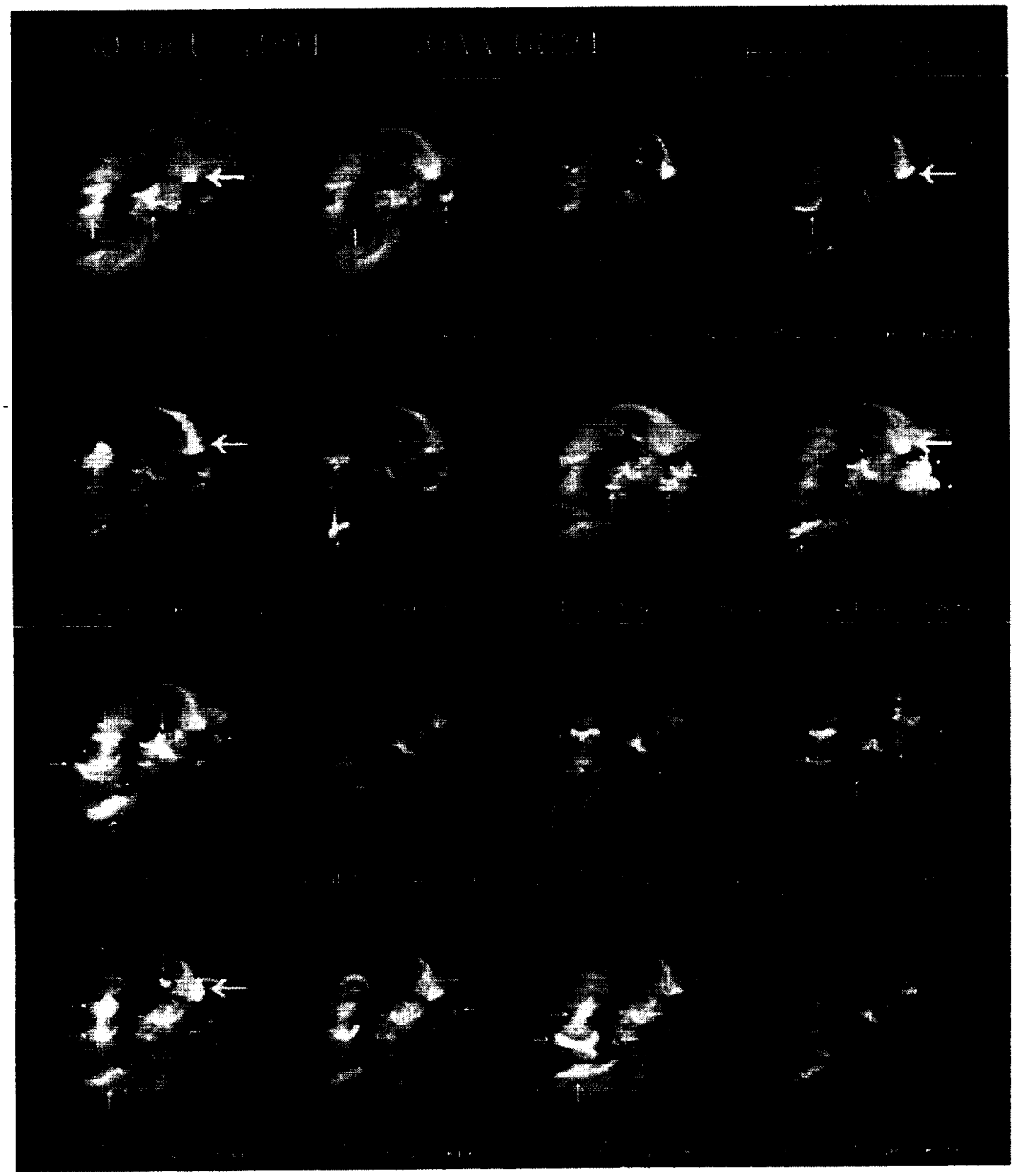

Fig. 4. A time sequence of x-ray images from *Yohkoh*, showing successive transient brightenings in active region loops.

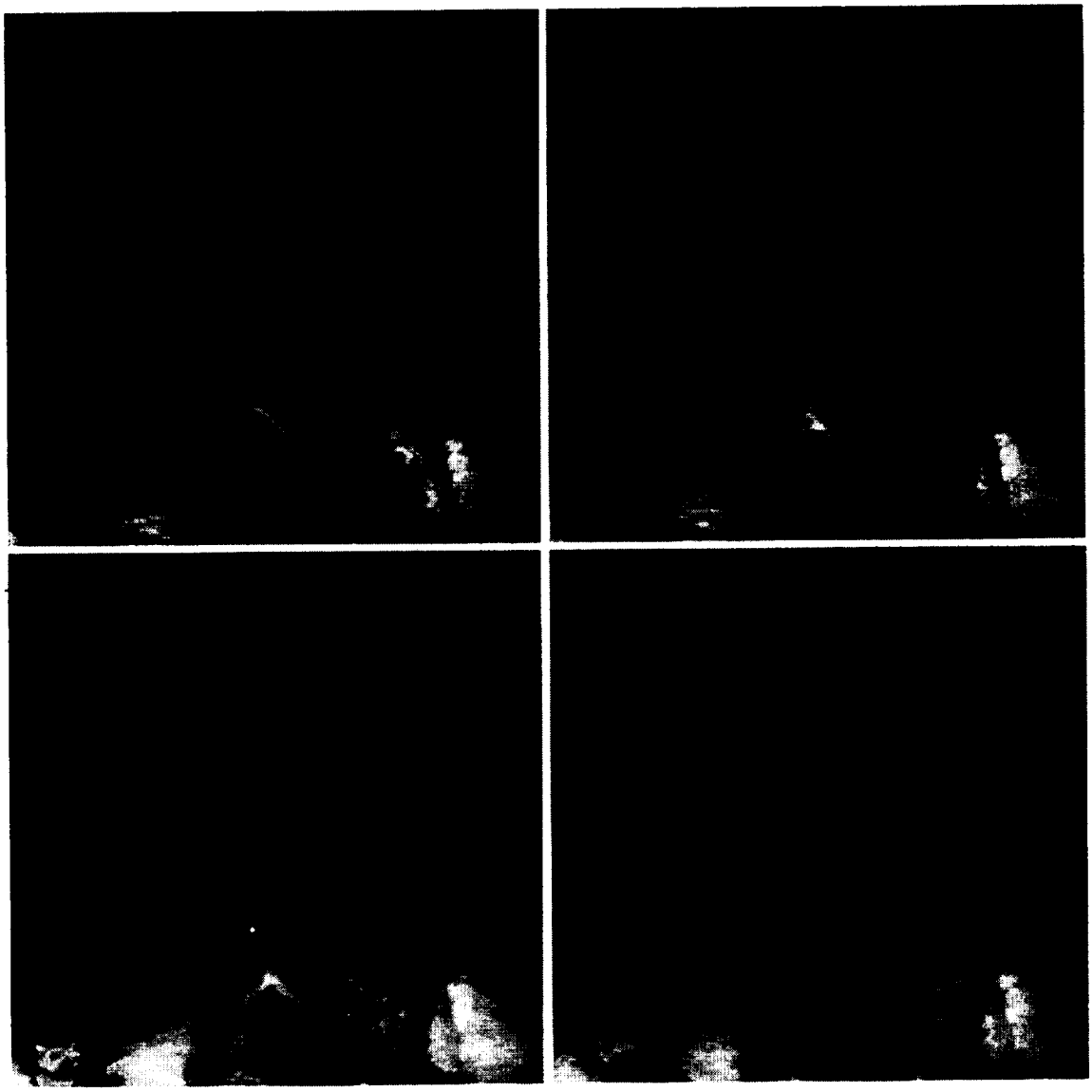

Fig. 5. The 'scorpion' flare, a large filament eruption event observed by the *Yohkoh* SXT on 26 Feb. 1992.

during the flare decay stage is often invoked.

4. Long-Term & Solar Cycle Variations

The most dramatic difference seen in coronal imaging data between solar minimum and other phases of the solar cycle is the vast increase in the number of x-ray bright points (XBP) seen at minimum (Golub 1980). There is considerable controversy concerning the nature of XBP, i.e. whether they represent new magnetic flux reaching the surface, or reprocessed magnetic

flux from previous active region emergence (see Harvey-Angle 1993 for a thorough review). However, the obervational fact is undeniable that at solar minimum the low corona is dominated by these small-scale features.

As an example, Fig. 6 shows a comparison between two x-ray images taken a few years apart. The top image was taken in 1973, during the declining phase of that cycle and the bottom image was taken in 1976, at solar minimum. The data were selected at times when the averaged sunspot numbers were nearly identical, so that the instantaneous level of flux emergence was not a factor. Nevertheless, there is a clear difference between the two observations in the number of small features seen: the solar minimum corona is seen to have triple the number of small-scale features. It even appears that there is very little structure in the corona other than that associated with the XBP.

Finally, the changes in x-ray luminosity and in structural composition of the corona as a function of phase in the magnetic cycle are again shown with dramatic clarity by the Yohkoh SXT. Figure 7 shows how the corona has evolved during four years of observations by the SXT. The overall soft x-ray luminosity has decreased by a factor of twenty in that time and the large-scale structure, representing the evolved magnetic field of large active regions, has been replaced by the weaker, less organized field structure of the numerous x-ray bright points.

5. Future Observations

With the launch of the Solar and Heliospheric Observatory (SoHO) by ESA and NASA at the end of 1995, a major new observational capability is added to the solar arsenal. Combined with the *Yohkoh* satellite and with the Transition Region and Coronal Explorer (TRACE) to be launched at the end of 1997, it would appear that solar physics is in a healthy state and that it can look forward to a decade of progress as this millenium closes.

While all of this is true, there are still many areas of solar and solar-terrestrial research which urgently require further attention, both on strictly scientific grounds and because of their direct importance to society. It is now becoming apparent that relatively small changes in the solar output can lead to major changes in the earth's climate, even if the direct cause is not yet clearly understood. Short-term variations, particularly mass ejections and high-speed solar wind streams, are now known to cause damaging effects at ground level, in the upper atmosphere, and in the near-earth space environment. Thus, the activity of the corona has direct consequences for power distribution networks, for the survival of satellites and astronauts in space, for long-range communications, and possibly even for long-term global climate changes.

A wide range of instrumentation will be used in attacking these prob-

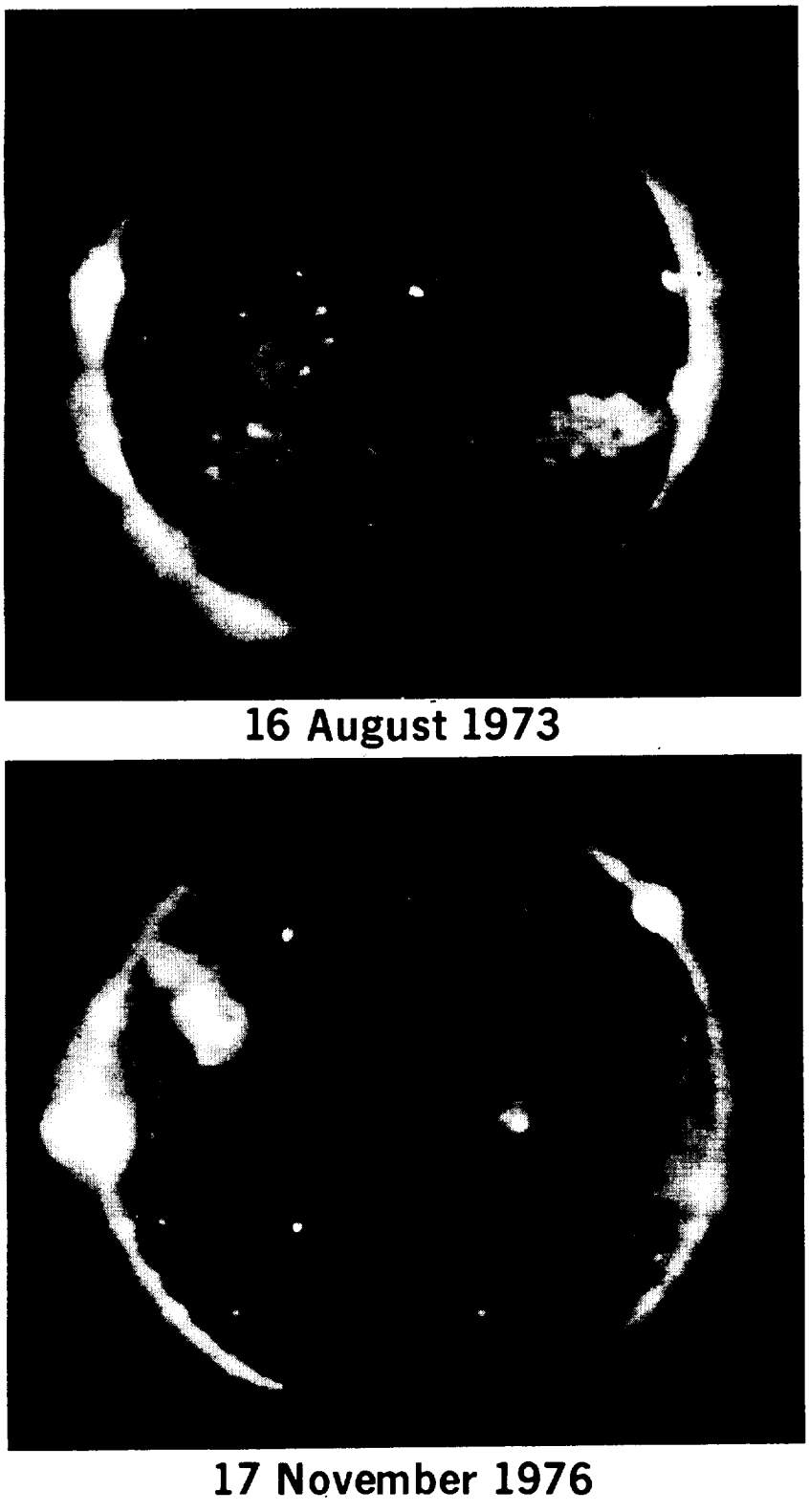

Fig. 6. Comparison of the XBP number density during the declining phase of the solar cycle (top) and solar minimum (bottom).

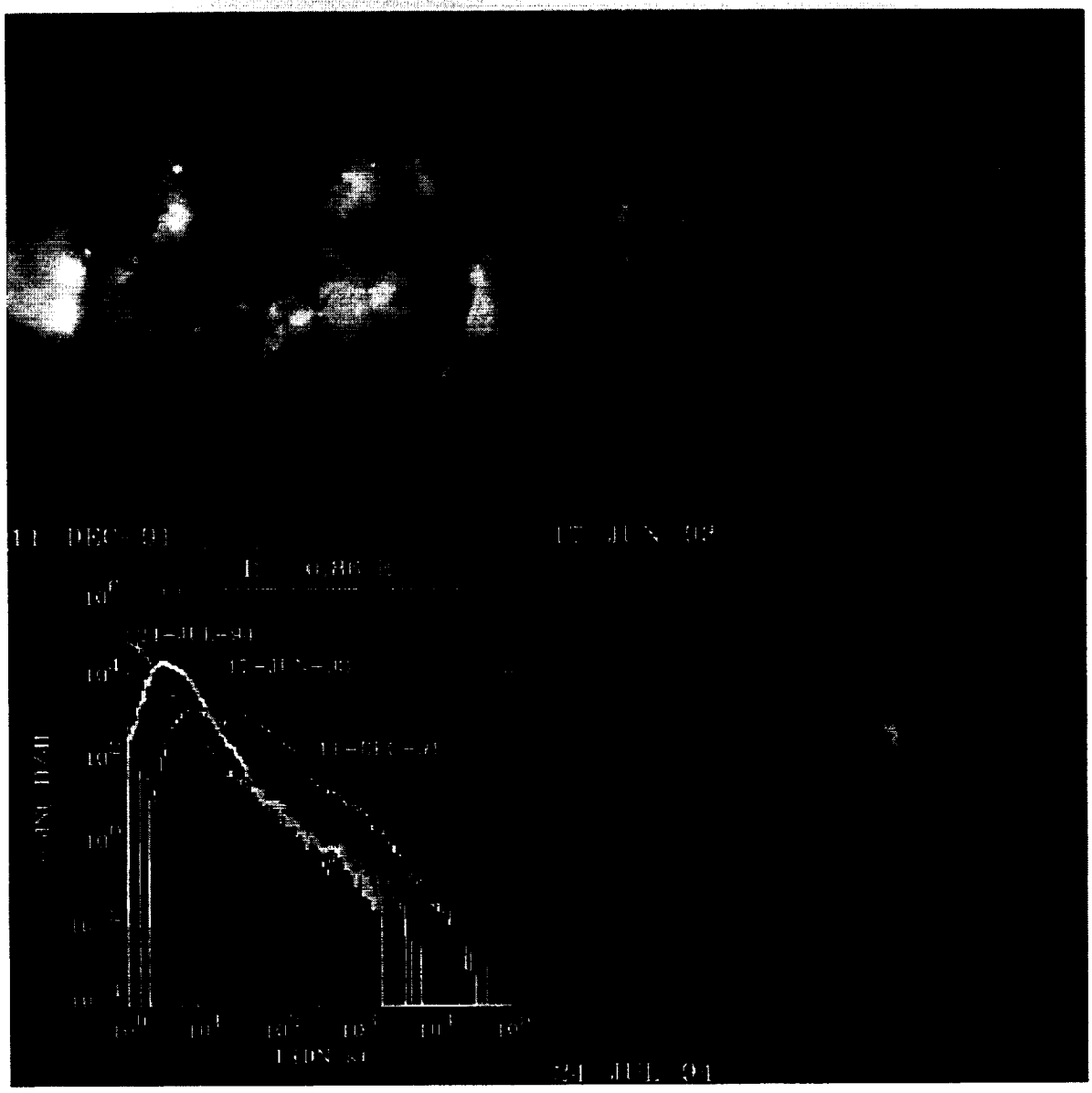

Fig. 7. Change in the coronal x-ray emission as a function of phase in the solar cycle, as seen by the Yohkoh SXT (photo courtesy H. Hara, NAOJ).

lems, including ground-based observing networks, NASA sounding rockets and other rapid, low-cost methods for putting instruments in space, and also larger missions such as the planned Solar-B observatory. A Solar Probe mission would allow direct *in situ* measurements relevant to coronal heating and solar wind acceleration, as well as offering the possibility of obtaining observations of the coronal structure with unprecedented effective spatial

resolution. It is, of course, impossible to predict how much of this will actually happen.

Acknowledgements

I would like to thank Dr. E. DeLuca for helpful discussions and Dr. T. Hartquist for a critical reading of the manuscript. I am also grateful to Drs. L. Acton, H. Hara and T. Shimizu for providing illustrations used in this chapter.

References

Baum, W.A., Johnson, F.S., Oberly, J.J., Rockwood, C.C., Strain, C.V. and Tousey, R.: 1946, 'Solar Ultraviolet Spectrum to 88 km', *Phys. Rev.* **70**, 781.

Dunn, R.B.: 1971, 'Coronal Events Observed in 5303Å; in *Physics of the Solar Corona*, ed. C.J. Macris, D. Reidel Publ. Co., Dordrecht-Holland.

Frazier, E.N. and Stenflo, J.O.: 1972, 'On the Small-Scale Structure of Solar Magnetic Fields', *Sol. Phys*, **27**, 330.

Golub, L.: 1991, 'X-ray Observations of Global Solar Activity', in *Flare Physics in Solar Activity Maximum 22*, ed. Y. Uchida, *et al.*, Springer-Verlag, Berlin.

Golub, L.: 1980, 'Solar X-ray Bright Points', *Phil. Trans. Royal Soc. London A* **297**, 595.

Golub, L., Herant, M., Kalata, K., Lovas, S., Nystrom, G., Pardo, F., Spiller, E. and Wilczynski, J.: 1990, 'Sub-arcsecond Observations of the Solar X-ray Corona', *Nature*, No. 6269, 842.

Golub, L., Krieger, A.S., Silk, J.K., Timothy, A.F. and Vaiana, G.S.: 1974, 'Solar X-ray Bright Points', *Astrophys. J. (Letters)* **189**, L93.

Harvey-Angle, K.L.: 1993, 'Magnetic Bipoles on the Sun', Ph.D. Thesis, U. of Utrecht.

Jones, B.B., Freeman, F.F. and Wilson, R.: 1968, 'XUV and Soft X-ray Spectra of the Sun', *Nature* **219**, 252.

Linsky, J.L.: 1980, 'Stellar Chromospheres', *Ann. Rev. Astron. & Astrophys.* **18**, 439.

Linsky, J.L. and Haisch, B.M.: 1979, 'Outer Atmospheres of Cool Stars, I"', *Astrophys. J. (Letters)* **229**, L27.

Narain, U. and Ulmschneider, P.: 1990, 'Chromospheric and Coronal Heating Mechanisms', *Space Sci. Rev.*, **54**, 377.

Orrall, F.Q. (ed.) 1981. *Solar Active Regions*, Colorado Assoc. Univ. Press, Boulder, Col.

Robinson, R.D., Worden, S.P. and Harvey, J.W.: 1980, 'Observations of Magnetic Fields on Two Late-Type Dwarf Stars', *Astrophys. J. Lett.* **23**, L155.

Sheeley, N.R., Jr. and Golub, L.: 1979, 'Rapid Changes in the Fine Structure of a Coronal Bright Point and a Small Coronal Active Region', *Sol. Phys.* **63**, 119.

Shimizu, T., Tsuneta, S., Acton, L.W., Lemen, J.R., and Uchida, Y.: 1992, 'Transient Brightenings in Soft X-rays Observed by the Soft X-ray Telescope on Yohkoh', *Publ. Astronom. Soc. Japan*, **44**, L147.

Shimizu, T.: 1994, 'Active Region Transient Brightenings', in *X-ray Solar Physics from Yohkoh*, eds. Y. Uchida, T. Watanabe, K. Shibata and H.S. Hudson, Universal Academy Press, Tokyo, Japan.

Tandberg-Hanssen, E. and Emslie, A.G. 1988. *The Physics of Solar FLares*, Cambridge University Press UK.

Vaiana, G.S., Krieger, A.S. and Timothy, A.F.: 1973, 'Identification and Analysis of Structures in the Corona', *Sol. Phys.* **32**, 81.

Vaiana, G.S., *et al.*: 1981, 'Results from an Extensive EINSTEIN Stellar Survey', *Astrophys. J.* **245**, 163.

Vaiana, G.S. and Rosner, R.: (1978), 'Recent Advances in Coronal Physics', *Ann. Rev. Astron. Astrophys.* **16**, 393.
Vaughan, A.H.: 1980, 'Comparison of Activity Cycles in Old and Young Main-Sequence Stars', *Publ. Astron. Soc. Pac.* **92**, 392.
Wilson, O.C.: 1963, 'A Probable Correlation Between Chromospheric Activity and Age in Main-Sequence Stars', *Astrophys. J.* **138**, 832.
Wilson, R.: 1964, 'The Zeta/Solar lines Between 170 Å and 220 Å; IAU Symp. No. 23, Liege, Belgium, ed. J-L Steinberg.

DIFFICULTIES IN OBSERVING CORONAL STRUCTURE

L. GOLUB
Smithsonian Astrophysical Observatory, Cambridge, MA 02128, U.S.A.

(Received 3 July 1966; accepted 29 October 1996)

Abstract. There has developed in recent years a substantial body of evidence to indicate that the temperature and density structure of the corona are far more complicated than had previously been thought. We review some of the evidence and discuss some specific examples: observations of a limb flare, showing that the cool Hα material is *cospatial* with the hot X-ray emitting material; simultaneous NIXT and *Yohkoh* SXT observations of an active region, showing that loops seen in one instrument are not seen in the other, and that the effect works in *both* directions; comparisons of extrapolated magnetic field measurements to the observed coronal structure, indicating that neither potential nor constant-α force-free fits are adequate. We conclude with a description of two new instruments, the TRACE and the TXI, which will help to resolve some of these difficulties.

1. Overview

The importance of magnetic fields in determining the structure of the solar outer atmosphere has long been recognized. Billings (1966) notes that magnetic fields 'are employed, as a matter of fact, to explain all departures from a nonspherical [sic] distribution of matter in the corona, including the loop structure of the corona over active regions...' Observations from sounding rockets in the late 1960s and early 1970s provided convincing evidence that loops structures, apparently outlining the magnetic field direction, are fundamental (Vaiana, Krieger, and Timothy, 1973) and the *Skylab* observations in 1973-1974 provided the impetus for constructing atmosphere models in which loop 'mini-atmospheres' are the fundamental constituent of the inner corona (Rosner, Tucker, and Vaiana, 1978; Craig, McClymont, and Underwood, 1978).

This atmosphere is dynamic and constantly varying. Low (1990) notes that the solar atmosphere is never truly quiescent or static, but adds that for the purpose of building models idealized static states may be used as an approximation to the physics underlying the apparent stability of long-lived structures. The extremely dynamic nature of the corona has been shown most effectively by the Soft X-ray Telescope (SXT) aboard the *Yohkoh* satellite: repeated transient loop brightenings in active regions (Shimizu *et al.* 1992), continual rapid expansion outward of structures at the tops of active regions (Uchida *et al.*, 1992), jets of X-ray emission, apparently associated with reconnection events (Shibata *et al.*, 1992), among others.

Thus, it is already clear that the simplest models of the corona – spherical or plane-parallel – are of limited applicability for interpreting the actual observations, and that the simplest loop atmosphere models – static loops – are also of limited usefulness. To these complications, we will add an additional set of worries, by

Solar Physics **174:** 99–114, 1997.

Table I
Observational questions about the solar corona

Q1.	Is the corona hot or cold at a given point in space?	A1.	Depends on the viewing method.
Q2.	Where is the 'base' of the corona?	A2.	Meaningful only for individual loops and probably unanswerable.
Q3.	What is the transverse scale size of coronal structures?	A3.	Our knowledge is limited by present instrumental resolutions.
Q4.	What is the relation between the coronal B and X-ray emission?	A4.	Data do not provide sufficient constraints.
Q5.	What does the hot corona look like?	A5.	Depends on the viewing method.

showing that it is not at all clear that we are even now in a position to say that we know what coronal loops look like, or to know how the real corona is constructed of such loops.

2. Case Studies

In order to illustrate the difficulties alluded to in the Overview, we will examine five specific 'case studies,' each involving a seemingly reasonable question about the corona. The questions addressed by these studies are listed in Table I, along with the answer to each question. The latter will be explained in the course of discussing each case. These examples are all taken from work related to flights of the Normal Incidence X-ray Telescope (NIXT) sounding rocket payload (Golub *et al.*, 1990) during the years 1989–1993.

2.1. A LIMB FLARE

On 11 Sept. 1989, the NIXT rocket was launched at the start of a small flare (GOES classification C5). However, during the five-minute flight, a second flare began in an active region at the limb (Herant *et al.*, 1991). Examination of the GOES X-ray light curves (Figure 1) indicates that the limb flare began at about 16:36 UT during the decay phase of the larger on-disk flare. The NIXT observations also began at 16:36 UT, with the last image taken at 16:41:35 UT; the peak of the limb flare in X-rays is at ~16:42 UT. Thus, the NIXT coverage could not have been better-timed.

Figure 2 shows simultaneous Hα and X-ray images of the flare at the time of the peak. The most striking aspect of this event seems to be the nearly identical size, shape and location of the flare in the two wavelength regimes. This similarity is confirmed by a cross-correlation between the two datasets, shown in Figure 3. The contour lines show the X-ray brightness and the shaded region shows the H brightness: the two overlap to within the accuracy of alignment. Thus it would

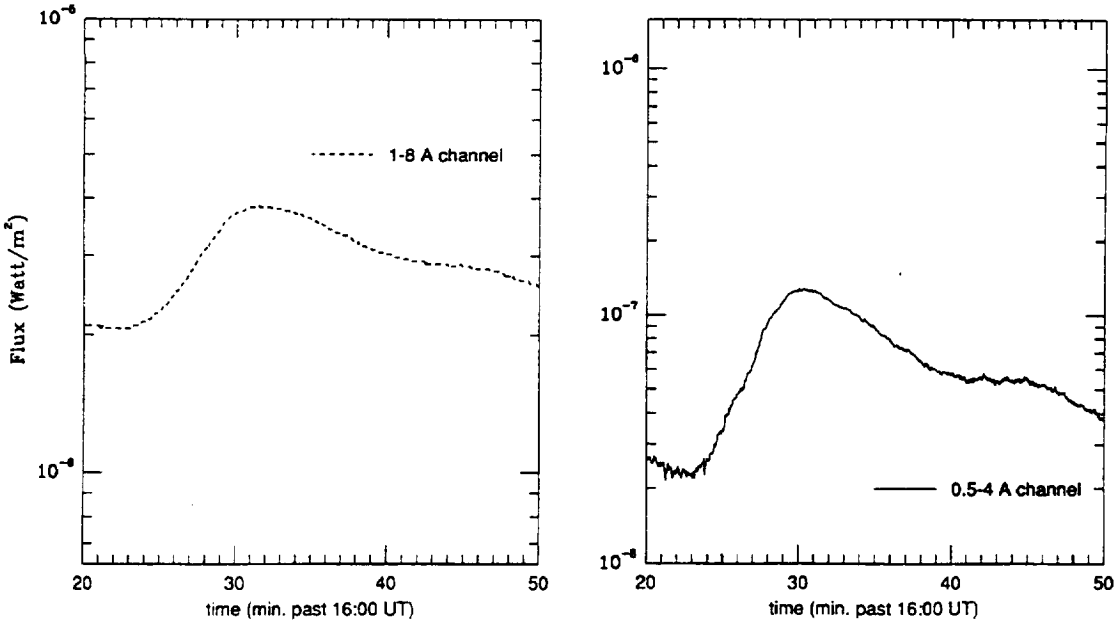

Figure 1. GOES 1–8 Å and 0.5–4 Å X-ray plots for 9 November, 1989.

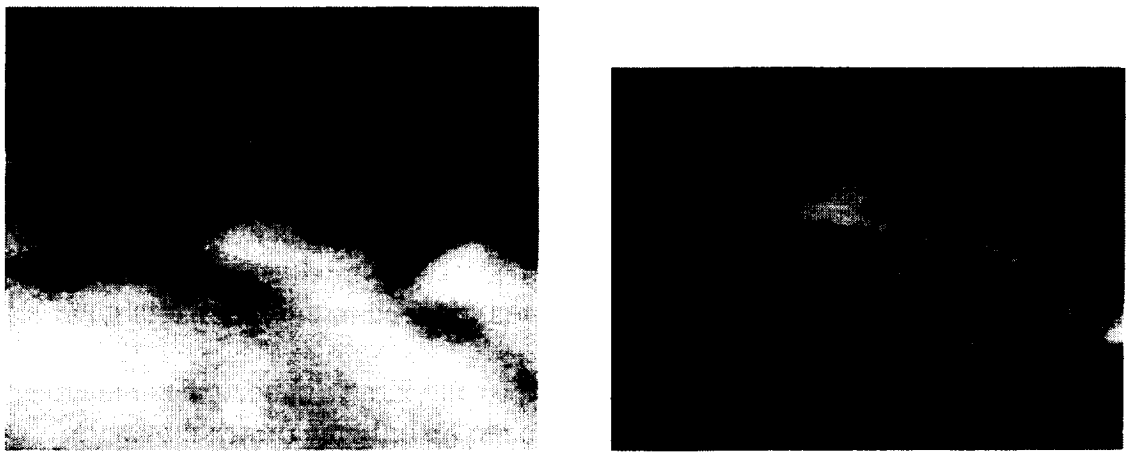

Figure 2. Simultaneous Hα and NIXT X-ray images of a limb flare.

appear that the corona is both hot (X-ray) and cool (Hα) at the same place at the same time.

Possible explanations exist, of course, for this apparent contradiciton. It is possible that the X-ray emission originates from a thin shell ahead of the advancing Hα region. Alternatively, hot and cool material may be intermingled on small spatial scales within the observed regions. The problem is not to come up with an answer, it is to come up with a correct answer.

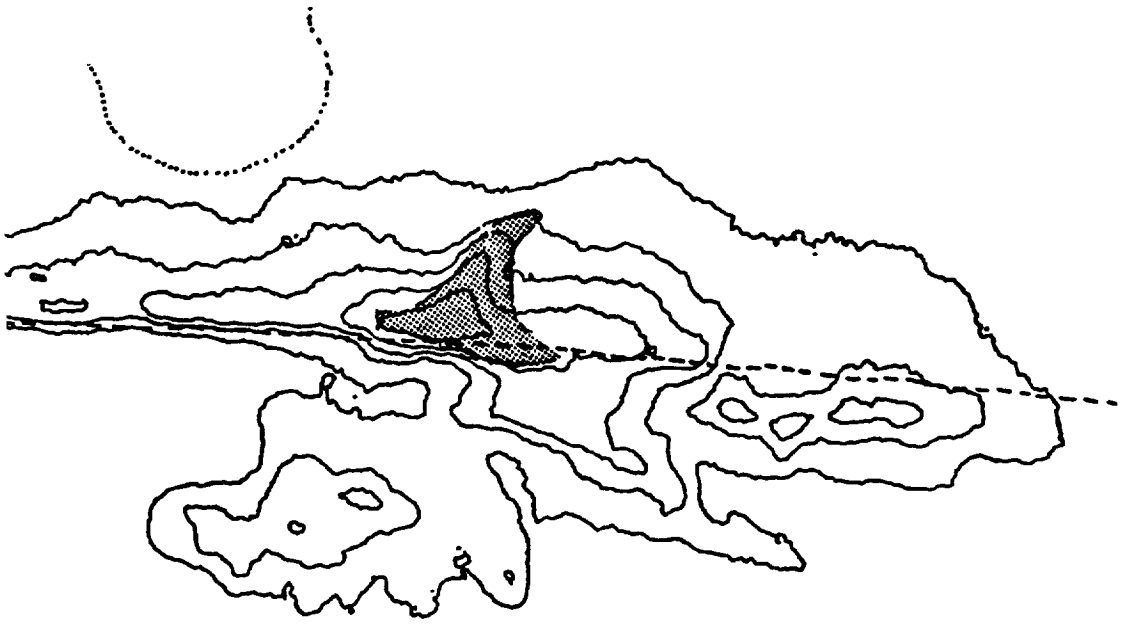

Figure 3. Relative positions of X-ray event and Hα material.

2.2. SIMULTANEOUS WHITE-LIGHT AND X-RAY IMAGING

Plane-parallel, or spherically symmetric models of the outer solar atmosphere treat the relation between temperature and height as one-dimensional, although not monotonic since the temperature at first increases with height but then decreases again. With the advent of loop model atmospheres, as described above, this fundamental view did not change in essence, but the temperature vs height relation is transplanted into each loop instead of into the atmosphere as a whole. However, a flight of the NIXT payload on 22 February 1991 provided a unique dataset which shows that a more complicated geometry is required in order to explain the observations.

The multilayer mirrors used in the NIXT to provide X-ray imaging also reflect visible light with $\approx$ 50% reflectivity. In order to record only the (much fainter) X-ray image, two stages of visible-light rejection are employed: an entrance aperture filter, which cuts the visible to $\approx$ 1% and a focal plane filter, which provides 10^9 reduction in the visible. During the launch phase of the February 1991 flight, a portion of the entrance aperture filter broke. The instrument, however, was designed so that the focal plane filter acts as back-up in the event of just such a failure. Thus, because the X-rays and the visible are reflected in the same way from the same mirror at the same time, we obtained simultaneous images of the visible disk and the corona. These are automatically coaligned and have the same plate scale, so that high precision (<1 arc sec) comparison between the two can be made.

Figure 4 shows a portion of the east limb from one of the exposures obtained on that flight. Note that there is a dark band at the limb, between the white-light solar limb and the bright coronal X-ray emission. We note several features of this

Figure 4. Portion of a combined NIXT/white-light image, showing a gap between the visible limb and the 'base' of the corona, 22 February, 1991.

gap: (1) it is most clearly evident when there is an X-ray emitting region behind the limb and no emitting region in front of the limb; (2) the thickness of the gap varies between equator and poles, or between active regions and large scale 'quiet' regions; (3) at both the inner (white light) and outer (X-ray) heights, the gap is quite sharp. The question we will address is, how is this gap to be interpreted?

The data from this flight have been analyzed by Daw, DeLuca, and Golub (1995), who find that a model in which the corona is viewed as consisting of a homogeneous set of loops, with temperature varying as a function of height in a uniform manner (Figure 5(a)) is not consistent with the data. In order to explain what is seen, it is necessary to use a model in which hot loops penetrate downward into an atmosphere having cool spicular material penetrating upward (Figure 5(b)). The two types of loops do not connect physically, but are interspersed along the line of sight. Thus, the gap is interpreted as the upward extent of spicular material, viewed along the line of sight at the limb and absorbing the X-rays emanating from loops behind the spicules.

We note that the soft X-rays in the NIXT data are strongly absorbed in spicular material, with about 10 arc sec path length required for e^{-1} absorption. The variation in thickness of the band indicates that spicules may extend farther in open field (e.g., coronal hole) regions than in higher temperature closed-loop regions, as reported by Huber *et al.* (1974). This interpretation of the NIXT data suggests that the footpoints of coronal loops cannot, in principle, be seen. When viewed at the limb,

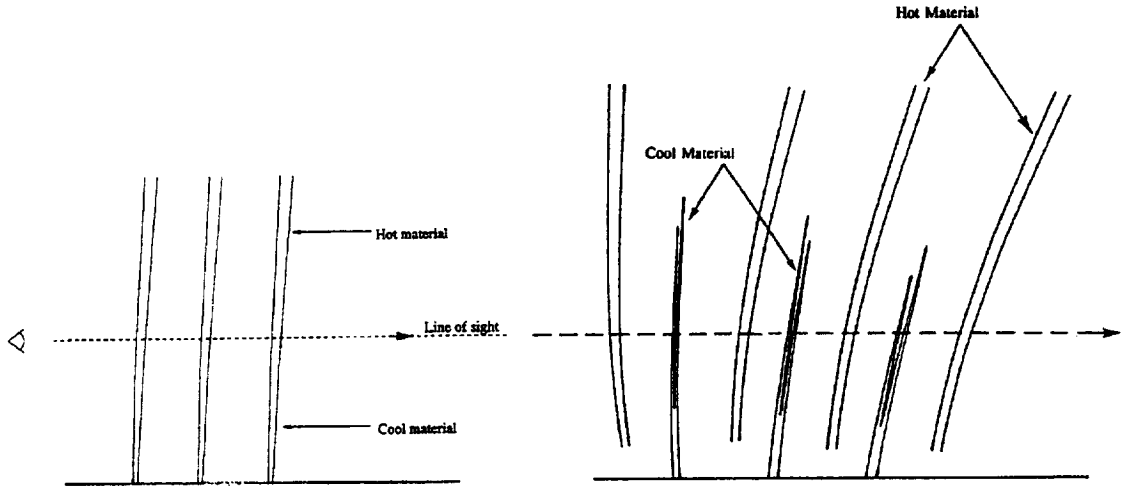

Figure 5. Two loop model atmospheres offering alternative explanations of the gap seen in Figure 4. Modified plane-parallel model on left does not fit the data.

they are obscured by the intervening spicule material; when viewed from above, the projection angle is such that the height of the coronal 'base' is very poorly determined. Depending upon the relative spatial density of hot vs cool structures, there may be a small range of locations near the center of the disk which allow for both viewing the loops at an angle and for viewing them unobstructed. However, this is not yet known.

2.3. ACTIVE REGION FINE STRUCTURE

The progress in X-ray optics, when applied to solar coronal imaging, has consistently revealed coronal fine structure down to the resolution limit of the observing instruments (see, e.g., articles by Giacconi, Golub, and Walker *et al.* in Linsky and Serio, 1993). An example is shown in Figure 6, a coronal X-ray image from the NIXT instrument, obtained on 11 July, 1991. There is clearly fine structure prevalent everywhere in the image and photographic analysis indicates that it reaches the combined limit set by the film and by the pointing stability of the rocket.

A quantitative analysis of the fine structure of several active regions observed by the NIXT was carried out by Gómez, Martens, and Golub (1993). By Fourier analyzing the images, they find a broad, isotropic power-law spectrum for the spatial distribution of soft X-ray intensities. The spectrum has a slope of $\alpha \approx -3$, which extends down to the resolution limit of the instrument at ≈ 0.75 arc sec.

A similar result has been obtained by Martens and Gómez (1992) from analysis of *Yohkoh* SXT data: the Fourier transform distribution is a power law (with somewhat smaller slope of ≈ -2.4) which extends down to the Nyquist frequency. Thus, for both cases in which the procedure has been carried out, the spatial structuring of the corona is seen to be limited by the resolution of the imaging instrument. The implication, since the Sun does not know what instrument we are

Figure 6. 11 July, 1991 NIXT image.

using to observe it, is that we have not yet fully resolved the coronal fine structure. Thus, the answer to Question 3, 'What is the transverse scale size of coronal structures?', is that we do not yet know.

2.4. MAGNETIC FIELD EXTRAPOLATION VS OBSERVED STRUCTURE

There have been only a limited number of attempts in recent years to carry out direct comparisons between high resolution coronal observations and magnetic field extrapolations, if we exclude attempts to explain the onset of flares by testing the non-potentiality of fields. For non-flaring regions, i.e., normal coronal structure, Poletto *et al.* (1975) and Sakurai and Uchida (1977) had reasonable success at the level of late 1960s and early 1970s resolution. More recently Sams, Golub, and Weiss (1993) found a general agreement between extrapolations and the structures seen in the NIXT, although close examination shows that the agreement is quite poor in detail. Metcalf *et al.* (1994) conclude, from comparison of vector magnetograph data (giving the locations of vertical currents) with *Yohkoh* SXT coronal data, that there is a very poor spatial and temporal correlation between the locations of the currents and the locations of bright coronal structures.

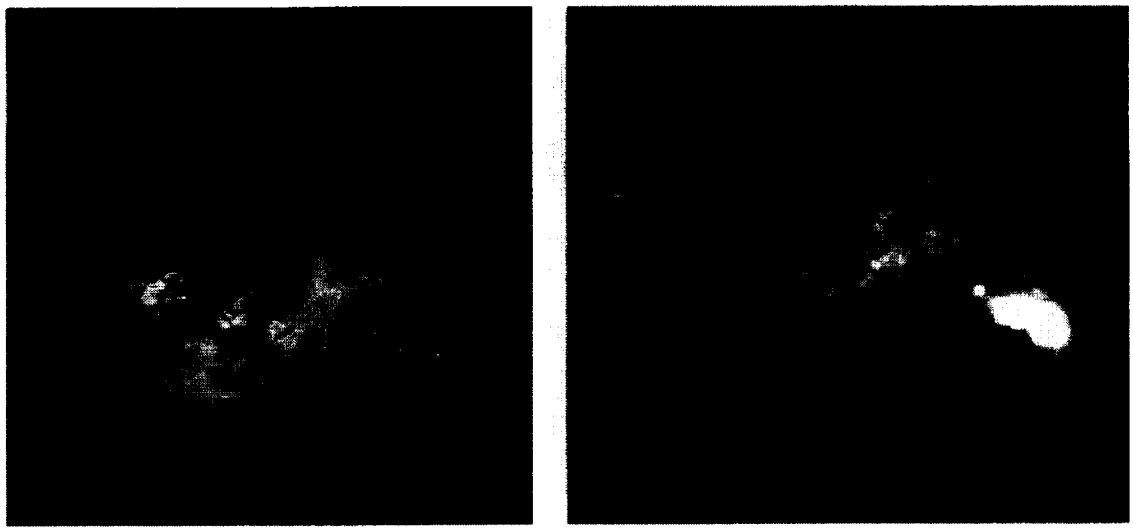

Figure 7. NIXT X-ray image of AR 6718 and KPNO magnetogram of the region.

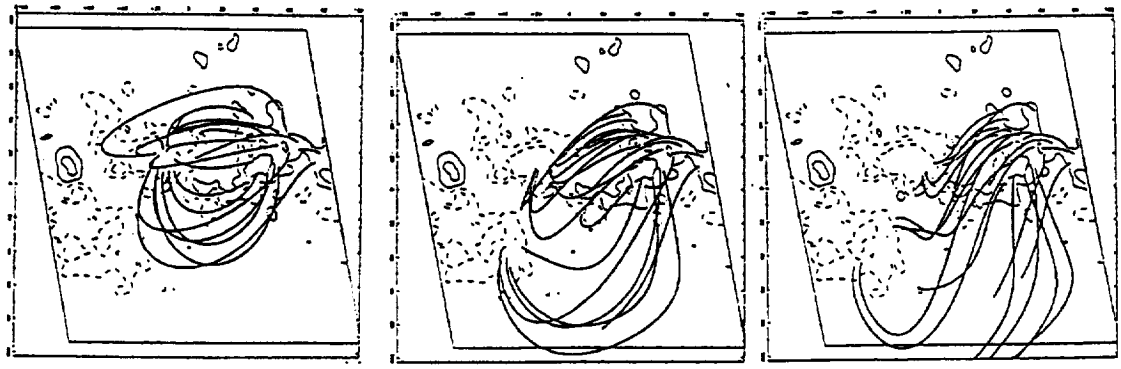

Figure 8. Magnetic field extrapolations of AR 6718, with three values of α.

In a recent study, Schmieder *et al.* (1996) have used high resolution NIXT data combined with Kitt Peak magnetogram and Multi-channel Double Pass (MSDP) spectrograph data, to study in more detail the relationship between the observed structure and the type of magnetic field extrapolation employed. The extrapolation code is based on the work of Alissandrakis (1981) as modified by Démoulin *et al.* (1996). A single active region, AR 6718 on 11 July, 1991, was chosen for study; an X-ray image of the region and the corresponding portion of the magnetogram are shown in Figure 7.

The first result is that a potential-field extrapolation does not represent the observed coronal structure at all, and that even a constant-α force-free field extrapolation is not adequate. Figure 8 shows extrapolations using three values of α. The left-most panel shows $\alpha = 0$, i.e., a potential field. Note that the connectivity of the field lines is entirely different from that of the observed structures. The two force-free fits in the middle and right-hand panels match portions of the region,

Figure 9. Comparison between *Yohkoh* (*top*) and NIXT (*bottom*) observations of an active region; arrows indicate structures seen in one of the instruments but *not* seen in the other.

but neither one in itself is a good fit. What we find is that the inner portion of the active region is well matched by the larger value of α while the outer portion of the region is matched by a lower α.

A possible interpretation of this result is that there is, with time, a relaxation of the magnetic field, as proposed by Heyvaerts and Priest (1984). In a highly-conducting plasma, small-scale processes dissipate magnetic energy much more rapidly than helicity $H \equiv \int \mathbf{A} \cdot \mathbf{B}\, dV$ (Taylor, 1974; Berger, 1985). With this constraint the magnetic field does not relax to a potential state, but to a linear force-free state. The gradient of α found in this region may be indicative of this ongoing relaxation process.

2.5. *Yohkoh* SXT vs NIXT comparison

In April 1993 the *Yohkoh* SXT carried out a special observing sequence simultaneous with a flight of the NIXT rocket. An inital comparison of the two datasets was carried out by Yoshida *et al.* (1995) for a quiet corona region. Because the SXT temperature response is somewhat harder than that of the NIXT (>2.5 MK for SXT vs 1–3 MK for NIXT) it was expected that the SXT would see the hotter top portions of coronal loops while the NIXT would see the lower portions or the footpoints. This was indeed generally seen to be the case in that study.

However, subsequent evaluation of the one active region on the disk on that day is showing a completely different and unexpected result. One expects that 'all X-ray images are alike,' so that the two should show roughly similar structures. Viewed from a distance, the two observations seem to be showing the same coronal features. However, detailed examination shows some remarkable discrepancies between the two.

Figure 9 shows the comparison of NIXT and *Yohkoh* SXT observations, with arrows pointing to three locations in the region. These are places where a structure or set of structures is visible in one of the images and *entirely invisible* in the other; the effect works both ways. Thus, if only one of these images were available, we would draw reonneous conclusions about the coronal structure, since there would be no indication at all that some structures are present.

The seriousness of this problem is obvious: if we intend to study the formation, stability and dynamics of coronal structures, one must first be able to see them. A partial solution to this problem is described in the next section.

3. Some Partial Solutions

The above discussion provides only a partial listing of some of the problems we are encountering in attempting to study the formation, heating, structuring and dynamics of the solar corona. In this section we describe two new instruments which will help to solve, or at least advance, some of these problem areas. The

TRACE instrument will have the highest spatial resolution ever used to observe the corona, as well as the ability to discriminate multiple temperature regimes and to view the atmosphere from the upper chromosphere up into the active region corona. The TXI is a rocket-borne payload which will have the capability of observing the entire sequence of successive ionization stages of a single element from $<10^6$ K to $>3 \times 10^6$ K, and will also determine flow velocities at these temperatures.

3.1. TRACE

The Transition Region And Coronal Explorer (TRACE) is designed to explore quantitatively the connections between fine-scale magnetic fields at the solar surface and the associated plasma structures in the solar outer atmosphere. The TRACE instrument uses multiple UV and normal-incidence XUV channels to collect images of atmospheric plasma from 10^4 K to 10^7 K. Many of the physical problems that arise in this portion of the atmosphere – plasma confinement, reconnection, wave propagation, plasma heating – arise throughout space physics and much of astrophysics as well. Although recent progress in, e.g., numerical MHD simulations has been substantial (viz., Low, 1990), use of these models requires close guidance by the observations, because the enormous range in parameter scale sizes cannot be realized in the computations.

The telescope provides true 1 arc sec resolution (1 pixel is 0.5 arc sec) and temporal resolution as short as a fraction of a second for bright sources. Table II lists the operating spectral bands, the associated temperatures and the portions of the atmosphere covered. The instrument uses four normal incidence coatings, one for broadband UV and three for narrow band XUV operation. The UV channel includes a set of narrow-band filters at the focal plane, thereby allowing sub-channels which detect portions of the atmosphere from the photosphere to the transition region. Selection of the XUV channels is based on a thorough analysis carried out by Golub, Hartquist, and Quillen (1989), who analyzed the spectral region accessible to normal incidence techniques and determined the best lines to use for particular atmospheric features of interest.

TRACE is launched on a Pegasus-XL into a polar, Sun-synchronous orbit, thereby providing continuous observation of the Sun. Continuous observing for about 8 months is planned over a 1-year baseline mission. TRACE produces data complementary with SOHO, and planning of the TRACE daily observations is being coordinated with those of SOHO.

The main components of the TRACE instrument are shown in Figure 10. The TRACE instrument consists of a 30-cm diameter Cassegrain telescope and a filter system feeding a CCD detector. Each quadrant of the telescope is coated for sensitivity to a different wavelength range. Light entering the instrument passes first through an entrance filter assembly which transmits only UV and soft X-ray radiation, thus blocking the solar heat from reaching the mirrors. A large rotating

Table II
TRACE spectral regions and observing parameters

Central wavelength (Å)	Width (Å)	Ion	Location
2500	Broad	Continuum	Photosphere
1700	Broad	T_{min}/Chrom.	
1570	30	C I, Fe II, Cont.	Photosphere
1550	30	C IV	Transition region
1216	84	H Lα	Chromosphere
284	14	Fe XV	Corona
195	10	Fe XII	Corona
		(+Fe XXIV)	Flares
171	9	Fe IX	Corona

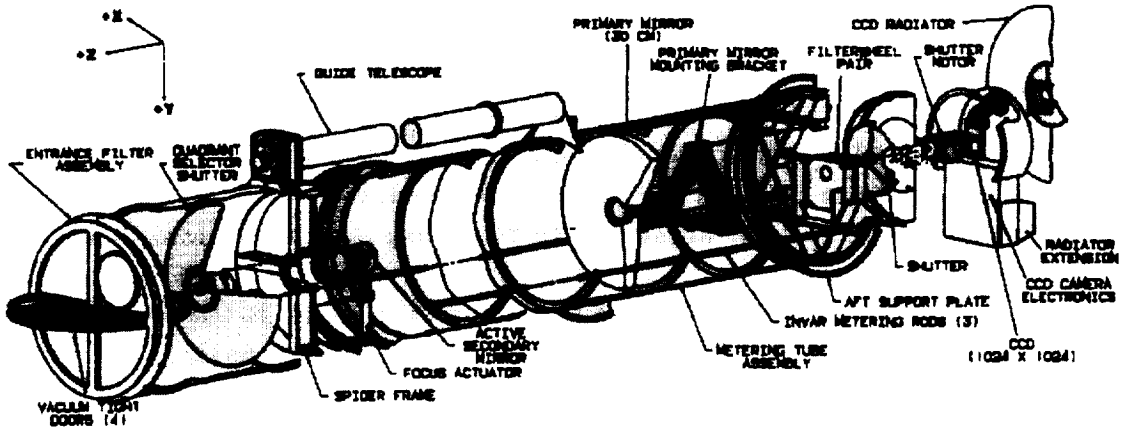

Figure 10. Major system components of the TRACE instrument.

quadrant shutter selects one quadrant at a time for viewing. The secondary mirror of the telescope is active, to correct for pointing jitter to better than 0.1 arc sec.

The converging beam from the secondary mirror passes through the central hole in the primary, where it encounters two filter wheels in series, each having three filters and one open position. These wheels contain both the XUV light-blocking and the UV passband filters. Finally, there is a focal plane shutter and a 1024×1024 CCD, for a field of view of 8.5×8.5 arc min. Mosaic observations are planned, for larger field and daily full disk data-taking. The TRACE launch is late in 1997, and mission lifetime is at least 8 months. Thus it will be observing during the rise phase of the new solar cycle.

Some of the scientific objectives of the mission are:

- Magnetic field structure and evolution.
- Coronal heating and magnetic fields.
- Onset of coronal mass ejections.
- Variability of X-ray bright points.

The mission and its objectives are described in more detail in Tarbell *et al.* (1994).

3.2. TXI

The Tuneable X-ray Imager (TXI) is a high-resolution coronal imaging instrument which has the ability to produce near-monochromatic images tuneable over a range of XUV wavelengths. The present design covers the wavelength range 170–220 Å, which includes the strong series of iron lines from Fe IX through Fe XIV, inclusive. Thus, the problem of 'missing' structures is solved, for the temperature range $\log T = 5.8$–6.4, because all of the successive ionization stages are isolated and recorded.

Figure 11 shows a schematic layout of the instrument. Spectral isolation is achieved by using a double-crystal monochromator, which feeds a broadband telescope, coated with an XUV multilayer having $\Delta\lambda \sim 30$ Å (FWHM). The monochromator is made as narrow-band as possible, which in this instance is ≈ 4 Å, and it is tuned by rotating the two plane mirrors in parallel. A Cowan–Golovehenko arrangement is used (Cowan, 1983), which has the highly desireable property that the entrance and exits beams stay fixed during tuning. Thus, there is no image motion in the focal plane as the wavelength is changed.

Table III shows the strongest lines in the TXI passband. Depending upon line strength and available exposure time, it appears possible to record data out to ≈ 220 Å; no data below 170 Å are recorded because aluminum light-blocking filters are used at the entrance aperture and at the focal plane. We note that line multiplets, such as Fe XII near 193 Å, do not smear the image, because this is a non-dispersive system.

The TXI sounding rocket program has just received approval from NASA to begin construction (May 1996). Present plans are to have the payload ready to fly by the summer of 1998. A summer launch is neccessary in order to reduce absorption by the residual atmosphere even at rocket altitudes. A minimum altitude of 100 miles is necessary for the wavelengths observed in this experiment, and a line of sight to the Sun as near normal to the plane of the atmosphere as possible is required. The launch therefore takes place around local noon in White Sands, NM.

3.3. THE SOLAR RADIO TELESCOPE

Of course, it is not only in the area of space-based instrumentation that solutions to the present set of problems in solar physics may be sought. In this section we describe a representative ground-based instrument, designed to map the magnetic field structure and topology in the corona.

A proposal for a dedicated Solar Radio Telescope which represents a major advance on current radio facilities is currently being explored (a report by D. Gary and T. Bastian will be available shortly). The ability to map solar magnetic fields

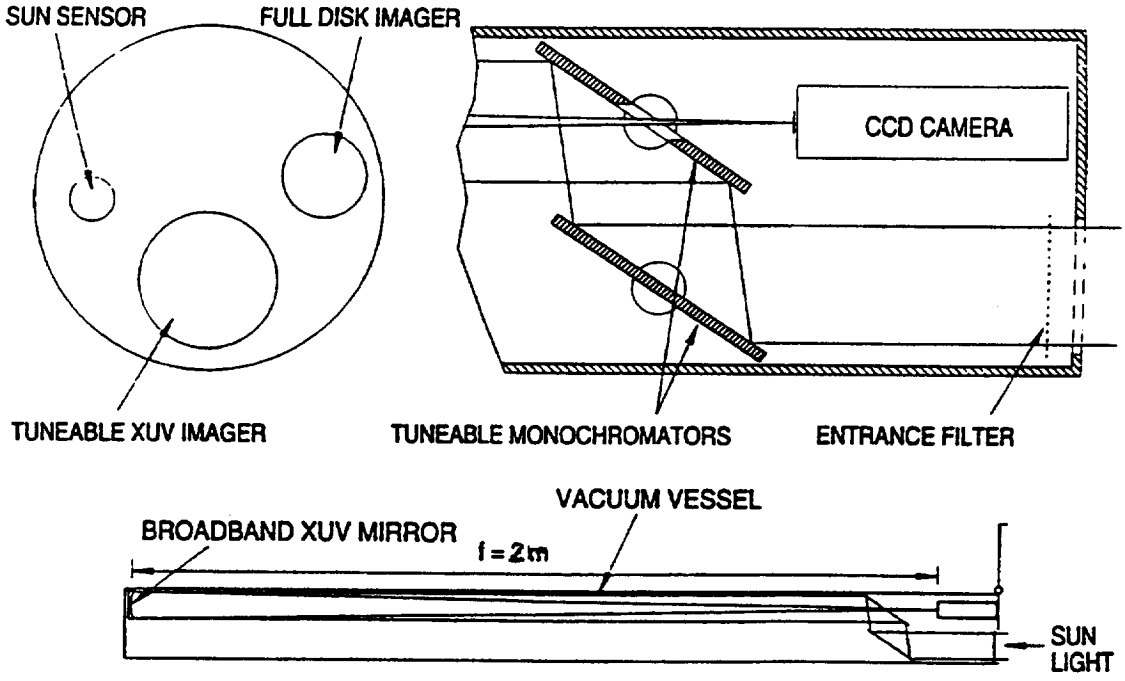

Figure 11. Schematic layout of the Tuneable XUV Imager.

Table III
Strongest lines in the TXI passband

Ion	Wavelength (Å)	log T
Fe IX	171.08	6.0
O V	172.17	5.4
O VI	172.94	5.5
	173.08	
Fe X	174.53	6.1
	177.24	
Fe XI	180.42	6.2
Si XI/Fe XII	186.88	6.2
Fe XI	188.22	6.2
Fe XXIV	192.03	7.3
Fe XII	192.40	6.2
	193.52	
	195.13	
Fe XIII	202.04	6.2
	203.82	
Fe XIV	211.32	6.3
He II	237.35	4.7

above coronal active regions is one of the major goals of this telescope. The features necessary to carry out such a goal are:

– the ability to make radio images of active regions on short time scales with high spatial resolution and high dynamic range;

– the ability to make images at many closely-spaced frequencies across a broad frequency range nearly simultaneously; and

– accurate polarimetry.

The proposed instrument which provides these features consists of an array which contains many small dishes (presently planned to be 40) with full-disk coverage, three large (~25 m) dishes to provide sensitivity and allow accurate calibration, and receivers which incorporate the frequency agile characteristics so successfully demonstrated by the OVRO array with a target range from 300 MHz to 30 GHz. This instrument would have 2.5 times as many baselines as the VLA, and requires a large correlator to handle them. Recent advances in broadband microwave components, large correlators and computers make such an instrument possible for a low cost. Considerable effort will also be expended on software for real-time processing of the data into a form (images and coronal field maps) suitable for immediate use by the broader solar community.

3.3.1. *Vector Magnetic Fields*

Finally, we mention the almost obvious point that vector magnetograms are crucially important in the comparison between surface fields and coronal structure/stability. Ground-based observations have progressed enormously, but there still remains the basic question: how much of the observed variability is due to atmospheric effects and how much is intrinsic to the source? This question has been answered in part by comparing observations taken simultaneously at widely-separated sites. However, the best way to answer the question and to obtain the highest quality observations, is to place a vector magnetograph in orbit.

Acknowledgements

Much of the work herein reported was supported by grants from NASA to the Smithsonian Astrophysical Observatory.

References

Alissandrakis, C. E.: 1981, *Astron. Astrophys.* **100**, 197.
Berger, M. A.: 1985, *Astrophys. J. Suppl.* **59**, 433.
Billings, D. E.: 1966, *A Guide to the Solar Corona*, Academic Press, New York.
Craig, I. J. D., McClymont, A. N., and Underwood, J. H.: 1978, *Astron. Astrophys.* **70**, 1.
Daw, A., DeLuca, E., and Golub, L.: 1995, *Astrophys. J.* **453**, 929.
Démoulin, P., Balala, L. G., Mandrini, C. H., Hénoux, J. C., and Rovira, M. G.: 1996, *Astron. Astrophys.*, in press.
Golub, L., Hartquist, T. W., and Quillen, A. C.: 1989, *Solar Phys.* **122**, 245.
Golub, L., Herant, M., Kalata, K., Lovas, S., Nystrom, G., Pardo, F., Spiller, E., and Wilczynski, J.: 1990, *Nature* **6269**, 842.

Gómez, D. O., Martens, P. C. H., and Golub, L.: 1993, *Astrophys. J.* **405**, 767.
Herant, M., Pardo, F., Spiller, E., and Golub, L.: 1991, *Astrophys. J.* **376**, 707.
Heyvaerts, J. and Priest, E. R.: 1984, *Astrophys. J.* **137**, 63.
Huber, M. C. E., Foukal, P. V., Noyes, R. W., Reeves, E. M., Schmahl, E. J., Timothy, J. G., Vernazza, J. E., and Withbroe, G. L.: 1974, *Astrophys. J.* **194**, L115.
Linsky, J. F. and Serio, S. (eds.): 1993, *Physics of Solar and Stellar Coronae*, Kluwer Academic Publishers, Dordrecht, Holland.
Low, B. C.: 1990, *Ann. Rev. Astron. Astrophys.* **28**, 491.
Martens, P. C. H. and Gómez, D. O.: 1992, *Publ. Astron. Soc. Japan* **44**, L187.
Metcalf, T. R., Canfield, R. C., Hudson, H. S., Mickey, D. L., Wülser, J. P., Martens, P. C., and Tsuneta, S.: 1994, *Astrophys. J.* **428**, 860.
Poletto, G., Vaiana, G. S., Zombeck, M. V., Krieger, A. S., and Timothy, A. F.: 1975, *Solar Phys.* **44**, 83.
Rosner, R., Tucker, W. H., and Vaiana, G. S.: 1978, *Astrophys. J.* **220**, 643.
Sakurai, T. and Uchida, Y.: 1977, *Solar Phys.* **52**, 397.
Sams, B. J., III, Golub, L., and Weiss, N. O.: 1993, *Astrophys. J.* **399**, 313.
Schmieder, B., Démoulin, P., Aulanier, G., and Golub, L.: 1996, *Astrophys. J.*, in press.
Shibata, K. *et al.*: 1992, *Publ. Astron. Soc. Japan* **44**, L173.
Shimizu, T., Tsuneta, S., Acton, L. W., Lemen, J. R., and Uchida, Y.: 1992, *Publ. Astron. Soc. Japan* **44**, L147.
Tarbell, T. D., Bruner, M., Jurcevich, B., Lemen, J., Strong, K., Title, A., Wolfson, J., Golub, L., and Fisher, R.: 1994, *Proc. of the 3rd SOHO Workshop*, ESA SP-373.
Taylor, J. B.: 1974, *Phys. Rev. Letters* **33**, 1139.
Uchida, Y., McAllister, A., Strong, K. T., Ogawara, Y., Shimizu, T., Matsumoto, R., and Hudson, H. S.: 1992, *Publ. Astron. Soc. Japan* **44**, L155.
Vaiana, G. S., Krieger, A. S., and Timothy, A. F.: 1973, *Solar Phys.* **32**, 81.
Yoshida, T., Tsuneta, S., Golub, L., Strong, K., and Ogawara, Y.: 1995, *Publ. Astron. Soc. Japan* **47**, L15.

TXI EXPERIMENT
PROJECT INITIATION CONFERENCE
23 MAY 1996

AGENDA

	TOPIC	PRESENTER
1.	SCIENCE	GOLUB
2.	EXPERIMENT DESIGN EXPERIMENT CONCEPT VEHICLE CONFIGURATION - EXPERIMENT SECTION PROPOSED VEHICLE EXPERIMENT WEIGHT	NYSTROM
3.	EXPERIMENT DESIGN - ELECTRONICS SYSTEM BLOCK DIAGRAM DATA REQUIREMENTS POWER REQUIREMENTS	VIOLA
4.	EXPERIMENT DESIGN - COMMAND AND TELEMETRY COMMAND REQUIREMENTS-UPLINK TELEMETRY REQUIREMENTS-DOWNLINK	LICATA
5.	EXPERIMENT REQUIREMENTS POINTING FLIGHT PROFILE LAUNCH WINDOW GROUND OPERATIONS	NYSTROM/ GOLUB
6.	PROGRAMMATIC TOPICS PROGRAM MILESTONES NASA FURNISHED EQUIPMENT TESTING	NYSTROM
7.	SUMMARY	ALL

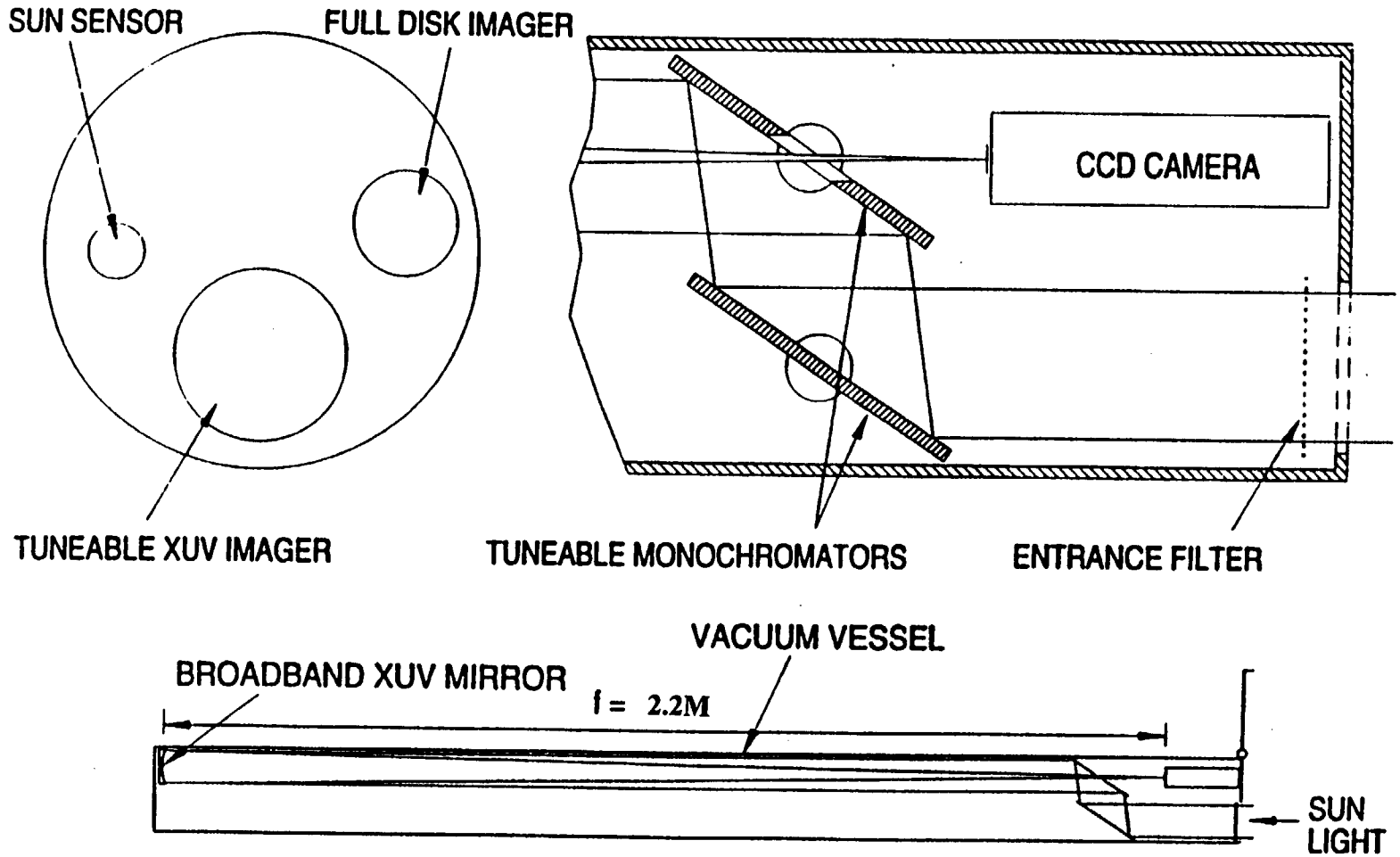

Figure 2.4 Schematic diagram of the TIXAS instrument package.

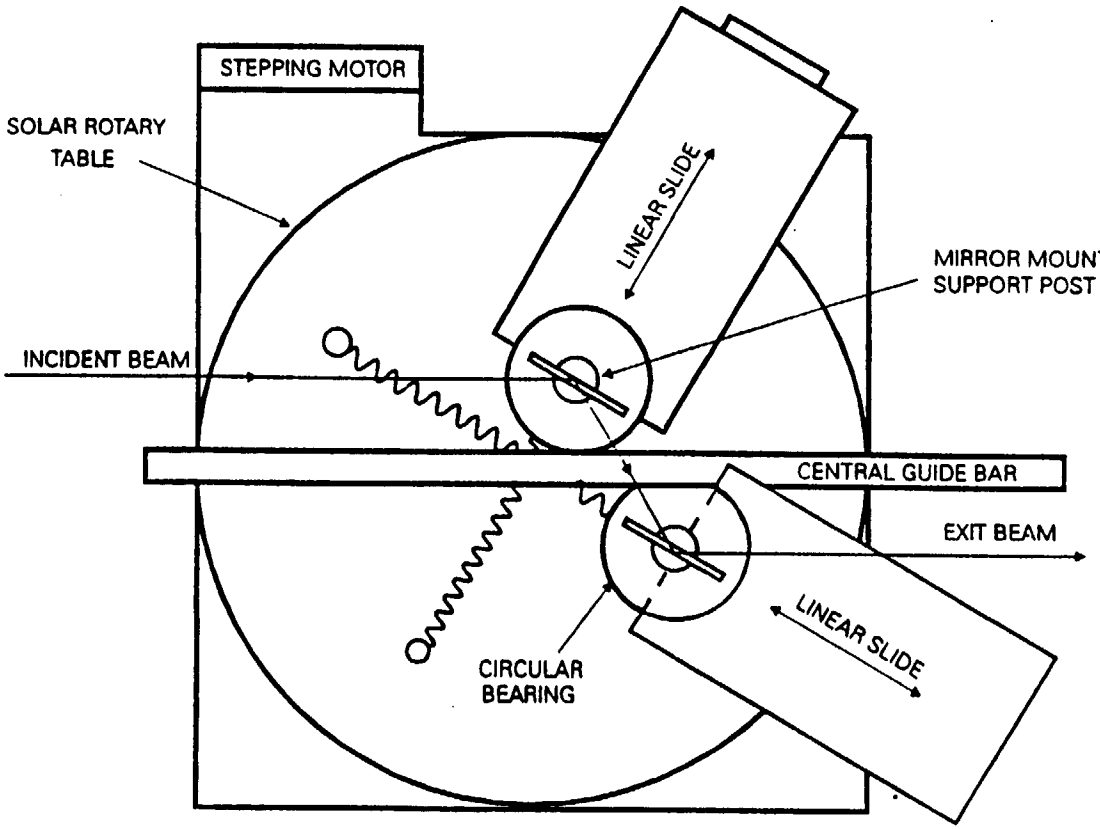
STEPPING MOTOR
SOLAR ROTARY TABLE
LINEAR SLIDE
MIRROR MOUNT SUPPORT POST
INCIDENT BEAM
CENTRAL GUIDE BAR
EXIT BEAM
LINEAR SLIDE
CIRCULAR BEARING

Table 2-1.

Physical and Optical Parameters of the TXI Instrument

Wavelength Range:	171 – 210 Å (at 10 % of peak) 171 – 230 Å 1 % of peak)
Analyzer Bandwidth:	4 A
Collecting Aera:	75 cm^2 geometric 2.5 cm^2 net @ peak
Focal Length:	3 meters
Resolution:	2 K x 2 K
Pixel Size:	0.35 arcsec

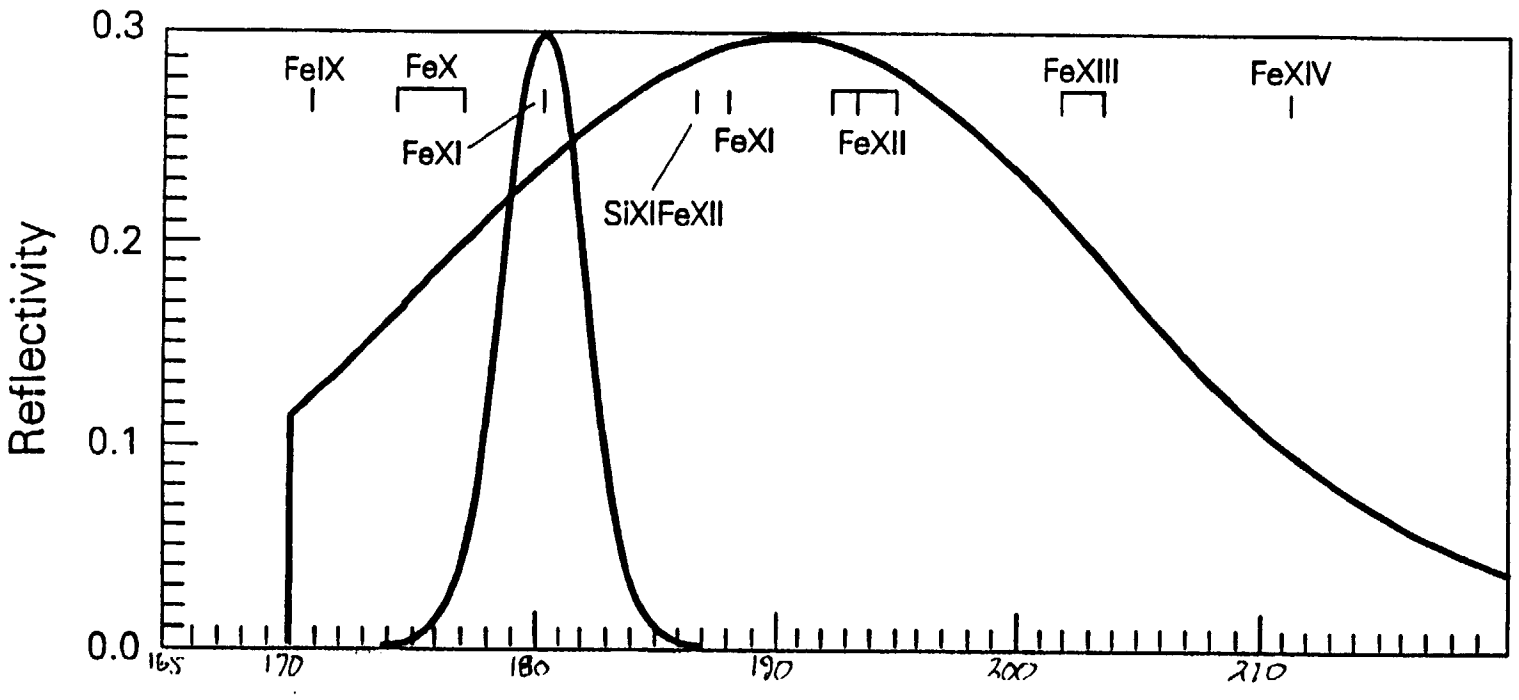

Table 2-2.

Strongest Emission Lines Within the TXI Passband.

Ion	λ(A)	log T_m	Countrate (cts/sq.arcsec/sec)
Fe IX	171.08	6.0	360
O V	172.17	5.4	44
O VI	172.94	5.5	30
	173.08		
Fe X	174,53	6.1	350
	177.24	6.1	210
Fe XI	180.42	6.2	890
Si XI/Fe XII	186.88	6.2	670
Fe XI	188.22	6.2	570
Fe XXIV*	192.03	7.3	–
Fe XII	192.40	6.2	1100
	193.52	6.2	580
	195.13	6.2	530
Fe XIII	202.04	6.2	160
	203.82	6.2	240
Fe XIV	211.32	6.3	160
He II	237.35	4.7	30

*weaker line, is strong in flares and possibly in transient loop events

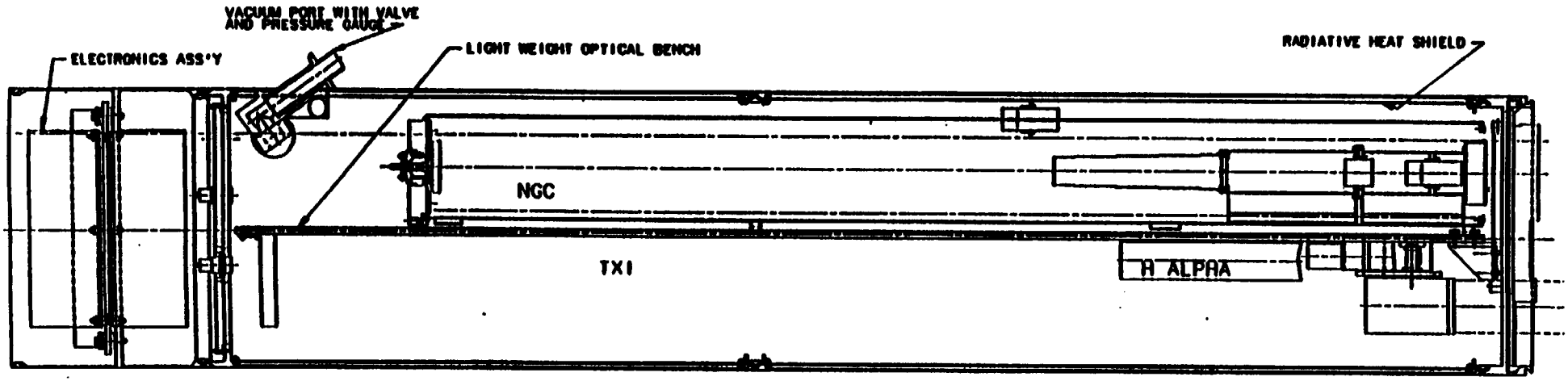

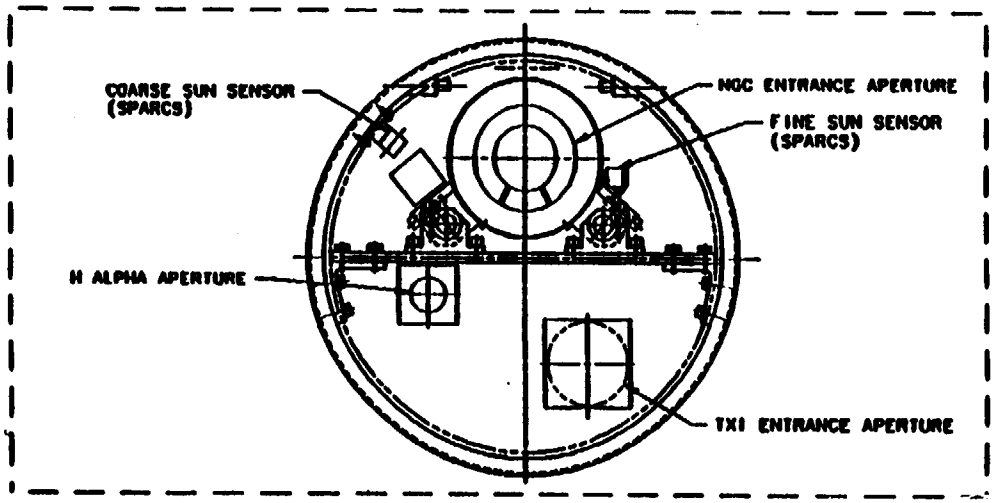

TXI ROCKET EXPERIMENT

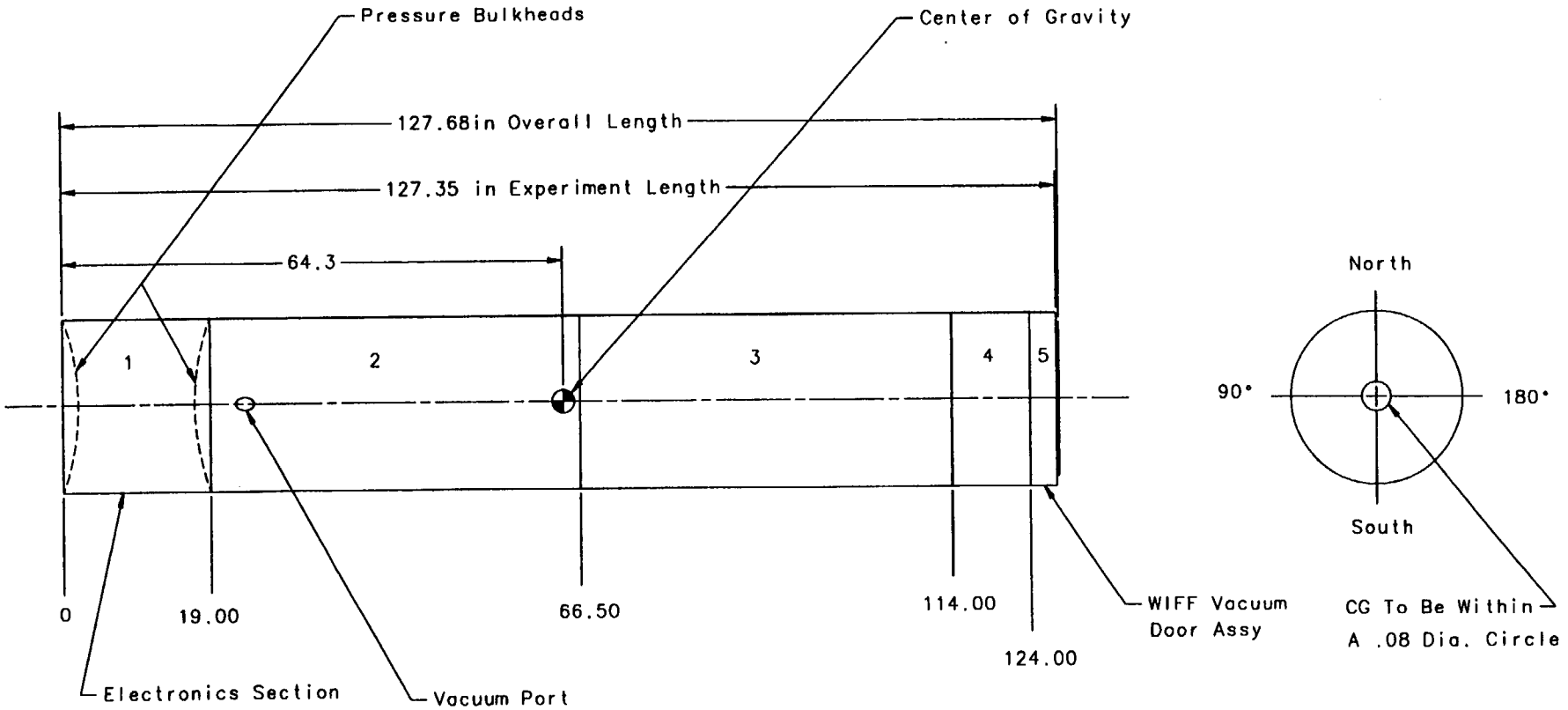

EXPERIMENT WEIGHTS:

VEHICLE	339.5
EXPERIMENT	151.8
TOTAL	491.3 LBS

TXI-VEHICLE
EXPERIMENT SECTION

DIFFERENCES FROM NIXT
1 LENGTH + 3.8 inches
2 REQUEST MARK TO Booster

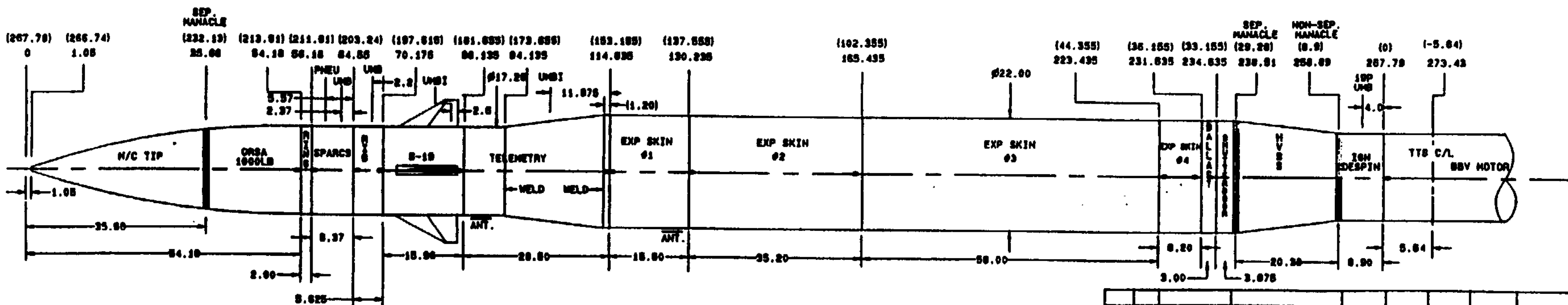

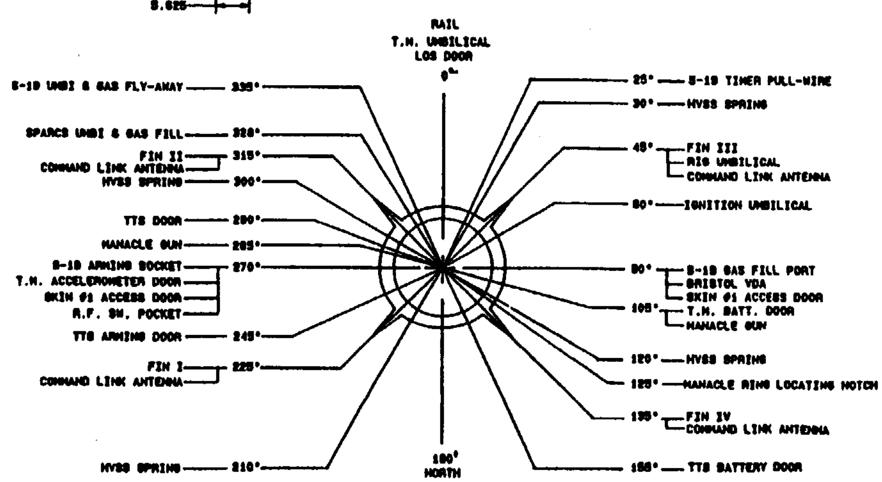

LOOKING FWD

4 FIN - 7.8 MRL LAUNCHER

ITEM	QTY.	DWG.NO.	DESCRIPTION	WT.	C.G.	I_x	I_y	MATERIAL
29	1		P/L REENTRY					W/BALLAST
28	1		P/L CONTR. W/GAS					W/BALLAST
27	1		P/L LAUNCH CONFIG					W/BALLAST
26								
25	1		BALLAST					
24								
23	1		P/L REENTRY	892.70	190.227	10.847	770.264	W/O BALLAST
22	1		P/L CONTR. W/GAS	910.70	194.804	10.619	699.823	W/O BALLAST
21	1		P/L LAUNCH CONFIG	1046.181	144.852	12.003	1170.062	W/O BALLAST
20								
19	1		SBV MOTOR CASING	546.0	378.65	12.66	565.53	
18								
17								
16								
15	1		TTS (IN MOTOR)	13.875	273.43	.182	.182	
14	1		IGN/DESPIN W/TTS	49.316	262.10	.382	.248	
13	1		HVSS	40.0	246.10	.780	.842	
12	1		SHUTTER DOOR	41.6	237.25	.562	.154	
11	1		BALLAST RING	10.5	233.135	.258	.130	
10	1		EXPERIMENT	453.0	178.08	5.927	118.565	
9	1		TELEMETRY W/GAS	135.0	102.08	1.457	2.701	
8	1		GAS IN T.M.	9.0	89.95	.048	.033	
7	1		S-19	72.6	77.01	.580	.654	
6	1		RIG	26.0	67.10	.226	.126	0.025" F/F SKIN
5	1		SPARCS GAS	14.0	59.10	.024	.032	
4	1		SPARCS W/GAS	65.0	59.10	.523	.343	
3	1		RING	10.5	55.10	.175	.091	
2	1		N.C. TIP	23.3	26.75	.05	.27	
1	1		1K ORSA N.C.	122.0	41.60	.65	2.40	

GOLUB

ESTIMATED DATA 3-12-90

UNIT OF PROJECT: 36.070	SCALE: 1/10	DR. A.J.GOBLE
NEXT ASSEMBLY		CHK. A.J.GOBLE
NATIONAL AERONAUTICS AND SPACE ADMINISTRATION		
PAYLOAD ASSEMBLY GOLUB1990		D-36-17554

D-36-17554

TXI EXPERIMENT WEIGHT SUMMARY	
COMPONENT DESCRIPTION	WEIGHT (Pounds)
EXPERIMENT	
Experiment Section	
Optical Bench	35
Turn Table	27.5
Mirror Assembly	11.5
Detector Assembly	10.0
Ancillary Equipment	
SPARC's Sensors	4.5
Hα Camera	7.0
Vacuum Gauges and Valve	8.3
TBD Camera Assembly	12.0
Electronics	
Electronics	24
Cables, Connectors, Misc.	12.0
TOTAL EXPERIMENT WEIGHT	151.8
VEHICLE	
Rocket Skin Sections	230
Thermal Shields	30
WIFF Vacuum Door	38.2
Balance Weights	10
Vacuum Pumping Port	3.3
Bulkheads	28
TOTAL VEHICLE WEIGHT	339.5
TOTAL EXPERIMENT AND VEHICLE	491.3

TXI INSTRUMENT

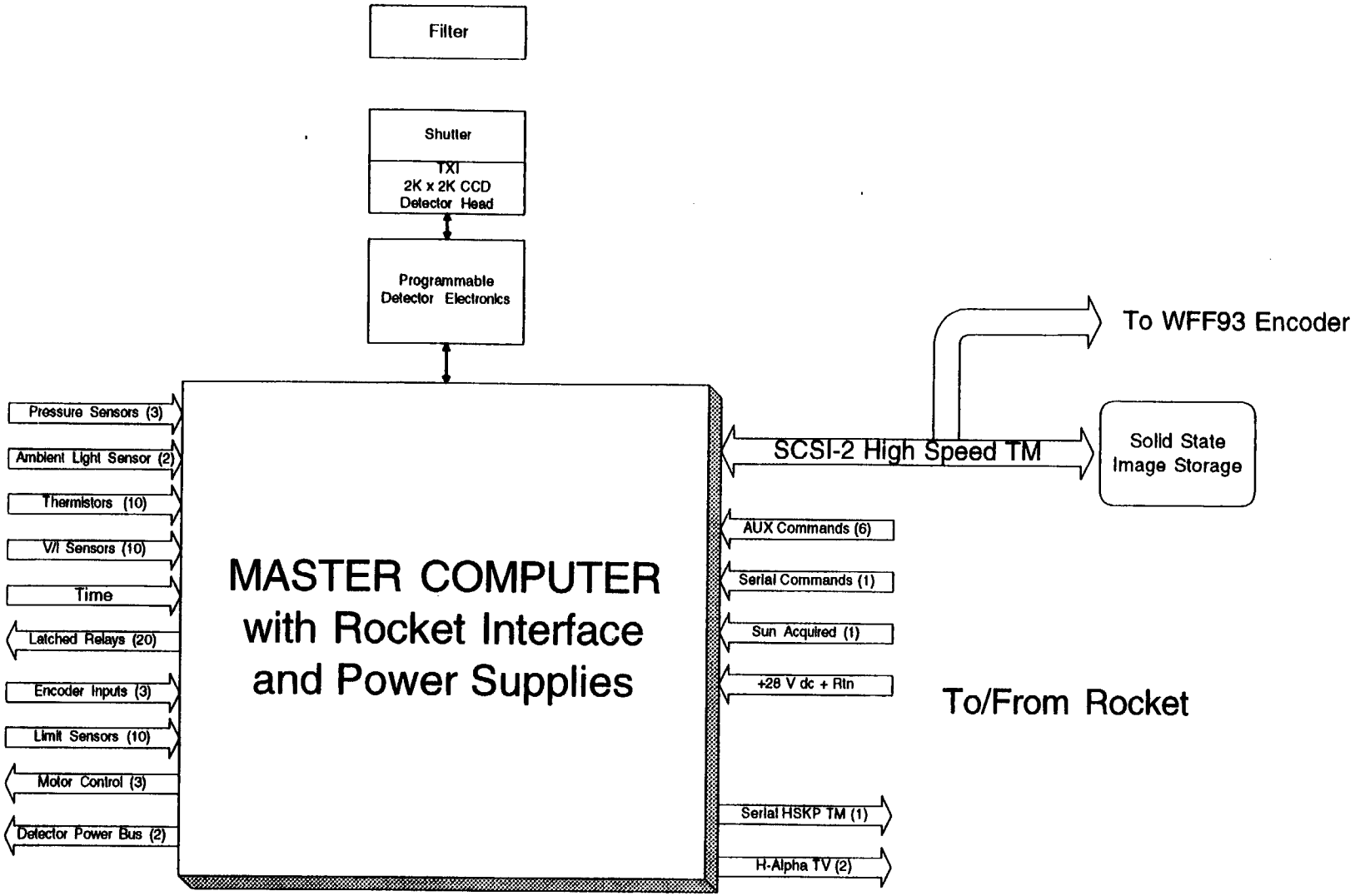

TXI MASTER COMPUTER

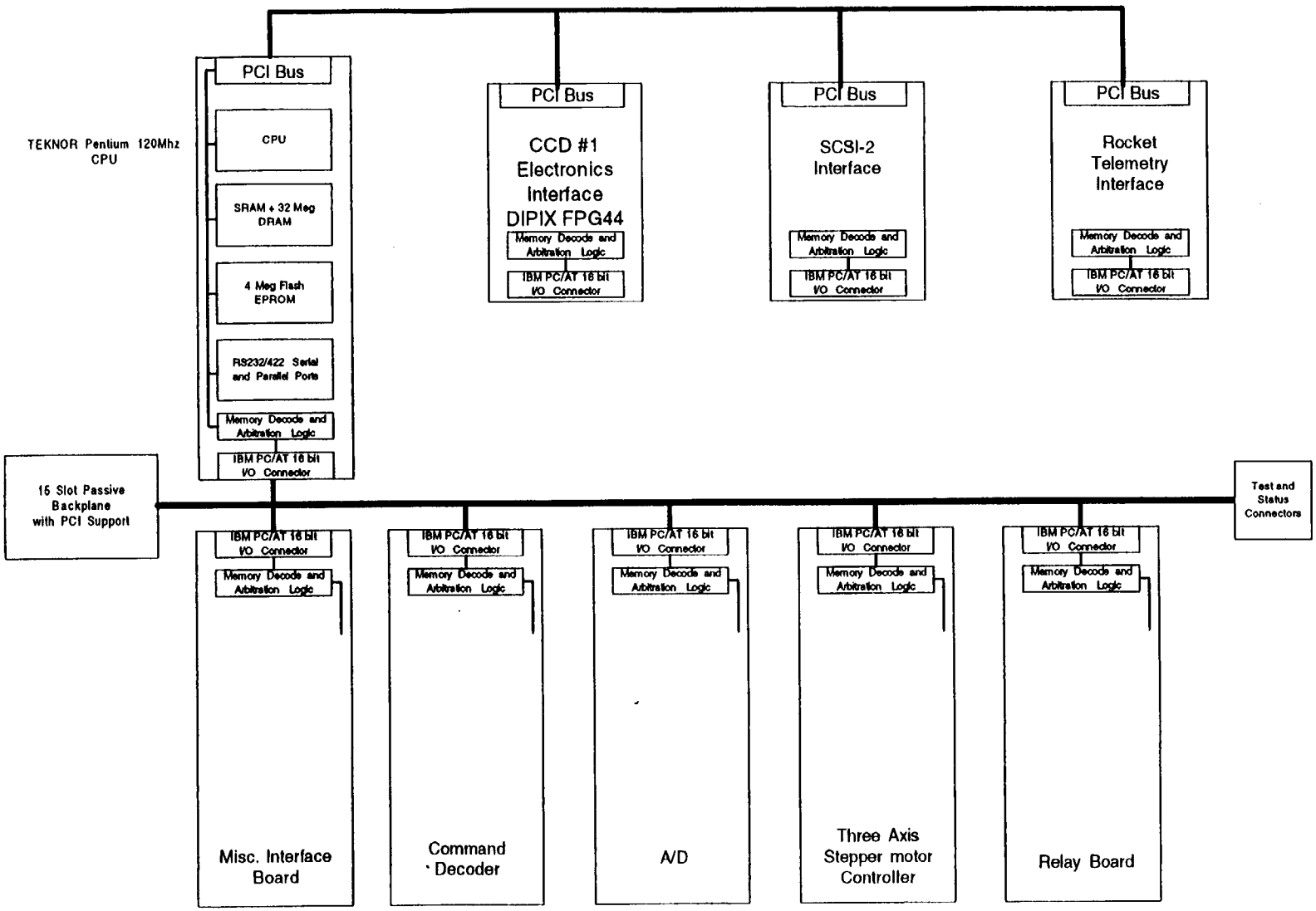

POWER

TXI Instrument Will Require:

1. +28 V dc +/- 4 V dc
2. 15 Amps at a nominal +28 V dc Peak Power
3. 20 Amps at a nominal +28 V dc Steady State Power

HIGH SPEED TM IMAGE DATA

SAO requires all High Speed TM data (ie 16 bit digital data words and a write strobe) available for our GSE in Real Time during the flight

SAO requires all High Speed TM data on D.A.T. tape in raw data form (ie 16 bit digital data words) for analysis Post Flight.

TXI TELEMETRY REQUIREMENTS

- Command Uplink

  1. Serial commands using the RS422 format.
  2. Six Set/Reset commands for manual operation.

- Downlink for Housekeeping
  1. Serial data using RS422 format.

- Downlink for Science Data
  1. 10Mb/sec WFF93 High Rate PCM Encoder

- Two TV Transmitters needed
  1. H_{α} Camera
  2. TBD Camera

- Blockhouse
  1. Use of 20 Umbical lines for External power, and TM checks

TXI GSE

Downlink for Science Data

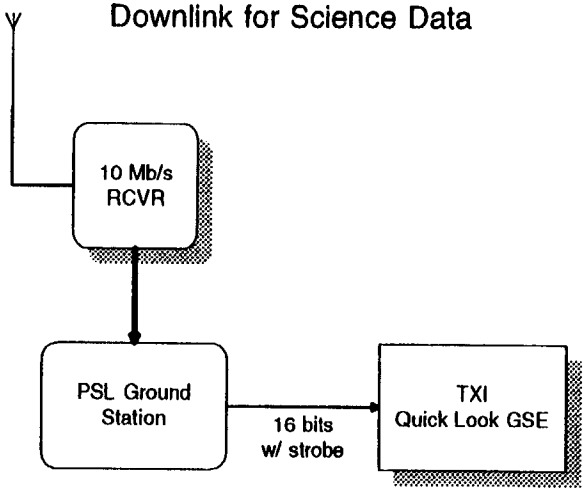

TXI Telemetry Requirements
CMD Uplink - HSKP Downlink

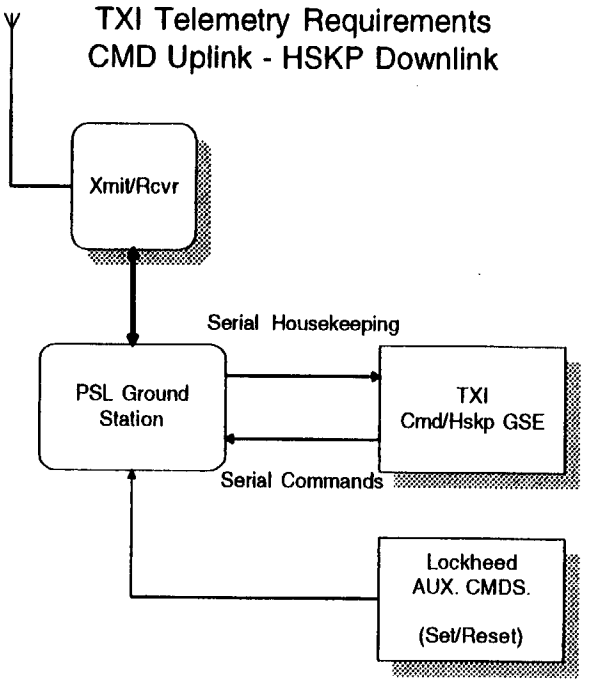

TV

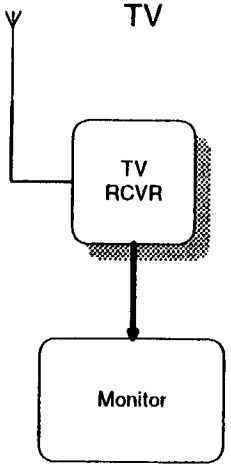

Blockhouse

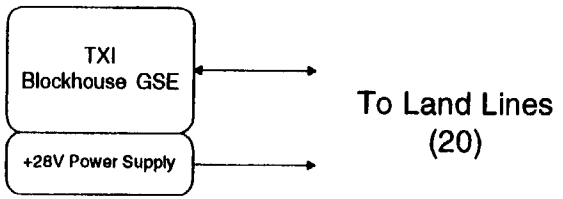

TXI ROCKET EXPERIMENT

POINTING REQUIREMENTS

ACCURACY:

THE TXI EXPERIMENT REQUIRES A POINTING ACCURACY TO BE WITHIN ONE ARC-MINUTE OF THE DESIRED POSITION.

STABILITY:

THE POINTING STABILITY MUST NOT EXCEED A PEAK TO PEAK ERROR VALUE OF ONE-HALF ARC-SECOND IN THE PITCH AND YAW AXIS WITH A MAXIMUM ROLL RATE OF 0.2 ARC-SECONDS PER SECOND ABOUT THE ROLL AXIS.

ABSOLUTE ROLL ANGLE ORIENTATION IS NOT REQUIRED. IT MUST ONLY BE SUFFICIENT TO GUARANTEE THE ACCURACY REQUIREMENT.

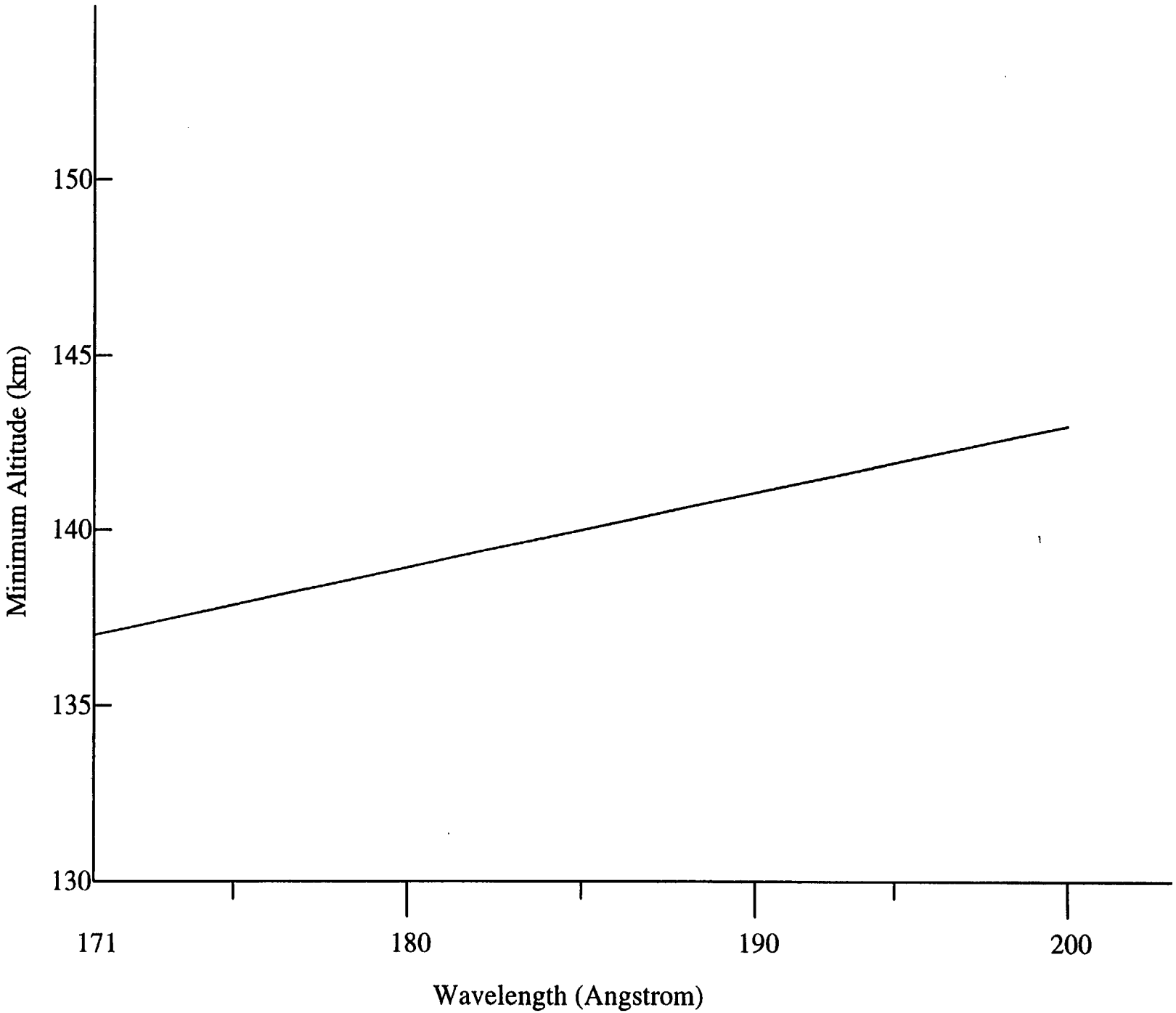
Minimum Altitude (km)
150
145
140
135
130
171
180
190
200
Wavelength (Angstrom)

TXI Observing Sequence

Time	Wavelength	Exposure (sec)
T+105	171	20
T+130	171	10
+145	175	10
+160	178	10
+185	180	3
+190	180	10
+205	182	10
+220	188	10
+235	192	10
+250	195	3
+255	195	10
+270	195	30
+305	203	10
+320	211	10
+335	203	10
+350	195	10
+365	192	10
+380	188	10
+395	175	3
+400	175	3
+405	175	3
+410	175	10
+425	171	10
+440	171	10
+455	171	10
etc.		

TXI ROCKET EXPERIMENT

LAUNCH WINDOW

THE TXI EXPERIMENTS SCIENCE REQUIRES THAT LAUNCH OCCUR WITHIN ± ONE MONTH OF THE SUMMER SOLSTICE AND WITHIN ± ONE HOUR OF LOCAL NOONTIME.

GROUND OPERATIONS

THE TXI EXPERIMENT WILL REQUIRE THAT THE EXPERIMENT BE EVACUATE PRIOR TO LAUNCH AND THAT ITS OVERALL TEMPERATURE NOT BE ALLOW TO CHANGE MORE THAN ± 10 DEGREES. THESE ARE SIMILAR TO THE NIXT EXPERIMENT REQUIREMENTS.

TXI ROCKET EXPERIMENT

MILESTONES

1. PROJECT INITIATION CONFERENCE (PIC)	23 MAY 1996
2. PRELIMINARY DESIGN CONFERENCE (PDR) (CDR-VEHICLE COMPONENTS)	DEC, '96
3. VEHICLE DRAWINGS TO WIFF	FEB, '97
4. CDR - EXPERIMENT	JULY, '97
5. VEHICLE PARTS TO SAO	DEC, '97
6. TEST PROGRAM - WSMR	MAY-JUNE, '98
7. LAUNCH	JULY, '98

TXI ROCKET EXPERIMENT

NASA SUPPLIED EQUIPMENT

1. SPARCS POINTING SYSTEM (DIGITAL OR ANALOG)

2. VEHICLE
   A. ROCKET SKINS WITH INTERNAL HEAT SHIELD
   B. VACUUM DOOR ASSEMBLY
   C. BULKHEADS (2)
   D. VACUUM PORT
   E. ROCKET SKIN PULLER (VACUUM SEALS)

3. WSMR VACUUM PUMPING SYSTEM

4. WSMR VIBRATION TEST FACILITIES

TXI ROCKET EXPERIMENT

TESTING

THE PRESENT TESTING PHILOSOPHY IS TO PERFORM SUBSYSTEM TESTING TO ENSURE EXPERIMENT OPERATION AND CALIBRATION.

THE EXPERIMENT FLIGHT QUALIFICATION TESTING IS PLANNED TO OCCUR A MONTH BEFORE THE FIRST POSSIBLE LAUNCH DATE. THE REASON FOR THIS APPROACH IS OUR DESIRE TO HAVE A LAUNCH OCCUR WITHIN THE SECOND CONTRACT YEAR. IF THE TESTING PROVES TO BE SUCCESSFUL, THAN LAUNCH ACTIVITIES COULD PROCEED., IF A FAILURE OCCURS, THEN THE LAUNCH WOULD BE DELAYED UNTIL THE FOLLOWING YEAR.

TUNEABLE X-RAY IMAGER FOR SOLAR CORONAL STUDIES

EXPERIMENTER'S DATA PACKAGE FOR FLIGHT 36.151 US-GOLUB

Leon Golub, Principal Scientific Investigator

SMITHSONIAN ASTROPHYSICAL OBSERVATORY
60 Garden Street
Cambridge, MA 02138

AND

MAX-PLANCK-INSTITUT FÜR AERONOMIE

D-37191 Katlenburg-Lindau

APPROVED

Leon Golub, SAO cfA

G. Nystrom, SAO cfA

TABLE OF CONTENTS

LIST OF TABLES / FIGURES / APPENDICES

1.0 DESCRIPTION OF EXPERIMENT

1.1 Introduction

We have completed and successfully flown the normal incidence X-ray telescope (NIXT) designed for very high spatial resolution studies of the solar corona. The telescope has been designed to fly on a Terrier/Black Brandt vehicle, and makes use of multilayer coatings to achieve usable reflectivity in the soft X-ray regime. The fifth flight of this telescope occurred July 11, 1991 at 1726 hours UT as part of an eclipse experiment. With this flight, we reached our design goal of 1/2 arc-second spatial resolution. The new TXI payload adds a wavelength tuning

The primary reason for using multilayer coatings at XUV and soft X-ray wavelengths is because no single surface layer coating can provide acceptable reflectivity at wavelengths shorter than ~300Å when used at normal incidence. For instance, at 173Å the best materials have R~.001. However, by precise deposition of 50 alternating layers of Mo and Si, mirrors with R~50% have been produced. When normal incidence mirror designs are employed, the immediate advantage is greatly improved image quality. The NIXT telescope recorded the highest resolution solar corona photographs ever taken on its last three flights. With the improvements now under way, we expect to improve on that performance.

1.2 Science Goals

The experiment has two purposes associated with a single scientific goal. We are trying to obtain high spatial resolution images of the solar corona and to develop a two-dimensional imaging detector sensitive to X-rays and XUV radiation.

The overall purpose is to study activity in the solar corona with sufficient spatial, spectral, and temporal resolution to understand the physical mechanisms responsible for coronal heating and dynamics.

Our analysis of NIXT and **YOHKOH** SXT data from the simultaneous observations carried out in April 1993, shows that the coronal structures seen in the two instruments can be totally different: loops seen in Fe XVI are not visible at all in Fe XVII, and vice versa. Our goal in designing the TXI has therefore been to observe all of the successive ionization stages of a single element (Fe), so that the plasma has nowhere to hide. By tuning through the range of x-ray wavelengths, and combining all of the observed ionization stages, we will build up a complete characterization of the corona in the temperature range

covered (log T = 5.8 - 6.4). The TXI design also allows detection of plasma flows by a suitable positioning of the monochromator passband, and detection of polarization of the x-rays via a 90° rotation of the instrument about the line-of-sight direction.

1.3 Scientific Uses and Expected Performance

The results from our last three NIXT flights and recent measurements of X-ray multilayer performance have shown that true sub-arc-second resolution combined with usable reflectivity are now realistic possibilities in a space instrument. We are thus in a position to begin implementing a qualitatively new kind of observing program for solar coronal studies.

The major strength of the multilayer technique will be evidenced when several sets of mirrors are flown at the same time, each one tuned to a different portion of the spectrum. This will allow simultaneous imaging and spectroscopy for both qualitative and quantitative analysis. Alternatively, at wavelengths longer than ~100Å, where the multilayers have sufficient bandwidth, the addition of a dispersive element, such as a double-reflection monochromator will permit the same type of diagnostics to be carried out. At the present time we anticipate three major areas of solar studies in which the rocket instrument will have an immediate impact:

1. **Fine Structure of Coronal Loops.** Present observations are insufficient to constrain theoretical parameters in studies of the heating and dynamics of the hot ($>10^6$K) plasma-filled magnetic structures that are found in the corona. At this time we do not know the radiant temperature and density structure within these loops, the magnitude of coherent plasma flows within them, or the relative importance of transient vs. steady-state heating processes. Additionally, the possible presence of isolated magnetic islands within a loop may be amenable to observation at the higher spatial resolution that we expect to achieve.

2. **Flare Onset and Reconnection.** At the sub-arc-second level of resolution, the possibility exists, particularly in the large-scale class of solar flares known as prominence eruptions, that we may be able to directly image the reconnection regions in which magnetic flux is annihilated and converted to the energy that powers a flare. In a sense these reconnection boundary layers are purely theoretical constructs, since they have not been observed on the Sun. Predicted sizes begin about one order of magnitude below present observational capabilities. Thus, with

the order of magnitude improvement in image quality we may begin to resolve these questions.

3. **Emerging Magnetic Flux.** X-ray studies from Skylab showed that most of the magnetic flux emerging from the solar interior is in small scale "shredded" or intermittent form. The overall balance between large active regions and small emerging flux regions is a function of phase in the solar cycle and is such that the total amount of magnetic flux emerging is nearly constant; the solar cycle can thus be visualized as an oscillation in the wave number distribution of emerging flux.

This observational constraint on magnetic dynamo theories remains to be tested on smaller spatial scales. Previous limitations due to the instrumental resolving power have left undecided the question of how much flux emerges at scale sizes below ~10 arc-seconds. It is certain that at some small spatial scale, magnetic diffusion will dominate so that the size spectrum of emerging flux will be cut off. However, the presently observed spectrum is such that the integrated contribution of small regions increases in importance down to the observational limit. If we are able to observe the turnover at spatial scales obtainable by this new instrumentation, then we will be able to directly test theories for magnetic flux emergence and diffusion.

1.4 Scientific Investigation: Flight Results

The most readily observable manifestation of a solar flare is a brightening in Hα of a well-defined area of the Sun. Although there is now general agreement that the energy release takes place in the corona, explaining chromospheric observations is of capital importance for any model of the physical processes that takes place in a flare.

A two-ribbon flare appears in Hα as the brightening of two parallel ribbons separated by a dark filament of rising coronal matter. The standard picture calls for some kind of catastrophic instability, either triggered by the shear of the field lines induced by the motion of the footprints in the photosphere, or generated by the interaction of the field and the current flowing in the filament (Van Tend and Kuperus, 1978 and Martens and Kuin, 1989). Reconnection of field lines then occurs beneath the rising filament with the magnetic energy released in the current sheet being transported down to the chromosphere either by a beam of particles or by heat conduction (or both) along the flux tubes.

In 1989 and 1991 we used real-time satellite data combined with a t-2 minutes launch hold, which is called a flare-wait mode. This allowed us to launch during the rise phase of a solar flare. This mode of operation was highly successful in that we obtained extremely good X-ray data at the peak of a solar two-ribbon flare. We also had the good fortune to observe the start of another separate flare event during our flight. The data obtained in the September 11, 1989 flight have provided a totally new view of solar flares in the corona, and do not fit any present theoretical model of how flares occur. Our data are thus presenting a challenge to flare theorists by forcing reexamination of the models.

For flight 36.151 the launch date will be determined by the presence on the Sun of at least one active region with well-developed sunspots. This can be predicted with a ~50% confidence one solar rotation (~27 days) in advance, and can be known with high confidence (>90%) three days in advance. Thus, a tentative launch date can be set one month prior to launch, and a go/no-go decision can be made 3 days prior.

2.0 SYSTEM DESCRIPTION

2.1 Electronic Systems and Telemetry

The Electronic system has three prime functions:

1. Control the operation of two CCD detectors. This would include the exposure and readout sequencing.
2. Control the operation of the TXI monochromator for wavelength selection and control the indexing of aperture mask on the calibration telescope.
3. Control the command and housekeeping operation.

The electronic design will utilize two on-board computers, one for the prime science operation, and the second for the command, housekeeping, and monochromater operation. The Image Processing Computer (IPC) is based around a Teknor 166Mhz pentium Single Board Computer (SBC) running on a passive PCI bus backplane. This SBC will control the image acquisition of both CCD detectors.

The detector on the tunable x-ray imaging side is being designed by the instrument's co-investigators at the Max Planck Institute. It is an image intensified detector based on a Kodak 2k x 2k CCD. The detectors pixel size is 15 microns^2.

The detector on the XUV telescope side is being designed by SAO. It is based on a Site 1k x 1k back-side illuminated CCD. The detectors pixel size is 24 microns. It will be cooled by a thermal electric cooler (TEC) operating against

a passive cold-block. The cold-block is designed to have sufficient energy to cover the flight plus up to 1.5 hours of hold time.

In a pre-programmed sequence, the IPC will initiate exposures and transfer the image data (after appropriate processing and formatting by two dedicated PCI bus frame grabber boards) to the rocket telemetry interface, for transmission to the ground by two 10Mbit data downlinks, and to an on-board storage device, for post-flight retrieval. The housekeeping will use a ISA computer bus backplane, and will use off-the-shelf data acquisition boards from National Instruments operating under LabView software.

The TXI block diagram number TXI-5100, shows the TXI electronic system. The command telemetry, data telemetry, telemetry interface, flight battery, and video telemetry are supplied by NASA. The experiment will be powered by a 28V battery. The power requirements are 28 volts @ 15 amps steady state, 20amps peak for 1 second. NASA will provide and service the batteries. A latching change-over relay will switch the experiment between external and internal power. The experiment's battery power will be applied a few minutes before launch. External power will be used for all testing excepting flight system testing.

The TXI telemetry Requirements are the following:

Command Uplink
1. One RS232 serial command link
2. Six Auxiliary set/reset for manual control
3. Three Momentary pulse commands

Downlink for Science data
1. Two 10Mb/sec WFF93 High Rate PCM Encoders
   (Sixteen bits and strobes)

Downlink for Housekeeping
1. One RS232 serial encoder
2. Four 10bit digital words and strobes
3. Thirty two Analog (0 to 5V)
   One TV transmitter for the H~Camera

Blockhouse (pre-flight operations)
1. 20 Umbical lines between the blockhouse and experiment
   for pre-launch check-out.

TABLE 2.1 - LATCH COMMANDS

SAO FUNCTION	SPARCS NOMENCLATURE
MANUAL MODE SET Lock out Automatic Sequence Enable Manual Mode	Aux-2 Set
MANUAL MODE RESET Return to Automatic Sequence Disable Manual Mode	Aux-2 Reset
START EXPOSURE Manual Mode (shutter open)	Aux-3 Set
END EXPOSURE (shutter close- read camera)	Aux-3 Reset
RESTART (terminate exposure in progress)	Aux-4 Set
Return to normal sequence	Aux-4 Reset
SPARE	Aux-5 Set
SPARE	Aux-5 Reset
SPARE	Aux-6 Set
SPARE	Aux-6 Reset
MASTER RESET ENABLE	Aux-7 Set
MASTER RESET DISABLE	Aux-7 Reset
MASTER RESET COMMAND	Momentary 1 (Pulsed)
CAMERA RESET COMMAND	Momentary 2 (Pulsed)
SPARE	Momentary 3 (Pulsed)

2.2 Optical Systems

2.2.1 TXI Experiment

The TXI experiment's optical system is an on-axis design which employs two flat (multi-layer coated) fold mirrors arranged to make an X-ray Monochromater of the Cowan-Golovchenko (Mills and King 1983; Craig *et al.* 1988) arrangement. In this arrangement, the two flat mirrors allow the entrance and exit beams to remain fixed, while the wavelength is changed by their rotation. The exit beam is directed to a spherical telescope mirror which focuses the solar image onto a CCD Detector by passing the beam through a central hole in the second flat mirror. This allows the telescope mirror to be used on-axis thereby minimizing optical aberrations. The optical system is described on SAO drawing TXI-002, Titled: Optical schematic - TXI.

2.2.2 Calibration Telescopes

There are four calibration telescopes of identical design, excepting their coatings which set their wavelength bandpass. The telescopes all share a common detector where only one telescope is imaged at a time. An indexing mask with one open aperture provides the telescope selection while covering the entrance apertures of the non-active telescopes. The optical configuration is a spherical telescope mirror tilted one degree to the incoming beam that focuses the solar image on a CCD detector; SAO drawing TXI-003, Titled: Optical schematic-Calibration experiment describes the optical system. The four telescope mirrors are equally spaced on a circle centered about the detector. This allows the tilt angle to be uniform for all telescopes and minimizes the tilt angle. The system focal ratio is such that the image tilt on the detector is well within the depth of focus so that no image degradation is observed.

2.2.3 H-Alpha Camera

A precision Day-Star Corporation Hydrogen Alpha (Hα) filter unit having a narrow bandpass (~0.6Å) centered on the Hα line (6563.28Å) with a 2.5 cm aperture was selected as the filter. The filter is placed behind a 712.6 millimeter (two lens) EFL telephoto lens system which images the full Sun on a Sony Electronics model XC-77 CCD video camera. The optical path is straight and un-vignetted. The H-Alpha Camera is mounted to the TXI optical bench and aligned parallel to TXI experiment. A similar system was flown successfully on

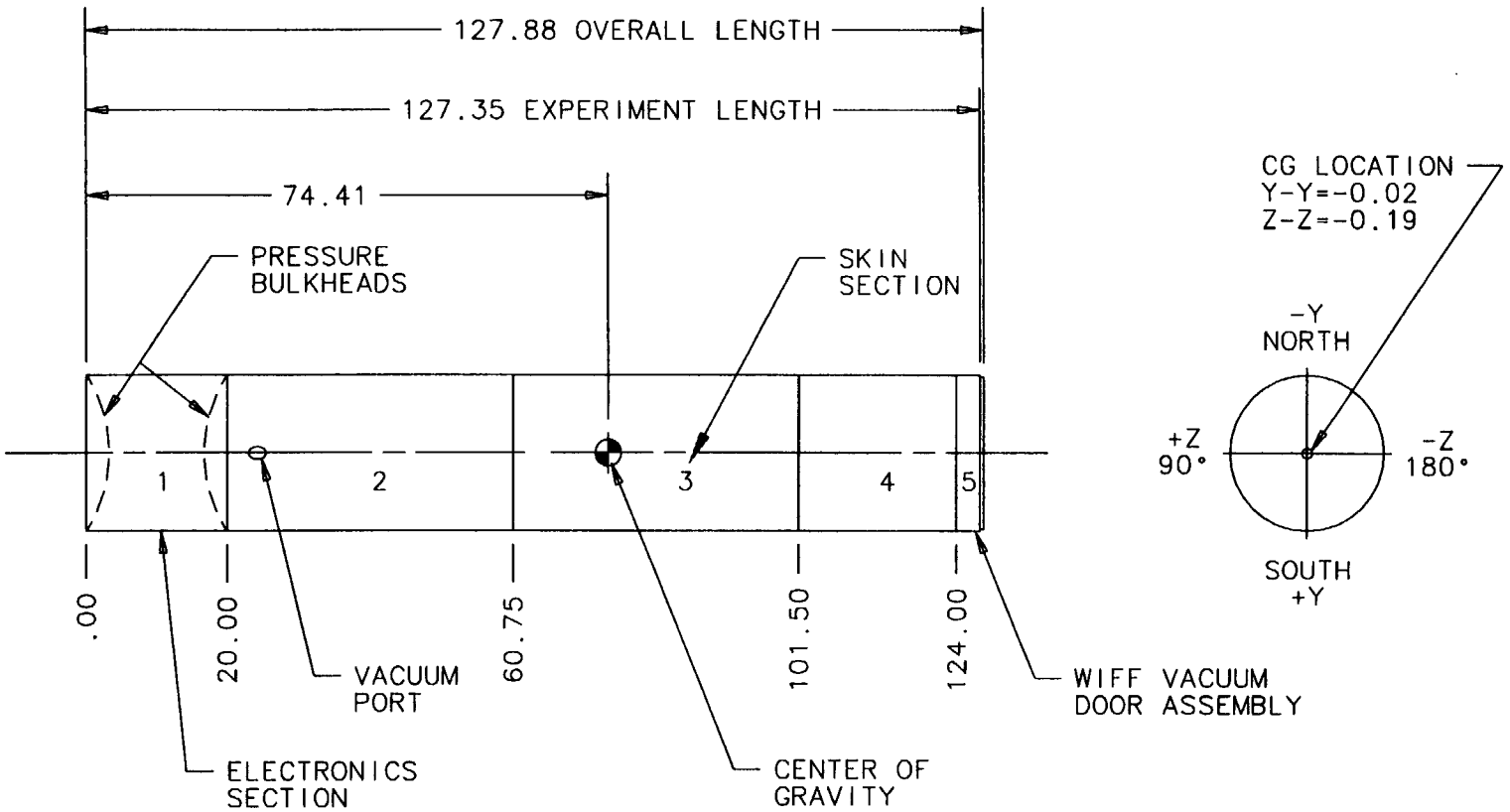

Figure 2-2.
TXI Center of Gravity Location

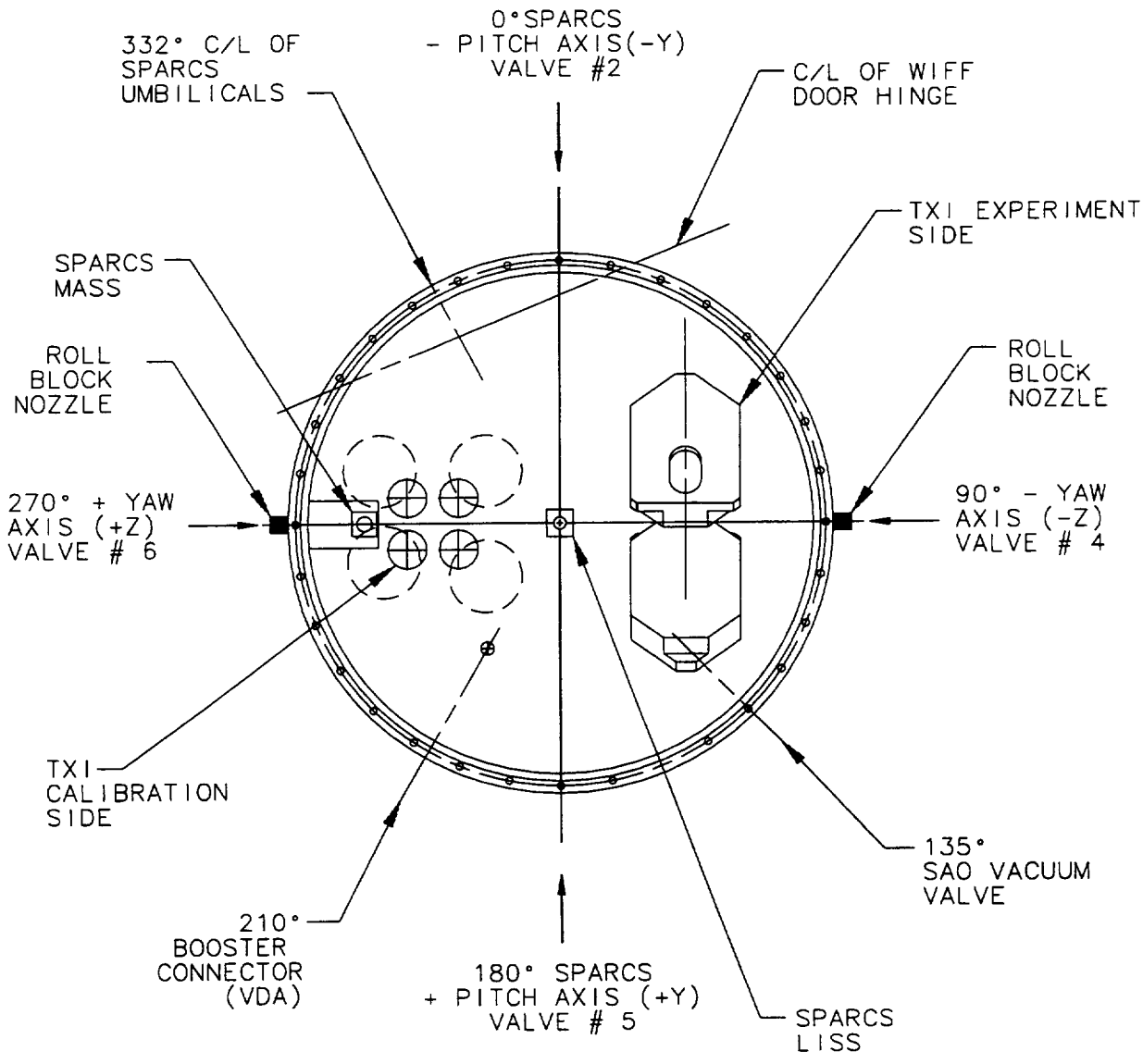

Figure 2-1.
TXI Angular Orientations WSMR-Tower

all the NIXT rocket flights and proved that adequate sensitivity can be attained to record the Hα image with sufficient resolution to allow sunspot recognition for aspect determination. This new Camera system has higher resolution coverage and will produce extremely sharp, highly contrasted images which will make pointing confirmation achievable.

2.2.4 SPARCS Pointing Sensors

The TXI telescope will be pointed and stabilized on the Sun by a SPARCS pointing and control system including a RIG (Roll Stabilization Gyro) unit. No attempt is made here to describe the SPARCS system; however, the MASS and LISS Sensors mounting, and co-alignment both to each other and to the TXI telescope will be described.

The MASS sensor is mounted by a rigid bracket attached directly to the rocket vehicle in the WIFF vacuum door assembly. The MASS Sensor is located on the +Z axis (285°) so that its control axes are properly aligned to the vehicle's axis within ±2° per Lockheed-SPARCS Group's instructions. It is positioned 200 mm radially outward from the vehicle's X-X axis and 25 mm back from the leading edge of the separation flange. This positioning guarantees a full unobstructed 70° FOV cone for the sensor.

The LISS (Fine Sun Sensor) assembly is mounted to the TXI's optical bench and positions the sensing element on the rocket's central axis, thereby yielding the largest unobstructed field of view. The control axes (pitch, yaw) of the LISS sensor are aligned within ±1° of the control axis per the Lockheed-SPARCS Groups instructions. The LISS will also be placed behind an aperture stop that only allows the optical beams to pass and thereby shields all other components from being illuminated by the solar beam.

The sensors will be aligned to the TXI telescope either by centering using an auto-collimation telescope to the TXI's focal plane and then erecting the sensors orthogonal to it by standard auto-collimation techniques or by centering a solar image on the TXI focal plane and then using the SPARCS pin hole target.

2.3 Mechanical Systems

2.3.1 Telescope Design

The major mechanical design consideration is the ability to achieve proper optical alignment and positioning of the optical elements including the detectors, while not introducing optical distortions or displacements from either mechanical or thermal stressing. This requirement must be satisfied for two environments. The first is in the laboratory where optical fabrication, testing, image evaluation and correction are performed. This laboratory environment is also roughly equivalent to what is expected during pre-launch activities. The second environment is the rocket flight. The rocket vehicle delivers severe vibration, shock and thermal loads to the experiment during its engine burn phase. The effect of these loads must be accounted for to ensure a successful experiment. The environmental design parameters are stated in Table 2-2, below.

TABLE 2-2 DESIGN PARAMETERS

PARAMETER	LABORATORY	LAUNCH
Temperature 72°F	±10°F	±3°F
Vibration	3.0g rms (3-400 Hz) all axes	19.1g rms (20-2000 Hz) all axes
Shock/Transient	3.0g decaying to 0 in 6 cycles	25g decaying to 5 g in 4 cycles

The design developed must satisfy these parameters. The experiment makes a kinematic attachment to the rocket vehicle at the main structural joint used to join rocket skin sections 3 and 4 together. This attachment comes from the central housing which contains a rigid platform used to house the Monochromator assembly and the experiment's two X-ray detector heads and their preamplifier electronics. This platform forms an optical bench for these components while also providing an interface for a conical tube made from Titanium. The Titanium tube has a sufficiently low Coefficient of Thermal Expansion (CTE) to guarantee that the telescope mirrors mounted to its end flange will remain in sharp focus over the expected temperature range while its conical shape provides rigid structural support. All five telescope (TXI plus 4 Cal.) mirrors mount to the end flange and incorporate the necessary motions to align and focus

them. The aperture stops for all telescopes are placed immediately next to the WIFF vacuum door on a rigid panel used to light seal the experiment's entrance aperture. The panel is also used to reject the solar thermal input, thereby minimizing thermal distortions within the optical systems. The panel also has an indexing aperture to uncover one Calibration telescope mirror at a time.

2.3.2 Electronics

The electronics, except for the power system are enclosed in two (2) computer enclosures. The enclosures are attached to the vehicle by vibration isolators to attenuate the vehicle dynamics. The electronic section will be pressurized.

2.3.3 Ancillary Systems

The telescopes are enclosed within the rocket vehicle skin sections numbered 2-5 with the ends sealed by a WIFF vacuum door and an aft bulkhead. This forms a vacuum tight enclosure. The WIFF vacuum door assembly allows for automatic opening and closing of the experiment's entrance aperture and provides protection from re-entry heating and dirt. The WIFF door requires a special battery operated unit to recycle the door during ground testing. The vacuum is achieved through an experiment valved pull-away port located in section 4. A standard thermocouple gauge and gauge controller are provided for initial evacuation and pressure monitoring during ground testing. This gauge will be compared with a Datametrics 600 internal flight gauge to determine experiment pressure. The internal gauge is used to determine experiment pressure during the launch and flight phases. The experiment must have a pressure below 1000 microns in order to launch. The gauge output is 0 to 5 volts dc, which corresponds to 1-1000 μ.

2.3.4 Experiment Weight Summary

The experiment weight summary is shown on table 2-3.

2.3.5 Angular Orientations

The experiment angular orientations are shown in Figure 2-1. The axis notations are according to the SPARCS group's drawings for a rail launched vehicle. The X-X axis is the vehicle's central axis with +X towards the motor.

2.3.6 Mass Moments of Inertia

The mass moments of inertia and the products of inertia for all axes are listed in Table 2-4. They are expressed in SI units of Kg-meter^2 and are about the experiment center of gravity (C.G.). The WIFF vacuum door assembly has been included in these calculations.

2.3.7 Center of Gravity

The experiment is composed of five sections having a total length of 127.68 inches, as shown on Figure 2-2. The C.G. location is for the TXI experiment including the WIFF vacuum door. Section 5 has been designed for attachment of ballast and/or trim weights. These weights have not been included in our C.G. calculations because they are intended to be added to trim both the Spin (X-X) axis and/or to position the Center of Pressure, if required. Therefore their positioning within the vehicle is unknown. The WIFF vacuum door assembly is also included in these calculations as it is an integral part of the experiment/vehicle.

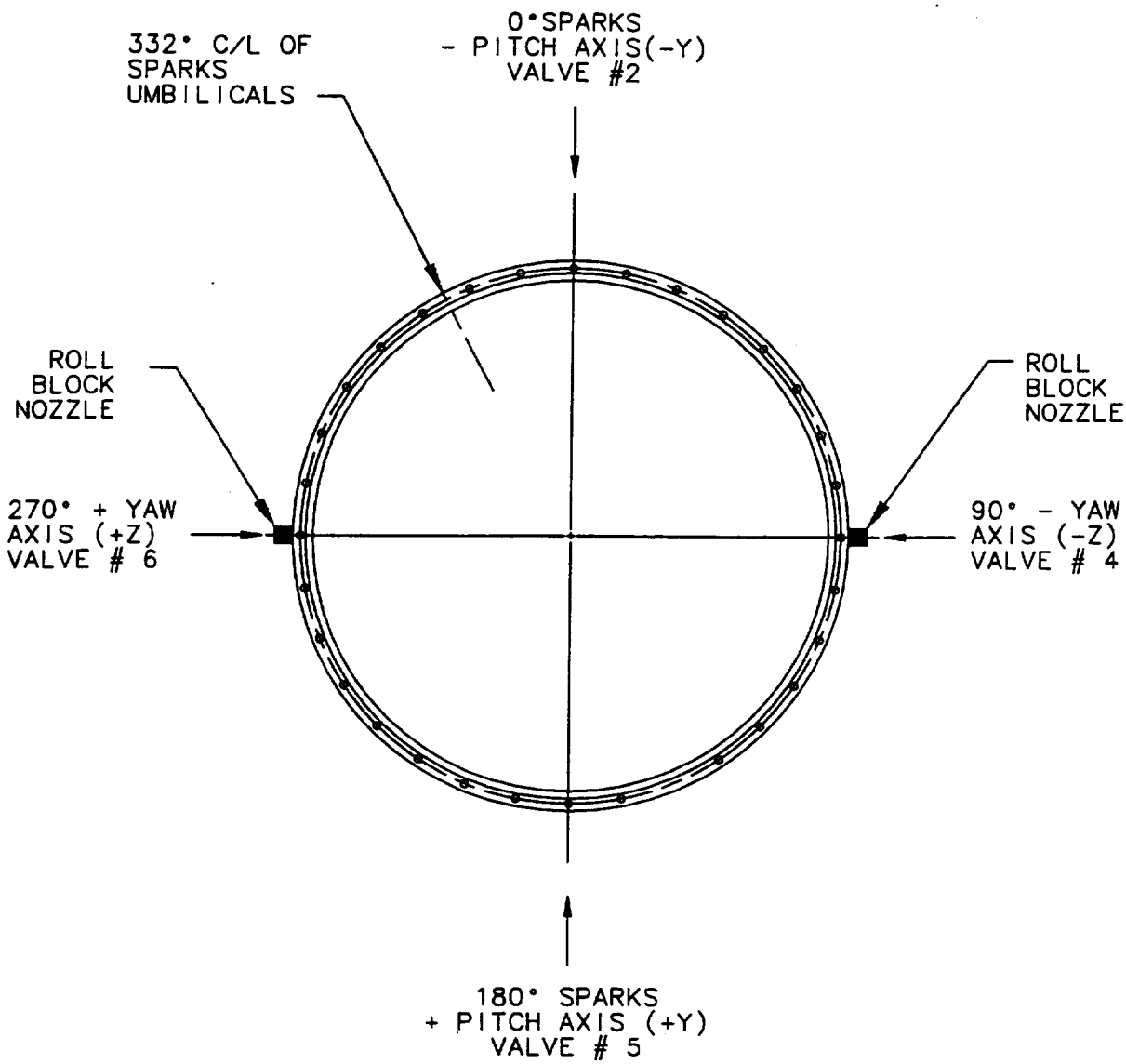

Figure 2-1.
TX1 Angular Orientations WSMR-Tower

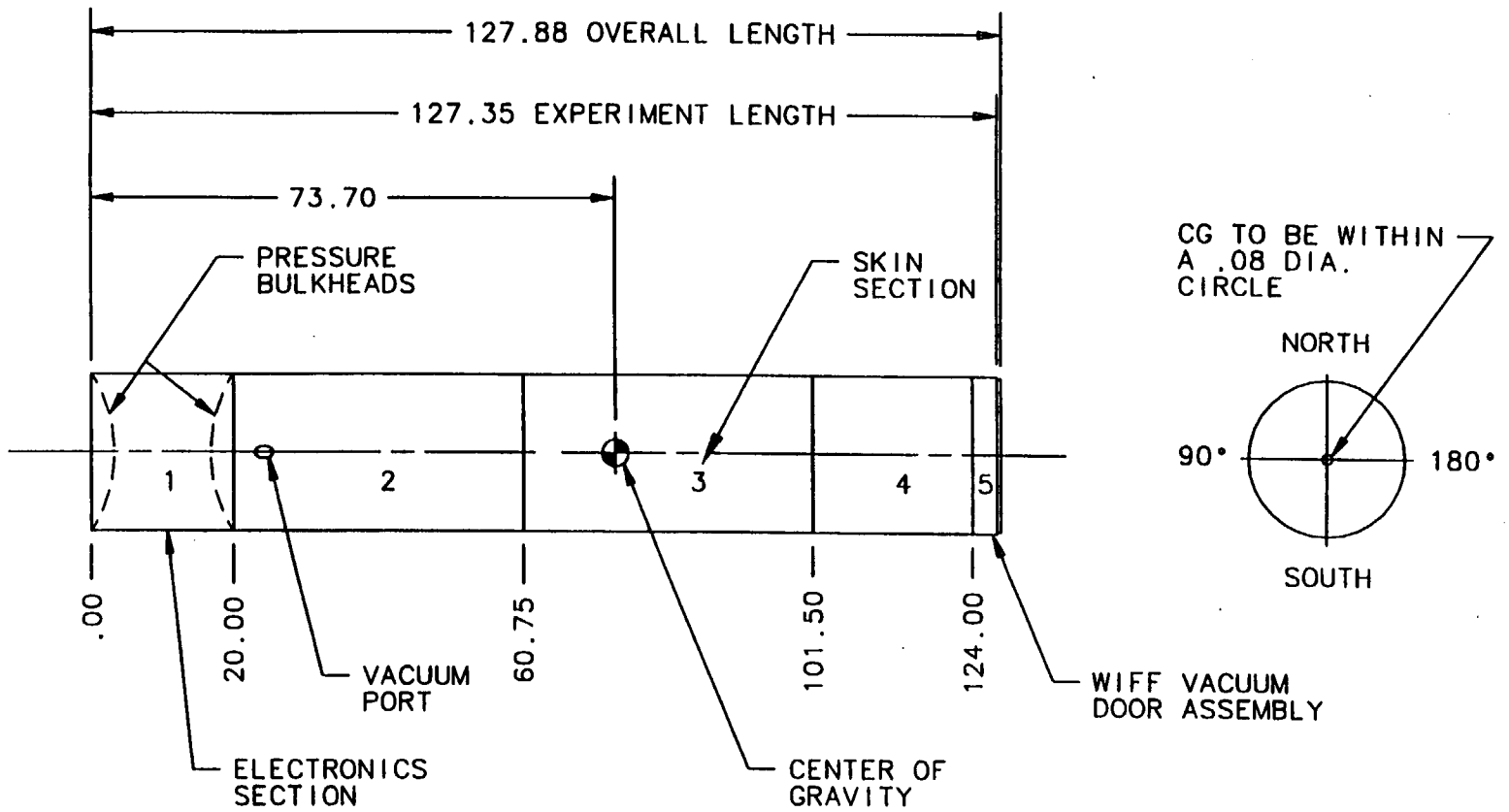

Figure 2-2.
TXI Center of Gravity Location

TABLE 2-3 EXPERIMENT WEIGHT SUMMARY	
COMPONENT DESCRIPTION	WEIGHT (Pounds)
EXPERIMENT	
Experiment Section	
TXI Focal Plane Assembly	41.0
Calibration FP Assembly	28.6
Telescope Tube Assembly	56.5
Forward Aperture Assembly	16.3
Ancillary Equipment	
SPARCS LISS Sensor	2.0
Hα Camera	7.0
Vacuum Gauge and Valve	6.5
Electronics	
Electronics	23.9
Cables, Connectors, Misc.	12.0
TOTAL EXPERIMENT WEIGHT	194.5
VEHICLE	
Rocket Skin Sections	249.2
Thermal Shields	27.0
WIFF Vacuum Door	38.2
Vacuum Bulkhead	13.5
Pressure Bulkhead	13.5
Ballast allotment	15.0
SPARCS Mass Sensor	0.8
TOTAL VEHICLE WEIGHT	367.2
TOTAL EXPERIMENT AND VEHICLE	551.7

TABLE 2-4 MASS MOMENTS/PRODUCTS OF INERTIA ABOUT EXP. CG			
AXIS	X	Y	Z
X	11.7	-2.0	0
Y	-2.0	241	0
Z	0	0	243
SI UNITS $Kg-M^2$			
NOTE: WIFF Vacuum Door Assembly included in these calculations.			

3.0 POINTING REQUIREMENTS

The SPARCS pointing accuracy must be within one arc-minute of the sun center. The pointing stability must not exceed a peak-to-peak error value of one-half arc-second in the pitch and yaw axis with a maximum roll rate of 0.2 arc-second per second about the roll axis. Absolute roll angle orientation will be specified at the time of flight and needs an angular positioning accuracy of ± 10 degrees.

4.0 LAUNCH WINDOWS AND REQUIREMENTS

Launch window is mid-April to end of August, and within one hour of local Noon (solar meridian transit).

5.0 MISSION SUCCESS CRITERIA

The primary purpose of this flight is to obtain extremely high spatial resolution soft X-ray images of the solar corona. The design goal of the TXI telescope is 0.25-.5 arc-second image quality. The exposure duration which is needed to record an image depends upon the solar activity level on the day of flight and upon the X-ray reflectivity of the mirrors and transmission of the filters (throughput). Under ideal conditions we may obtain images of the bright active region cores in a 1 second integration time. Under worst case conditions, we may need up to 30 seconds for an acceptable exposure.

The second purpose is to provide an in-flight calibration of the NASA TRACE satellite. We have selected the appropriate wavelengths to provide this calibration. The telescope design has been described in section 2.3.2.

5.1 Maximum Success Criteria

This flight's maximum success criterion is to achieve a full 430 seconds of stable solar pointing at the selected solar coordinates above an altitude of 110 kilometers. This will allow sufficient frames to be exposed onto the flight detectors based on an experiment initiation signal at 105 seconds. This permits the exposure sequences shown in Appendices A and B.

5.2 Minimum Success Criteria

The flight's minimum success criterion is to achieve 300 seconds of stable solar pointing at the selected solar coordinates above an altitude of 110 kilometers. This will allow a mimimun program to be carried out. The experiment has a redundant manual override capability which can be used if the flight experiences problems or the flight time is

projected to be shorter than 400 seconds. This allows selection of the prime flight exposures onto our detectors, based on an experiment initiation signal at 90 seconds or a manual override command. Also we must receive a high quality T/M signal over this length of time.

5.3 Exposure Sequence

The TXI detector flight exposure sequence is listed in Appendix A.

The Calibration detector flight exposure sequence is listed in Appendix B.

6.0 SUPPORT REQUIREMENTS

6.1 Instrumentation

One PCM telemetry unit configured to interface per our drawing number TXI-5100. This PCM unit's configuration and requirements will be specified at our upcoming working meeting at NASA-WIFF, currently schedule for 27 Febuary 1997. A TV transmitter and receiver are required to broadcast our Hα video TV signal in real time. Two 10 mega-bit channels are required for the prime science. We also request that a TV monitor displaying our Hα video be located at the SPARCS control station, and room be provided for positioning our GSE for both the TXI and XUV recording and display.

6.2 Vehicle

A Mark 80-boosted Black Brandt vehicle with an S-19 ascent stage is requested. This vehicle, with its associated launch support and the launch rail, is expected to be provided.

6.3 Guidance

The pointing and stabilization requirements are specified in Section 3.0. The experiment has been configured to attach a SPARCS-MASS sensor directly to the vehicle for coarse solar acquisition and a LISS sensor attached directly to the optical bench for fine control. Also a SPARCS RIG is required for roll stabilization.

6.4 Mechanical

We plan to integrate and test the experiment at WSMR. We will have portable optical measuring equipment at WSMR to evaluate alignment and telescope focus. We expect all fixtures required during integration and flight testing to be available at WSMR, such as vibration, dynamic balance,

etc. Experimenter personnel will be available to aid in these tasks. Also, we anticipate the need to use the SPARCS group's collimation telescope and Heliostat during the optical alignent and verification testing.

6.5 Recovery

The experiment employs CCD cameras and onboard memory for storage of scientific data. The CCD is sensitive to noise from excessive heating, therefore the vehicle has been thick anodized to minimize solar heating during the recovery phase. Also, the WIFF vacuum door will be closed during re-entry heating to keep dirt, brush, etc., from contaminating the experiment on impact. We request helicopter conveyance for two experiment team members to recover the payload quickly and survey possible damage.

6.6 Batteries

Battery power during flight is being provided by the SPARCS TM unit. Our power requirements are 28 volts with an average current draw of 15 amps, with peak draw of 20 amps for 1 sec.

6.7 Vacuum Station

A turbomolecular vacuum pumping system with roughing pump will be required for experiment evacuation at various WSMR test facilities, i.e., vibration qualification. The system must be appropriately valved to allow switching between pumps with a pumping line valve allowing fine control of the pumping speed and back-filling the system with dry nitrogen. The system employed during our NIXT flights is acceptable.

6.8 Rail Positioning

The rail position will be as shown in figure 2.1.

6.9 Special Considerations

The experimenter plans to provide all equipment (including spare parts) necessary to test, operate and evaluate experiment performance. The only specialized facility required is a collimator with projection target for CCD focussing.

7.0 FLIGHT QUALIFICATION AND/OR OPERATION STATUS OF EXPERIMENT SUB SYSTEMS

The TXI experiment will be tested to the NASA requirements for a new payload. We request that all this testing be performed at the WSMR test facilities. We will provide the necessary manpower to support the experiment testing activities.

8.0 FIELD OPERATIONS

8.1 WSMR ACTIVITIES

Our present plans call for the experiment to arrive at WSMR, starting in May-June 1998 to begin the flight test program. We anticipate this activity to take 10 working days.

If sucessful, then we would plan to proceed directly to its first flight.

8.1.1 Flight Checkout Procedure

The TXI experiment has multiple X-ray imaging telescopes, all having narrow band prefilters sealing their apertures. A functional checkout of the X-ray optical performance cannot be performed at WSMR. This is because a collimated X-ray source is unavailable. Our testing and evaluation for flight will be as follows:

1. Test electronics for correct operation through telemetry and GSE control.

2. Verify position of optical focus by making non-X-Ray detector images. This also checks detector operation and image processing.

3. Examine prefilters to assure blemish* free state.

4. Verify vacuum integrity of vehicle.

5. Verify filter status via light leak diodes.

* The prefilters must attenuate the solar spectrum by 10^{-4} (focal plane filter must be 10^{-8}). There cannot be any flaking of the coating or pinholes in the filter substrate film.

8.1.2 Flight Operations

Blockhouse LC36 Area

Smithsonian GSE display equipment will interface to the Lockheed ITS console. Most of the pre-flight check out will take place in this configuration.

Equipment needed:

1. One 8 channel Brush recorder.

2. Four 10 bit digital word displays.

ASCL LC-35

Used during the flight and pre launch telemetry checkout. The following equipment will be needed:

1. Command Console.

2. TV monitor displaying experiment Hα video signal.

3. One 8 channel Brush recorder.

4. One 10 bit word selector, with both analog and digital display capability.

5. Space for experiment VHS video recorder and monitor.

6. TV monitor displaying experiment housekeeping.

7. Quick look GSE for science data.

8.1.3 Pre-Flight and Flight Day Activities

In the evening before launch day, a series of exposures will be taken using our illumination system to ensure prefilter performance. Acceptable exposures are required for approval to launch the following day. An acceptable exposure means no indication of a light leak as detected by our detectors, ie increased counts.. The general flight-day checkout procedure is shown in table 8-1.

TABLE 8-1 GENERAL FLIGHT DAY CHECKOUT PROCEDURE	
TIME	EVENT
T-240 MIN	Begin Experiment Evacuation.
T-90	All personnel at their stations.
T-80	Perform Tower Functional Checkout Procedure.
T-60	Close Vacuum Valve.
T-58	Vent Vacuum Probe.
T-59	Verify Vacuum Pressure Steady.
T-30	Remove Vacuum Probe (now or as close to launch as possible).
T-25	O.K. to Launch.
T-15	Verify All Records Running Properly.
T-5	Experiment and T-M on External Power.
T-4	Verify GSE Telemetry Correct.
T-0	Launch.
T + 30	Verify vacuum valve open
T + 50	Hα Camera on
T + 69	Verify Hα Camera image
T + 89	Verify detectors on
T + 95	Verify Pointing Coordinates using Hα Camera Image.
T + 90 - End of Data Taking	Verify Pointing Stability and detector Sequencing.
T + (IF Required)	*Send Abort and manual Mode Commands as Required.
T +TBD	Verify WIFF Vacuum Door Closed.
T + TBD	Verify Experiment Power Off.
* Sent only if large pointing excursion or camera malfunction occurs.	

Time into flight* (Seconds)	Wavelength (Angstrom)	Exposure Time (Seconds)
T+105	171	20
130	171	10
145	175	10
160	178	10
185	180	3
190	182	10
205	188	10
220	192	10
235	195	10
250	195	3
255	195	10
270	203	30
305	211	10
320	203	10
335	195	10
350	192	10
365	188	10
380	175	3
395	175	3
400	175	3
405	175	3

* Times shown are preliminary and are subject to change based on NASA's Ballist analysis (Time vs. Altitude).

APPENDIX B

Time into flight* (Seconds)	Wavelength (Angstrom)	Exposure Time (Seconds)
T+105	171	10
120		10
135		30
170	195	10
185		30
220	284	10
235	188	30
270	304	10
285		30
320	171	10
335	195	10
350	284	10
365	171	10
380	195	10
395	171	10
410	195	10
Repeat last 2 steps until reentry		

NOTE: We are allowing 5 seconds in between exposures for readout. This time may be adjusted, based on actual operation.

* Times shown are preliminary and are subject to change based on NASA's Ballist analysis (Time vs. Altitude).

APPENDIX C

SAO DRAWING NUMBERS

TXI- 5100 - Titled: TXI - System Diagram

TXI- TBD - Titled: TXI - External Cabling Diagram

REFERENCES

1. Conrady, A.E. 1957, "Applied Optics and Optical Design" (Dover).

2. Thompson, K.P. 1980, Ph.D. Thesis, Univ. of Arizona.

3. Barbee, T.W., Jr., S. Mrowka, and M.C. Hettrick 1985, Appl. Opt., 24, 883.

4. Rosner, R., L. Golub, and G.S. Vaiana 1985, Ann. Rev. Astron. and Astryphy (in press).

5. Henry, J.P., E. Spiller and M. Weisskopf 1982, Appl. Phys. Lett., 40, 27.

6. Golub, L. 1984, Adv. Space Res., 4, 75.

7. Antonucci, E., R. Rosner and K. Tsinganos 1985, Ap.J. (in press).

8. Golub, L. 1980, Phil. Trans. R. Soc. London A, 297, 595.

9. Golub, L., E. Spiller, R.J. Bartlett, M.P. Hockaday, D.R. Kania, W.J. Trela and R. Tatchyn, 1984, Appl. Opt., 23, 3529.

NIXT PAPERS

1. Spiller, E., and L. Golub, "Fabrication and Testing of Large Area Multilayer Coated X-ray Optics".

2. Golub, L., G. Nystrom, E. Spiller and J. Wilczynski, "Construction of a Multilayered X-ray Telescope for Solar Coronal Studies from Space".

3. Golub, L., G. Nystrom, E. Spiller, J. Wilczynski, P. Takacz, and C. Welch, "X-ray/EUV optics for Astronomy, Microscopy, Polarimetry and Projection Lithography".

REVISIONS				
ZONE	LTR	DESCRIPTION	DATE	APPROVED
	1	INITIAL ISSUE		

MONOCHROMATOR TABLE	
GRAZING ∠	WAVELENGTH
39.5°	171 A°
45°	190 A°
51.8°	211 A°
54.9	220 A°

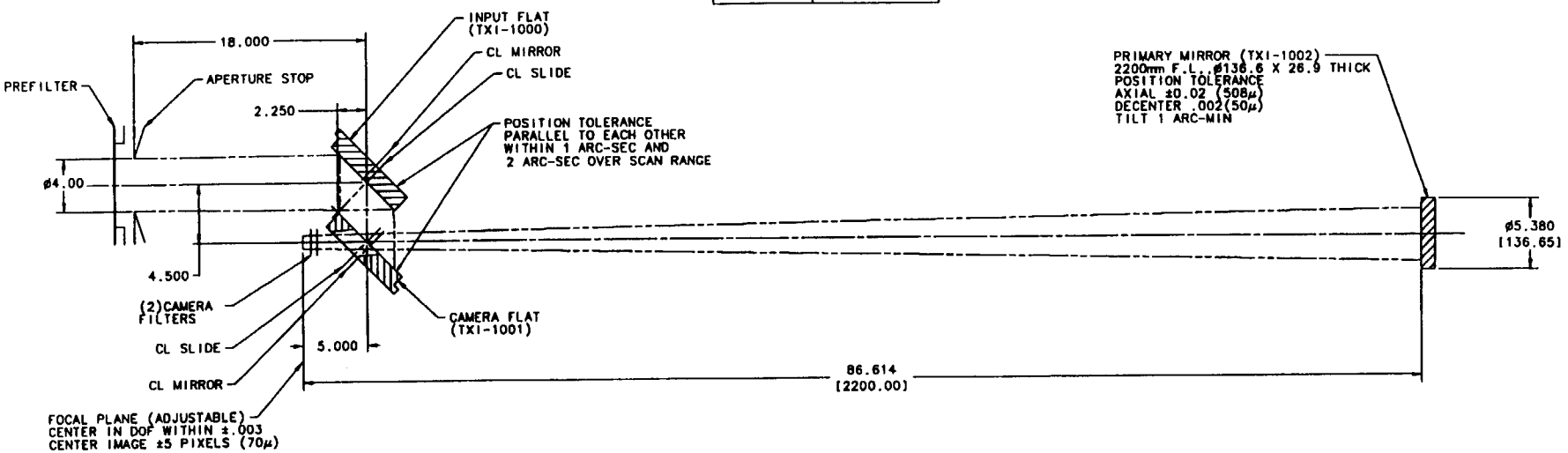

NOTES:

1. MATERIAL: N/A
2. FINISH: N/A
3. SYSTEM f NUMBER =21.635, DEPTH OF FIELD ± .0119 (302.89μ).
2. OPTICAL IMAGERY, SEE ZEEMAX FILE, TITLED X-RAY SCAN.

REMOVE BURRS AND BREAK SHARP EDGES	DR M.HONDA DATE 08-03-07	CHK DATE
UNLESS OTHERWISE SPECIFIED DIMENSIONS ARE IN INCHES	DSGN APPD DATE	
TOLERANCES ON FRACTIONS DECIMALS ANGLES .XX ±.01 .XXX ±.005 ±.25°	MANF APPD DATE	
SURFACE FINISH: 63	QUAL APPD DATE	
MATERIAL 1 FINISH 2	ENGR APPD DATE	
NEXT ASSY N/A	CONTRACT	

SMITHSONIAN ASTROPHYSICAL OBSERVATORY
CENTRAL ENGINEERING

OPTICAL SCHEMATIC TXI

SIZE	CAGE IDENT NO.	DWG NO.	REV
D	50944	TXI-002	1
SCALE 1/4	IDEAS V8.1	SHEET 1 OF 1	

REVISIONS				
ZONE	LTR	DESCRIPTION	DATE	APPROVED
	1	INITIAL ISSUE		

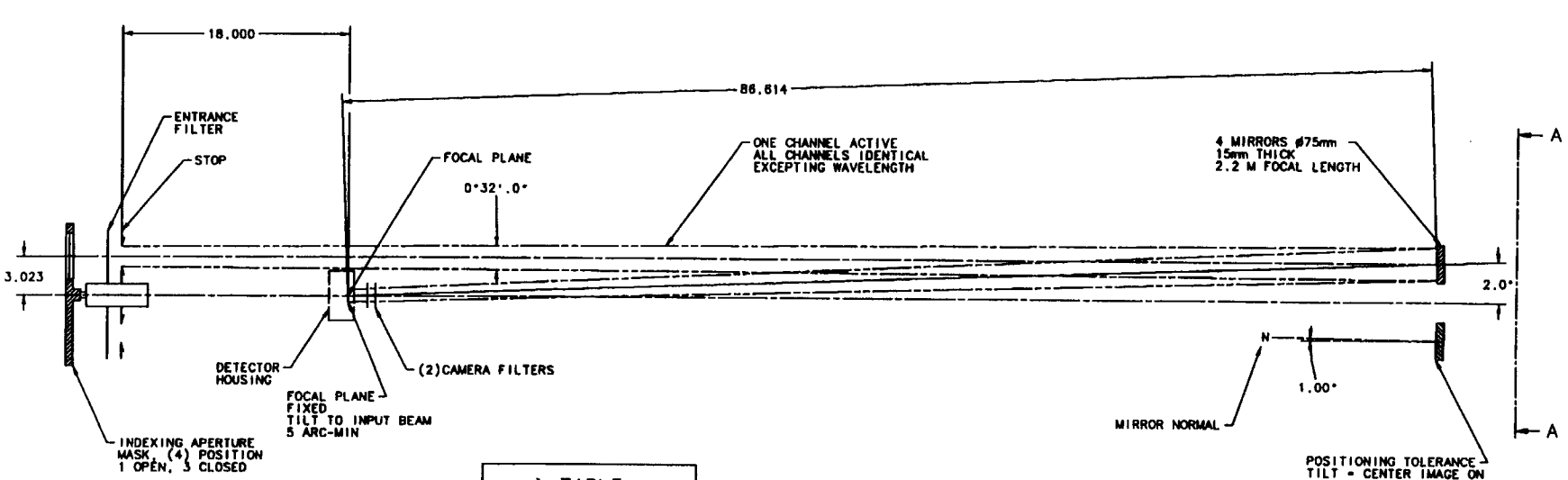

λ TABLE	
CHANNEL	λ
1	171 A°
2	195 A°
3	284 A°
4	304 A°

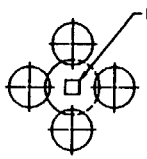

VIEW A-A

NOTES:

1. MATERIAL: N/A
2. FINISH: N/A
3. DEPTH OF FIELD = ±.017 (433μ)

REMOVE BURRS AND BREAK SHARP EDGES

UNLESS OTHERWISE SPECIFIED DIMENSIONS ARE IN INCHES

TOLERANCES ON FRACTIONS DECIMALS ANGLES

NEXT ASSY N/A

SMITHSONIAN ASTROPHYSICAL OBSERVATORY
CENTRAL ENGINEERING

OPTICAL SCHEMATIC CALIBRATION

SIZE	CODE IDENT NO.	DWG NO.	REV
D	50944	TXI-003	1

SCALE 1/4 IDEAS MS3 SHEET 1 OF 1

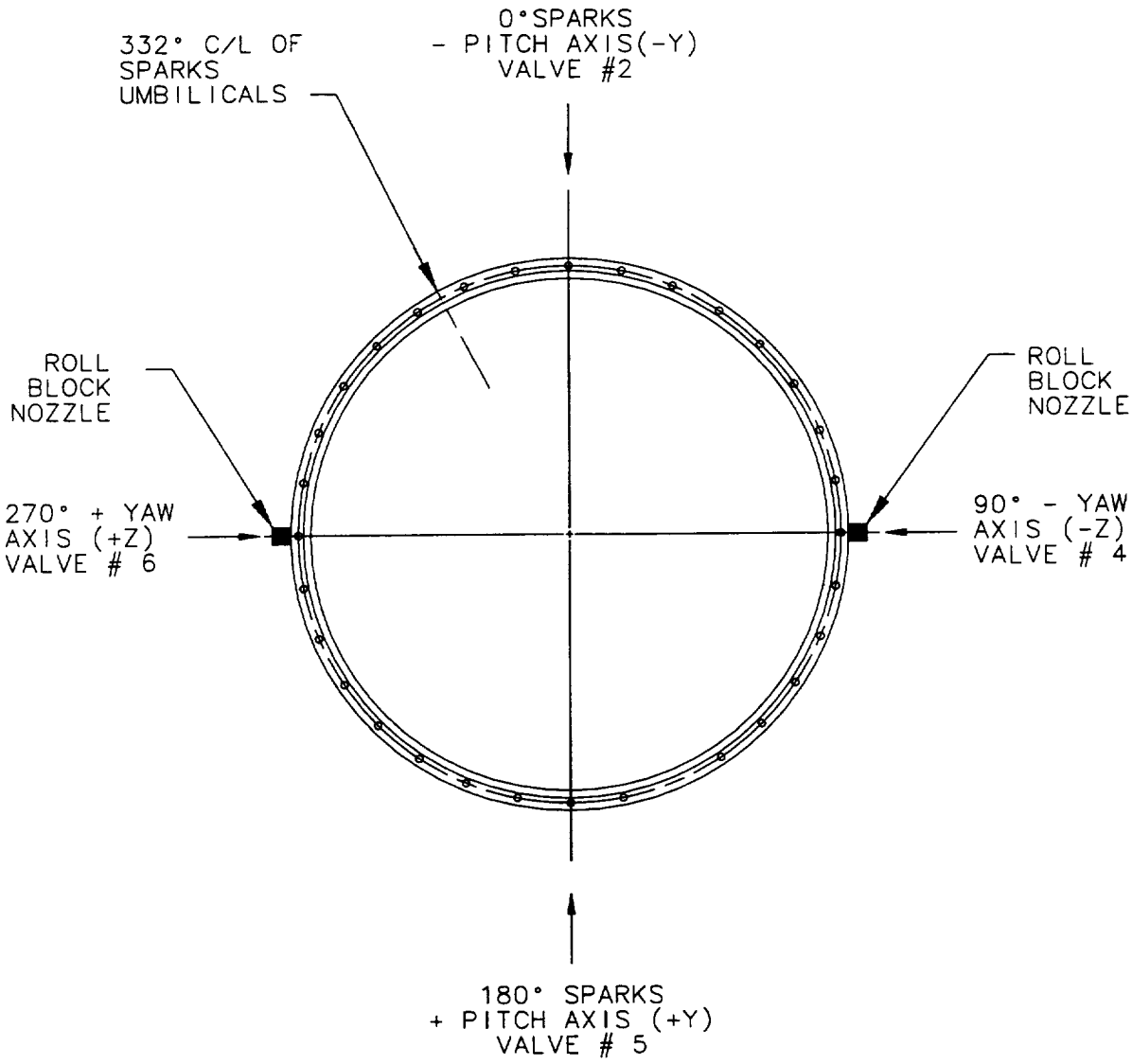

Figure 2-1.
TXI Angular Orientations WSMR-Tower

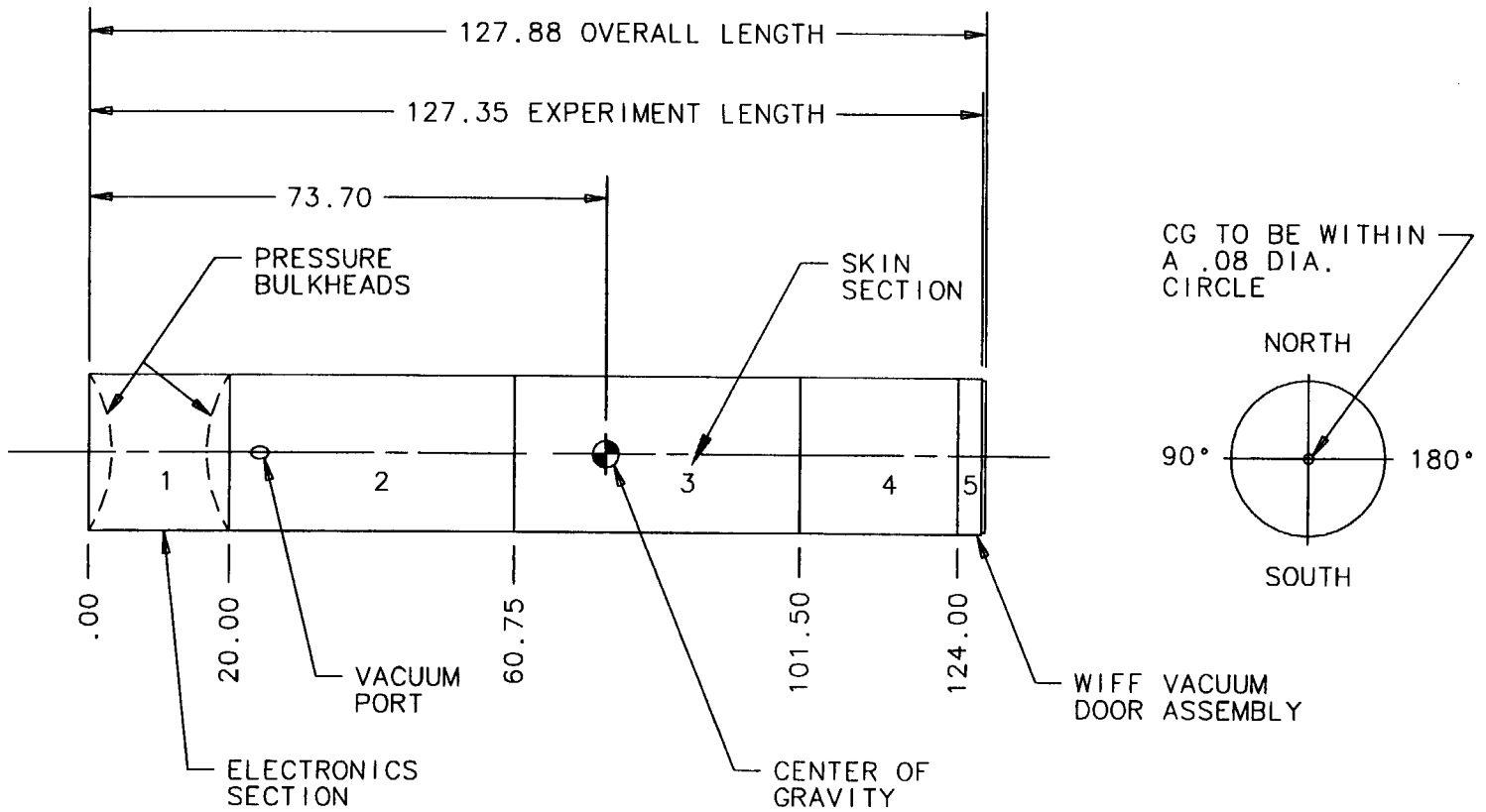

Figure 2-2.
TXI Center of Gravity Location

4.121
4.000

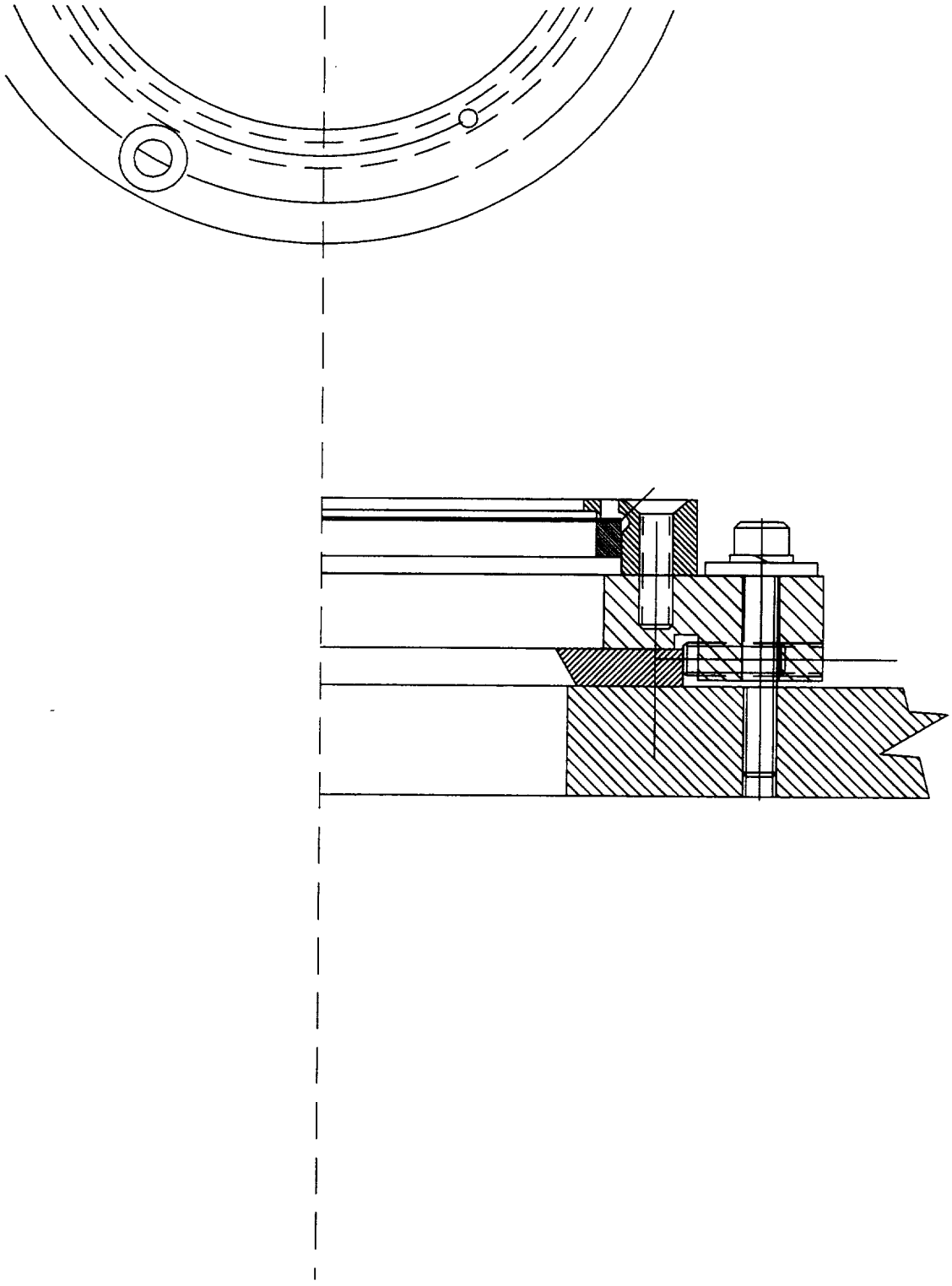

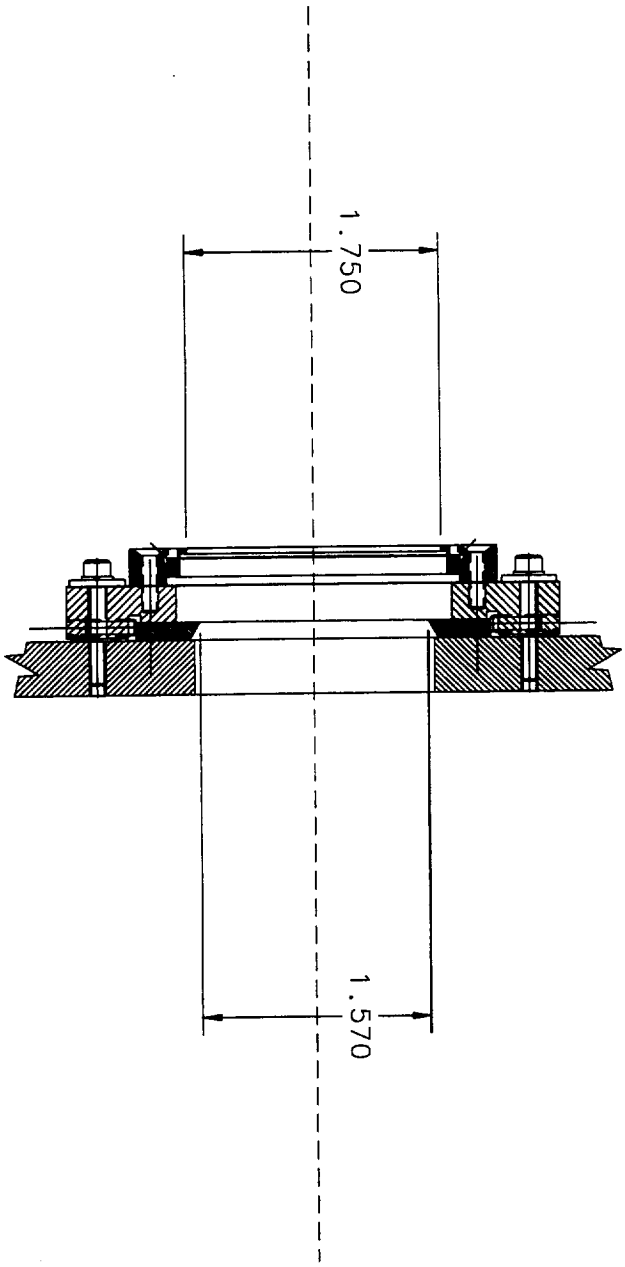
1.750
1.570

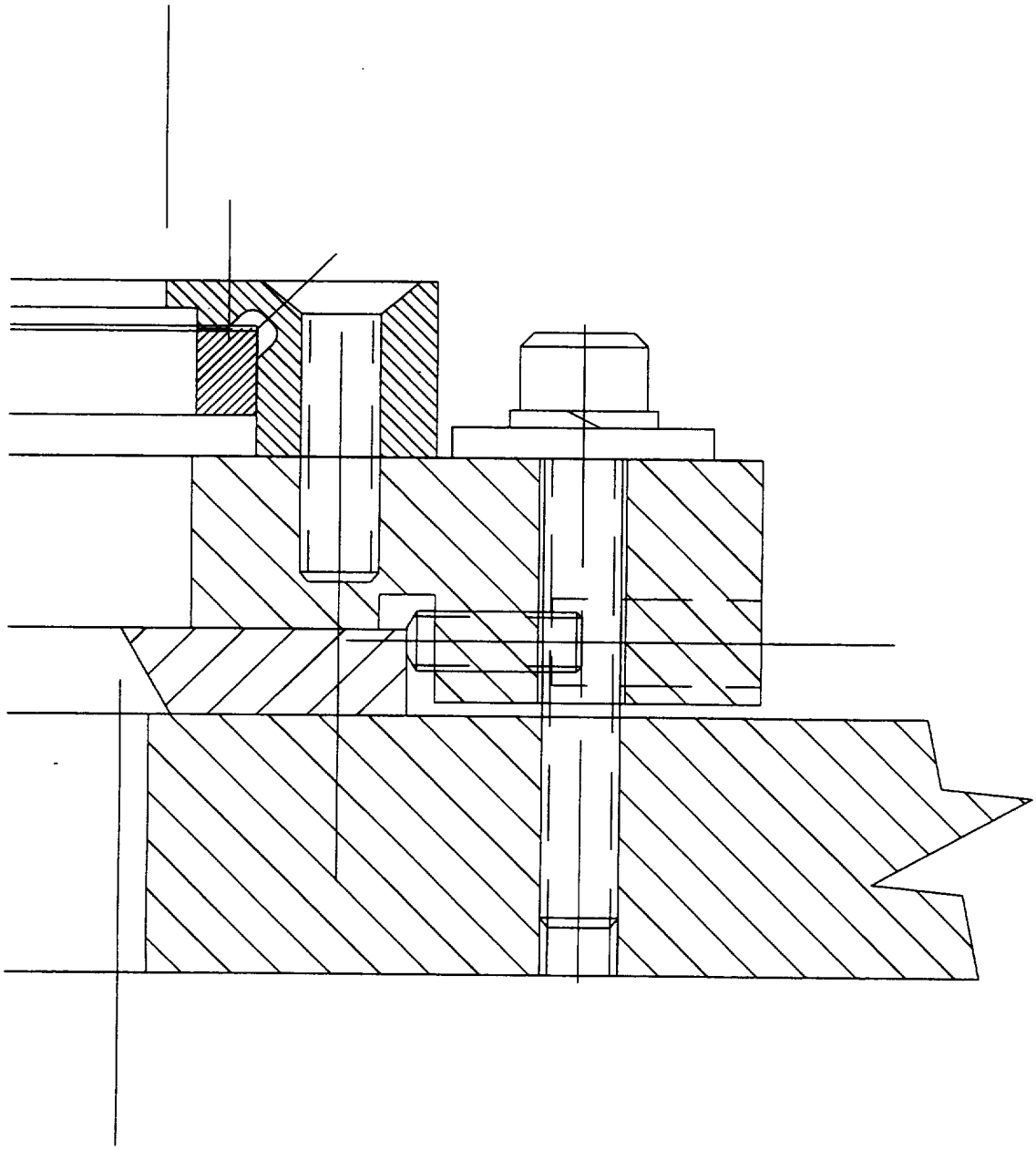

OPTIONAL FORM 99 (7-90)

FAX TRANSMITTAL

# of pages ▶ 5

To Chuck Tepstra	From Leon Golub
Dept./Agency	Phone # 617 495 7177
Fax # 303 447 3279	Fax #

NSN 7540-01-317-7368 5099-101 GENERAL SERVICES ADMINISTRATION

ZONE	LTR	REVISIONS DESCRIPTION	DATE	APPROVED
	2	REVISED PER DCR # 01		

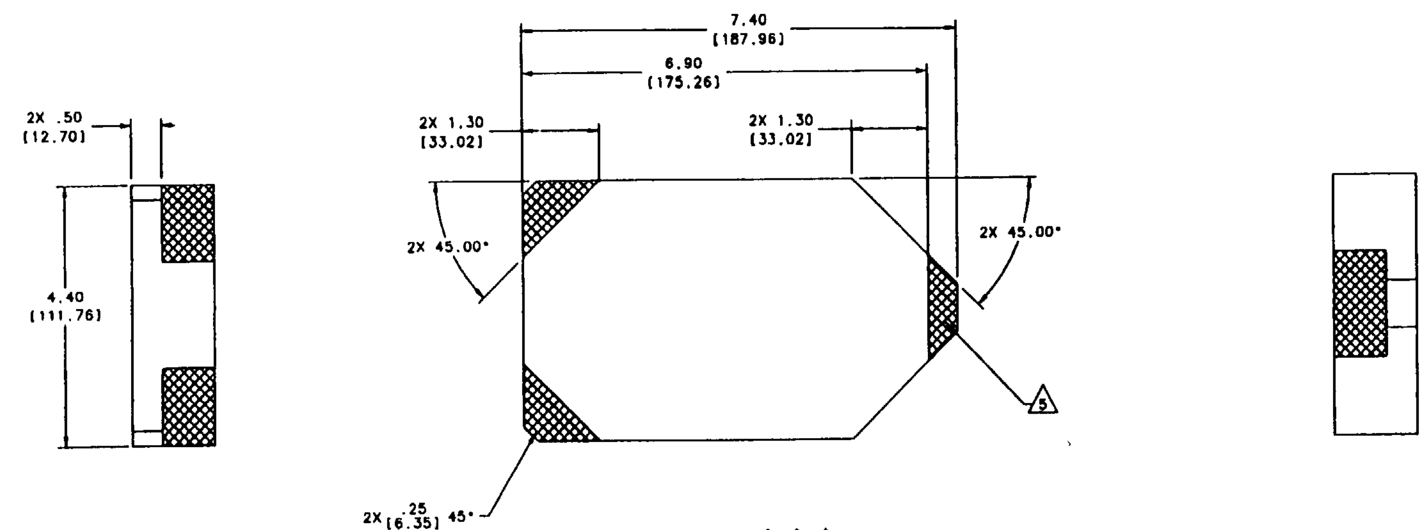

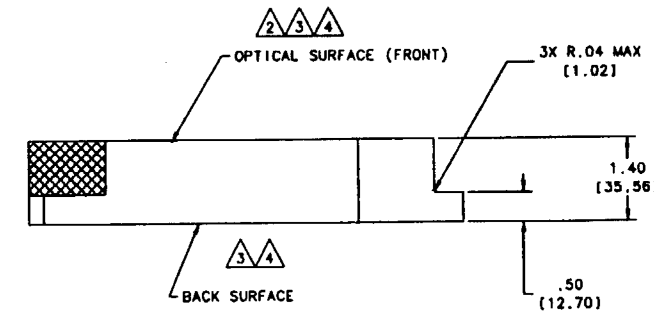

NOTES:

1. MATERIAL: FUSED SILICA, PREMIUM GRADE.
2. FINISH: ALL SURFACE FINISHES PER MIL-O-13830. OPTICAL SURFACE SHALL BE SUPER POLISHED TO A REQUIRED ROUGHNESS OF 3A° WITH A GOAL OF 1A°. BACK SURFACE, POLISH TO A SCRATCH/DIG TOLERANCE OF 40-20. ALL OTHER SURFACES TO BE MEDIUM GROUND TO AN 80/50 TOLERANCE.
3. SURFACE FIGURE: THE OPTICAL SURFACE TO BE FLAT AND SMOOTH TO A ~~PEAK TO VALLEY~~ TOLERANCE OF 1/40λ WHEN MEASURED AT 6328A° (STANDARD ZYGO INTERFEROMETER). EDGE EFFECTS CAN BE MASKED UP TO 4mm FROM EDGES. THE BACK SURFACE TO BE 1/2 TO 1/4λ WHEN MEASURED AS ABOVE. || RMS
4. THE OPTICAL SURFACE AND BACK BACK SURFACE TO BE PARALLEL TO EACH OTHER WITHIN 2 ARC-MINUTES.
5. SURFACES INDICATED BY CROSSHATCHING TO BE HYDROSULFURIC ACID ETCHED AFTER INITIAL OPTICAL FABRICATION AND PRIOR TO FINAL SURFACE FIGURING.

6 ALL EDGES TO HAVE EITHER A 1mm RADIUS OR A 1mm X 45° CHAMFER AT OPTICAL MANUFACTURERS DISCRETION.

7 ESTIMATED MASS IS 1.38 Kg.

8 DIMENSIONS IN BRACKETS ARE MILLIMETERS.

9 COATINGS: NONE

REMOVE BURRS AND BREAK SHARP EDGES
UNLESS OTHERWISE SPECIFIED DIMENSIONS ARE IN INCHES
TOLERANCES ON FRACTIONS ± DECIMALS .XX ± .01 .XXX ± .005 ANGLES ± .25°
MACH. FINI. N/A
MAT'L 1 FINI 2
NEXT ASSY TXI-501

DR M. HONDA DATE 08-30-96 | CHK DATE 12/23/96
DSGN APPD DATE
ENGR APPD DATE
CHKR APPD DATE
PROJ APPD DATE
CONTRACT

SMITHSONIAN ASTROPHYSICAL OBSERVATORY
CENTRAL ENGINEERING CAMBRIDGE, MA.

INPUT FLAT, FLIGHT

SIZE D | CODE IDENT NO. 50944 | DWG NO. TXI-1000 | REV 2

SCALE 1/1 | IDEAS MS 3.0 | SHEET 1 OF 1

REVISIONS				
ZONE	LTR	DESCRIPTION	DATE	APPROVED
	2	REVISED PER DCR # 01		

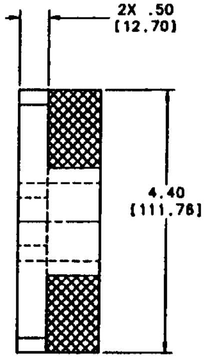

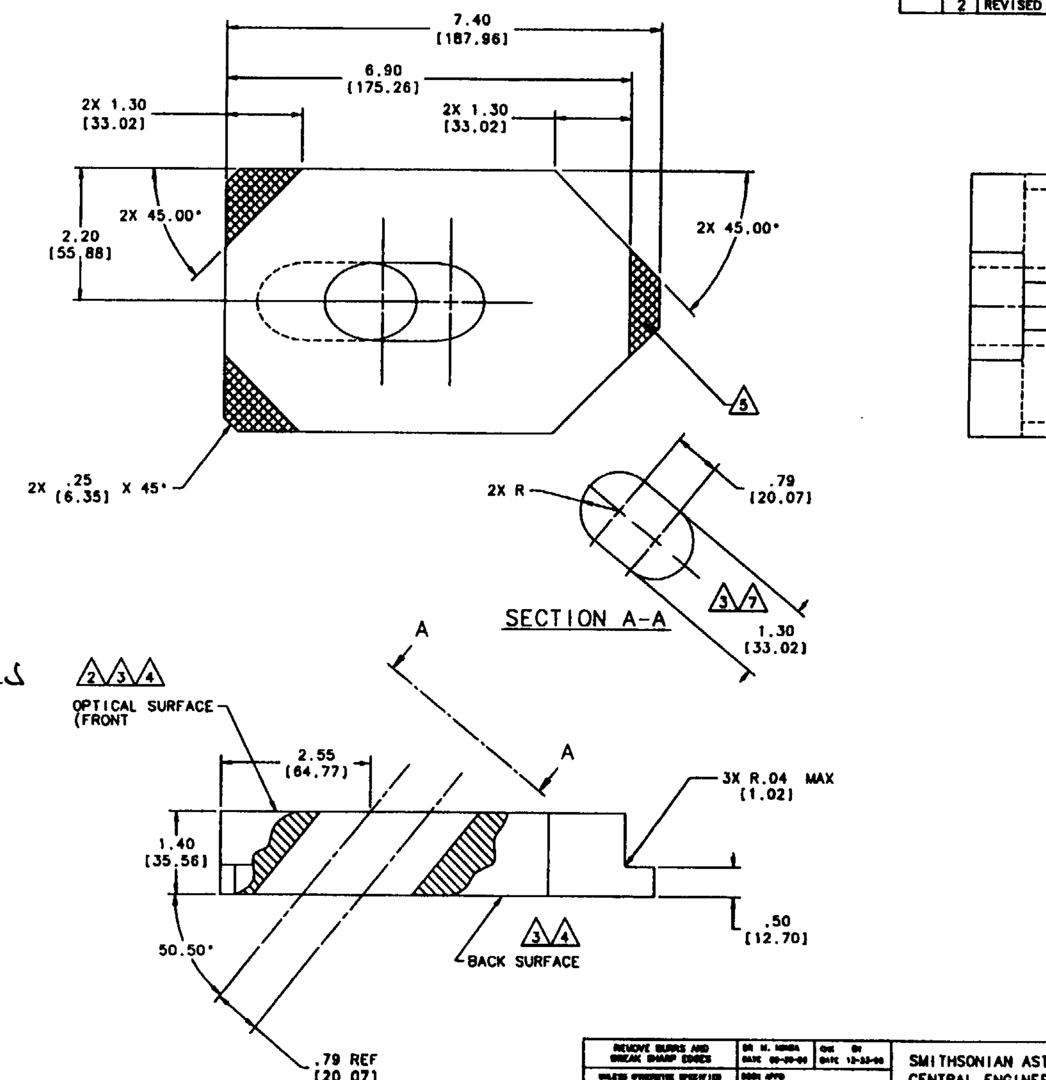

NOTES:

1. MATERIAL: FUSED SILICA, PREMIUM GRADE.

2. FINISH: ALL SURFACE FINISHES PER MIL-O-13830. OPTICAL SURFACE SHALL BE SUPER POLISHED TO A REQUIRED ROUGHNESS OF 3A° WITH A GOAL OF 1A°. BACK SURFACE, POLISH TO A SCRATCH/DIG TOLERANCE OF 40-20. ALL OTHER SURFACES TO BE MEDIUM GROUND TO AN 80/50 TOLERANCE.

3. SURFACE FIGURE: THE OPTICAL SURFACE TO BE FLAT AND SMOOTH TO A ~~PEAK-TO-VALLEY~~ TOLERANCE OF 1/40λ WHEN MEASURED AT 6328A° (STANDARD ZYGO INTERFEROMETER). EDGE EFFECTS CAN BE MASKED UP TO 4mm FROM EDGES AND 1 mm AROUND HOLE. THE BACK SURFACE TO BE 1/2 TO 1/4λ WHEN MEASURED AS ABOVE. / RMS

4. THE OPTICAL SURFACE AND BACK BACK SURFACE TO BE PARALLEL TO EACH OTHER WITHIN 2 ARC-MINUTES.

5. SURFACES INDICATED BY CROSSHATCHING TO BE HYDROSULFURIC ACID ETCHED AFTER INITIAL OPTICAL FABRICATION AND PRIOR TO FINAL SURFACE FIGURING.

6. ALL EDGES TO HAVE EITHER A 1mm RADIUS OR A 1mm X 45° CHAMFER AT OPTICAL MANUFACTURERS DISCRETION.

7. 1.40 (35.56mm) DIMENSION APPLIES AT OPTICAL SURFACE. A SLIGHT TAPER IS ALLOWABLE LEAVING A LARGER DIMENSION AT THE BACK SURFACE.

8. ESTIMATED MASS IS 1.22 Kg.

9. DIMENSIONS IN BRACKETS ARE MILLIMETERS.

10. COATINGS: NONE

REMOVE BURRS AND BREAK SHARP EDGES

UNLESS OTHERWISE SPECIFIED DIMENSIONS ARE IN INCHES

TOLERANCES ON

MAT'L: 1 FIN: 2

NEXT ASSY TX1-501

SMITHSONIAN ASTROPHYSICAL OBSERVATORY
CENTRAL ENGINEERING

CAMERA FLAT, FLIGHT

SIZE	CODE IDENT NO.	DWG NO.	REV
D	50944	TX1-1001	2

SCALE 1/1 | IDEAS MS3 | SHEET 1 OF 1

REVISIONS				
ZONE	LTR	DESCRIPTION	DATE	APPROVED
	1	INITIAL ISSUE		

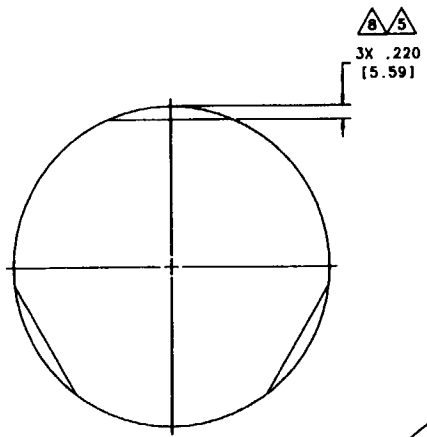

OPTIONAL 2

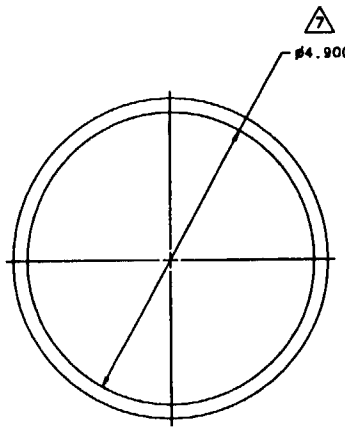

OPTION 1

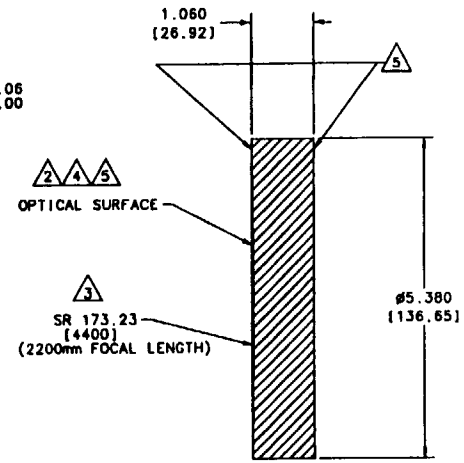

NOTES:

1. MATERIAL: FUSED SILICA, PREMIUM GRADE.
2. FINISH: ALL SURFACE FINISHES PER MIL-O-13830. OPTICAL SURFACE SHALL BE SUPER POLISHED TO A REQUIRED ROUGHNESS OF 3A° WITH A GOAL OF 1A°. BACK SURFACE, POLISH TO A SCRATCH/DIG TOLERANCE OF 40-20. ALL OTHER SURFACES TO BE MEDIUM GROUND TO AN 80/50 TOLERANCE.
3. THE MIRRORS FOCAL LENGTH SHALL BE 2200mm ±3mm.
4. SURFACE FIGURE: THE OPTICAL SURFACE TO BE SPHERICAL WITH A MAXIMUM ~~PEAK-TO-VALLEY~~ DEVIATION FROM AN IDEAL SURFACE OF 1/40λ WHEN MEASURED AT 6328A° (STANDARD ZYGO INTERFEROMETER). EDGE EFFECTS CAN BE MASKED UP TO 2mm FROM EDGES. THE BACK SURFACE TO BE 1/2 TO 1/4λ WHEN MEASUREDAS ABOVE. | RMS
5. THE BACK SURFACE AND FRONT FLAT SURFACE AREA MUST BE PARALLEL TO EACH OTHER AND PERPENDICULAR TO THE SPHERICAL GENERATION AXIS WITHIN 2 ARC-MINUTES.
6. ALL EDGES TO HAVE EITHER A 1mm RADIUS OR A 1mm X 45° CHAMFER AT OPTICAL MANUFACTURERS DISCRETION.
7. DIAMETER OF SPHERICAL SURFACE.
8. OPTION 2. FIGURE ENTIRE SURFACE THEN GRIND 3 FLATS AS SHOWN.
9. ESTIMATED MASS IS 1.04 Kg.
10. DIMENSIONS IN BRACKETS ARE MILLIMETERS.
11. COATING: NONE

REMOVE BURRS AND BREAK SHARP EDGES	DR. M. HONDA DATE 08-20-96	CHK DATE
UNLESS OTHERWISE SPECIFIED DIMENSIONS ARE IN INCHES	DSGN APPD DATE	
TOLERANCES ON FRACTIONS DECIMALS ANGLES ± .XX ± .01 ± .XXX ± .005 ± .25°	DSGN APPD DATE	
SURF. FIN:	DSGN APPD DATE	
MATL: 1 FINISH: 2	PROJ APPD DATE	
NEXT ASSY TXI-502	CONTRACT	

SMITHSONIAN ASTROPHYSICAL OBSERVATORY
CENTRAL ENGINEERING CAMBRIDGE, MA.

PRIMARY MIRROR

SIZE	CAGE IDENT NO.	DRG NO.	REV
D	50944	TXI-1002	1
SCALE 1/1	IDEAS MS 3.0	SHEET 1 OF 1	

⇒ TWO (2) OF THESE MIRRORS

REVISIONS				
ZONE	LTR	DESCRIPTION	DATE	APPROVED
	1	INITIAL ISSUE		

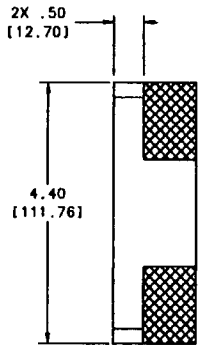

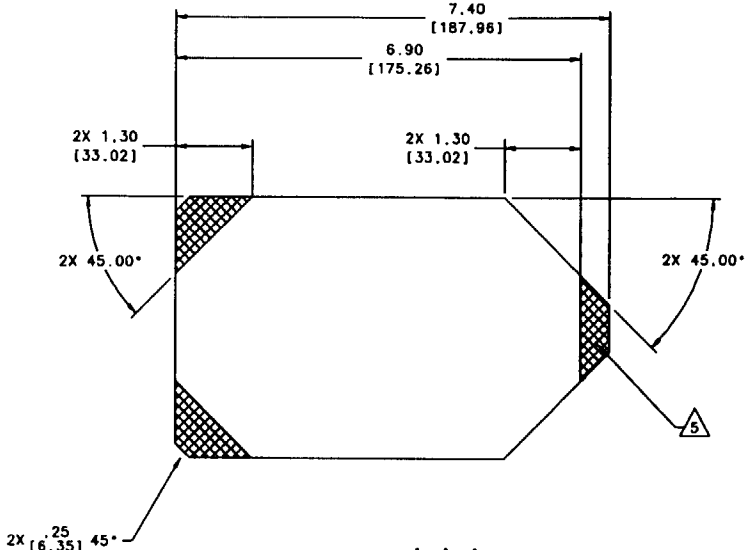

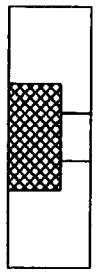

NOTES:

1. MATERIAL: FUSED SILICA, PREMIUM GRADE.
2. FINISH: ALL SURFACE FINISHES PER MIL-O-13830. FRONT AND BACK SURFACES SHALL BE POLISHED TO A SCRATCH/DIG TOLERANCE OF 40-20. ALL OTHER SURFACES TO BE MEDIUM GROUND TO AN 80/50 TOLERANCE.
3. SURFACE FIGURE: THE FRONT AND BACK SURFACES TO BE FLAT AND SMOOTH TO AN RMS TOLERANCE OF 1/4-1/8λ WHEN MEASURED AT 6328A° (STANDARD ZYGO INTERFEROMETER). EDGE EFFECTS CAN BE MASKED UP TO 2mm FROM EDGES.
4. THE OPTICAL SURFACE AND BACK SURFACE TO BE PARALLEL TO EACH OTHER WITHIN 2 ARC-MINUTES.
5. SURFACES INDICATED BY CROSSHATCHING TO BE HYDROSULFURIC ACID ETCHED AFTER INITIAL OPTICAL FABRICATION AND PRIOR TO FINAL SURFACE FIGURING.
6. ALL EDGES TO HAVE EITHER A 1mm RADIUS OR A 1mm X 45° CHAMFER AT OPTICAL MANUFACTURERS DISCRETION.
7. ESTIMATED MASS IS 1.38 Kg.
8. DIMENSIONS IN BRACKETS ARE MILLIMETERS.
9. APPLY AN OPTICAL COATING OF ALUMINUM WITH AN OVERCOAT OF 200-300A° OF SILICON DIOXIDE OR SILICON MONOXIDE.

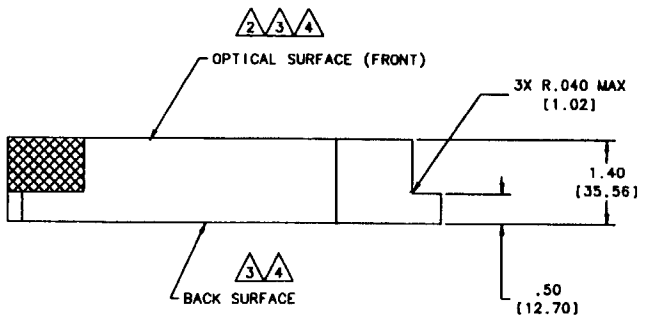

REMOVE BURRS AND BREAK SHARP EDGES	DR M. HONDA 00-10-94	CHK DATE
UNLESS OTHERWISE SPECIFIED DIMENSIONS ARE IN INCHES	DSGN APPD DATE	
TOLERANCES ON FRACTIONS DECIMALS ANGLES	DSGN APPD DATE	
MACH. FIN: N/A	CHKD APPD DATE	
MAT'L: 1 FINISH: 2	PROJ APPD DATE	
NEXT ASSY TXI-501	CONTRACT	

SMITHSONIAN ASTROPHYSICAL OBSERVATORY
CENTRAL ENGINEERING CAMBRIDGE, MA.

INPUT FLAT, TEST

SIZE	CODE IDENT NO.	DWG NO.	REV
D	50944	TXI-1003	1

SCALE 1/1 | IDEAS MS 3.0 | SHEET 1 OF 1

REVISIONS				
ZONE	LTR	DESCRIPTION	DATE	APPROVED
	2	REVISED PER DCR # 01		

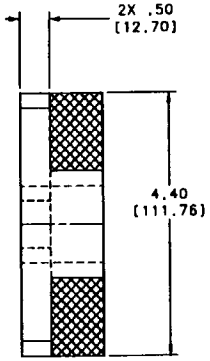

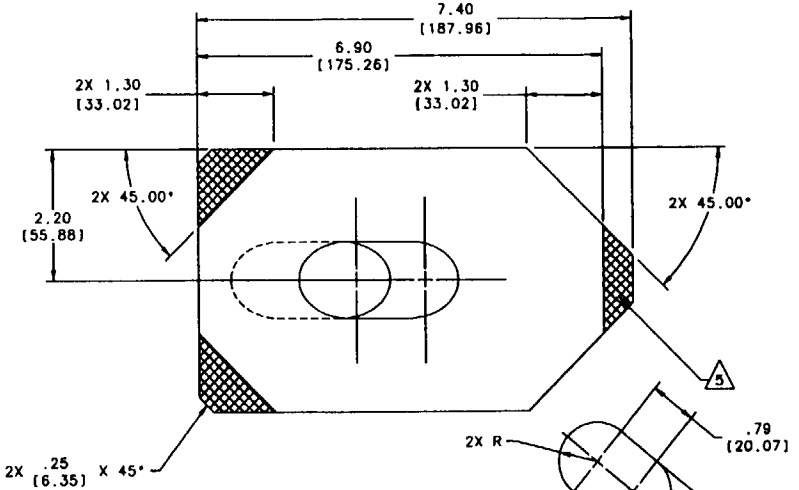

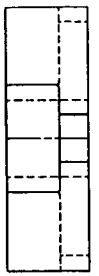

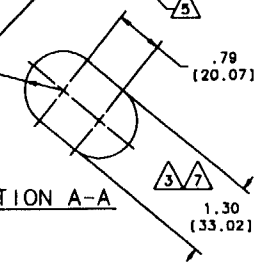

SECTION A-A

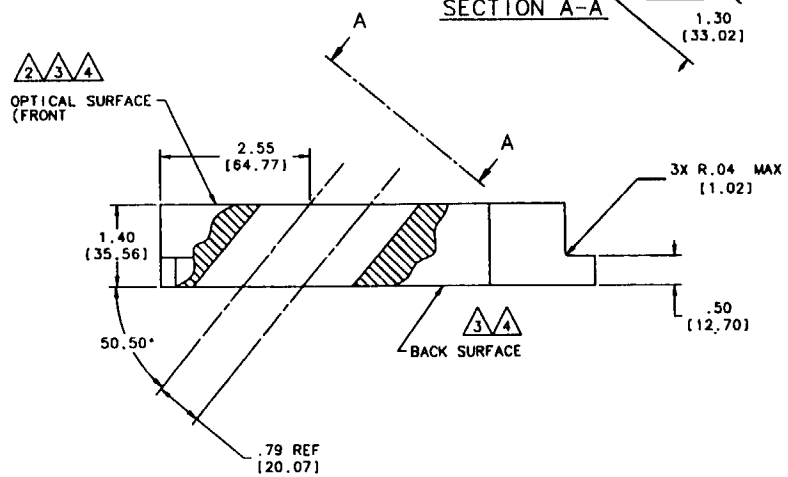

NOTES:

1. MATERIAL: FUSED SILICA, PREMIUM GRADE.
2. FINISH: ALL SURFACE FINISHES PER MIL-O-13830. FRONT AND BACK SURFACES SHALL BE POLISHED TO A SCRATCH/DIG TOLERANCE OF 40-20. ALL OTHER SURFACES TO BE MEDIUM GROUND TO AN 80/50 TOLERANCE.
3. SURFACE FIGURE: THE FRONT AND BACK SURFACES TO BE FLAT AND SMOOTH TO AN RMS TOLERANCE OF 1/4-1/8λ WHEN MEASURED AT 6328A° (STANDARD ZYGO INTERFEROMETER). EDGE EFFECTS CAN BE MASKED UP TO 2mm FROM EDGES AND 1 mm AROUND HOLE.
4. THE OPTICAL SURFACE AND BACK BACK SURFACE TO BE PARALLEL TO EACH OTHER WITHIN 2 ARC-MINUTES.
5. SURFACES INDICATED BY CROSSHATCHING TO BE HYDROSULFURIC ACID ETCHED AFTER INITIAL OPTICAL FABRICATION AND PRIOR TO FINAL SURFACE FIGURING.
6. ALL EDGES TO HAVE EITHER A 1mm RADIUS OR A 1mm X 45° CHAMFER AT OPTICAL MANUFACTURERS DISCRETION.
7. 1.40 (35.56mm) DIMENSION APPLIES AT OPTICAL SURFACE. A SLIGHT TAPER IS ALLOWABLE LEAVING A LARGER DIMENSION AT THE BACK SURFACE.
8. ESTIMATED MASS IS 1.22 Kg.
9. DIMENSIONS IN BRACKETS ARE MILLIMETERS.
10. APPLY AN OPTICAL COATING OF ALUMINUM WITH AN OVERCOAT OF 200-300A° OF SILICON DIOXIDE OR SILICON MONOXIDE.

REMOVE BURRS AND BREAK SHARP EDGES	DR: M. HONDA DATE: 08-30-96	CHK: DATE: 12-23-96
UNLESS OTHERWISE SPECIFIED DIMENSIONS ARE IN INCHES	DSGN APPD DATE	
TOLERANCES ON FRACTIONS DECIMALS ANGLES .XX ± .01 .XXX ± .005 ± .25°	MACH APPD DATE	
	ENGR APPD DATE	
MACH. FIN: N/A	PROJ APPD DATE	
MAT'L: 1 FIN: 2	CONTRACT	
NEXT ASSY TX1-501		

SMITHSONIAN ASTROPHYSICAL OBSERVATORY
CENTRAL ENGINEERING CAMBRIDGE, MA.

CAMERA FLAT, TEST

SIZE	CODE IDENT NO.	DWG NO.	REV
D	50944	TX1-1004	2

SCALE 1/1 | IDEAS MS3 | SHEET 1 OF 1